



Measurements of multijet event isotropies using optimal transport with the ATLAS detector

The ATLAS Collaboration

A measurement of novel event shapes quantifying the isotropy of collider events is performed in 140 fb^{-1} of proton–proton collisions with $\sqrt{s} = 13 \text{ TeV}$ centre-of-mass energy recorded with the ATLAS detector at CERN’s Large Hadron Collider. These event shapes are defined as the Wasserstein distance between collider events and isotropic reference geometries. This distance is evaluated by solving optimal transport problems, using the ‘Energy-Mover’s Distance’. Isotropic references with cylindrical and circular symmetries are studied, to probe the symmetries of interest at hadron colliders. The novel event-shape observables defined in this way are infrared- and collinear-safe, have improved dynamic range and have greater sensitivity to isotropic radiation patterns than other event shapes. The measured event-shape variables are corrected for detector effects, and presented in inclusive bins of jet multiplicity and the scalar sum of the two leading jets’ transverse momenta. The measured distributions are provided as inputs to future Monte Carlo tuning campaigns and other studies probing fundamental properties of QCD and the production of hadronic final states up to the TeV-scale.

Contents

1	Introduction	2
1.1	The Energy-Mover’s Distance	3
1.2	Event shapes via optimal transport	4
2	Event isotropies	6
3	The ATLAS detector, data and simulation	11
3.1	The ATLAS detector	11
3.2	Data	12
3.3	Simulation	12
4	Methodology	13
4.1	Jets	13
4.2	Event selection	14
4.3	Binning	14
4.4	Unfolding	14
5	Systematic uncertainties	15
5.1	Unfolding methodology: statistical uncertainties and non-closure	15
5.2	Choice of nominal Monte Carlo generator	15
5.3	Jet energy scale and resolution	16
5.4	Other experimental uncertainties	16
6	Results	16
7	Concluding remarks	29

1 Introduction

Event shapes are a family of observables used to describe the flow of energy in collider events [1]. Measurements of event shapes have been used to probe fundamental properties of QCD [2–26], to tune Monte Carlo (MC) models [27–29] and to search for physics beyond the Standard Model (SM) [30–34]. A novel class of event shape observables was recently proposed to quantify the isotropy of collider events [35]. These observables, broadly called *event isotropy*, measure how ‘far’ a collider event is from a symmetric radiation pattern in terms of a Wasserstein distance metric [36, 37]. Event isotropy observables are complementary to canonical event shapes such as thrust [2, 38, 39], sphericity [40, 41] and spherocity [42], which were designed to quantify how closely collider events resemble ‘pencil-like’ dijet events.

The Wasserstein distances used to define event isotropies are framed in terms of optimal transport problems, using the ‘Energy-Mover’s Distance’ (EMD) [43, 44]. This formulation is infrared- and collinear-safe by construction, avoiding pathologies related to low-energy particles or small-angled splittings that can affect other event shapes. Event isotropies are more sensitive to isotropic radiation patterns than other event shapes, isolating events with larger multiplicities of objects that are isotropically distributed. This behaviour differs from that of the thrust and sphericity, which interpolate between back-to-back dijet and

well-balanced trijet events. Event isotropies also exhibit larger dynamic ranges in the quasi-isotropic event-shape region than traditional event shapes [45]. This distinct behaviour implies that event isotropy observables have the potential to be powerful references for Monte Carlo developers, complementary to existing measurements. They also have the potential to increase the sensitivity of many measurements and searches for rare processes within and beyond the Standard Model with isotropically distributed signals and backgrounds, such as $t\bar{t}H$ [46, 47] or $t\bar{t}t\bar{t}$ [48, 49] production or searches for QCD instantons [50, 51], strongly-coupled hidden sectors [52, 53], models with large extra dimensions [54–58] or microscopic black holes [59–63].

ATLAS and CMS have performed differential measurements of many canonical event-shape observables at the LHC in minimum-bias [64, 65], multijet [66–68] and Z+jet [69, 70] final states. Earlier hadron-collider event-shape measurements were also performed by the CDF [71] and DØ [72] collaborations. The large Run 2 dataset [73] and advances in jet reconstruction performance [74] and MC modelling [75] allow the latest event-shape measurements to be made with fine binning and differentially in inclusive bins of jet multiplicity, N_{jet} , and the scalar sum of the leading and subleading jet transverse momenta, $H_{T2} = p_{T,1} + p_{T,2}$.

This paper presents normalised differential cross-section measurements of three event-isotropy observables, introduced in detail in Section 2. These measurements allow the shape of the event isotropy observables to be studied in detail; particularly by making comparisons with predictions from several cutting-edge Monte Carlo event generators. The methodology closely follows that used in the most recent ATLAS measurement of canonical event shapes [68], using anti- k_r jets with radius parameter $R = 0.4$ as the input objects for event shape calculations (Section 4.1) [76].

The structure of this paper is as follows. After these introductory remarks, an overview of the central phenomenological concepts used in this analysis is provided. Section 2 defines the three event-isotropy observables that are later measured, describing how they are calculated and some of their general properties. A description of the ATLAS detector, the Run 2 dataset and the simulated multijet events used in this analysis may be found in Section 3. In Section 4, details of the physics object reconstruction, event selection and unfolding procedure used in this analysis are given. A summary of the systematic uncertainties considered in the measurement is provided in Section 5. The main results of the analysis are presented in Section 6; afterwards, concluding remarks are made.

1.1 The Energy-Mover’s Distance

In order to compute how ‘far’ one event is from another, a well-defined mathematical definition of distance must be introduced. Event isotropy is computed using the Energy-Mover’s Distance (EMD) [43, 44] – an application of the well-known ‘Earth-Mover’s Distance’ from computer vision [77–81] to particle physics, using the p -Wasserstein metric [36, 37]. The EMD is defined as *the minimum amount of ‘work’ necessary to transport one event \mathcal{E} with M particles into another \mathcal{E}' of equal energy with M' particles, by movements of energy f_{ij} from particle $i \leq M$ in one event to particle $j \leq M'$ in the other:*¹

$$\text{EMD}_\beta(\mathcal{E}, \mathcal{E}') = \min_{\{f_{ij} \geq 0\}} \sum_{i=1}^M \sum_{j=1}^{M'} f_{ij} \theta_{ij}^\beta, \quad (1)$$

¹ In this analysis, the energies of the events compared in each EMD calculation are always normalised to each other, and so the EMD is presented here in a simplified form.

$$\sum_{i=1}^M f_{ij} = E'_j, \quad \sum_{j=1}^{M'} f_{ij} = E_i, \quad \sum_{i=1}^M \sum_{j=1}^{M'} f_{ij} = \sum_{i=1}^M E_i = \sum_{j=1}^{M'} E_j = E_{\text{total}} \quad (2)$$

where θ_{ij} is a pairwise distance between particles known as the *ground measure*, $\beta > 0$ is an angular weighting exponent, and E_{total} is the total energy in each event. The constraints defined in Eq. (2) ensure that the amount of energy moved from a particle is positive and does not exceed its initial energy, and that the total energy moved is conserved before and after the transport operation.

Equations (1) and (2) define an *optimal transport* problem between the energy flow in events \mathcal{E} and \mathcal{E}' , which may be solved using common scientific computing libraries. The open-source packages `EVENT_ISOTROPY` [82] (which implements event isotropy calculations using the `PYTHON OPTIMAL TRANSPORT (POT)` library [83]) and `WASSERSTEIN` [43, 44, 84] were both tested during this analysis, and were found to give compatible results.

In these measurements, the input objects to EMD calculations are anti- k_t jets with radius parameter $R = 0.4$ (reconstructed and calibrated as described in Section 4.1) [76]. The use of jets rather than per-particle inputs results in efficient optimal transport calculations because of the lower resultant object multiplicity per-event, and reduces sensitivity to non-perturbative QCD effects such as hadronisation. Experimentally, this choice provides a well-calibrated object with a precisely measured energy scale and energy resolution (Section 5.3) that has a clearly defined counterpart at particle level for use in the unfolding procedure (Section 4.4), and a measurement that is infrared- and collinear-safe.

1.2 Event shapes via optimal transport

References [35] and [44] interpret well-established event shapes such as the thrust and sphericity in terms of the geometric approach made possible by establishing a distance metric between different radiation configurations. This discussion is summarised in this section, but interested readers are referred to the original publications for a more thorough discussion.

Some canonical event-shape observables can be identified as the minimum EMD between a collider event and a manifold defined by a certain radiation pattern. For example, the simplest case considers the $\mathcal{P}_2^{\text{BB}}$ manifold, defined by the set of all back-to-back two-particle events with energy E_{BB}^i :

$$\mathcal{P}_2^{\text{BB}} = \left\{ \sum_{i=1}^2 E_{\text{BB}}^i \delta(\hat{n} - \hat{n}_i) \mid E_{\text{BB}}^i \geq 0, \hat{n}_1 = -\hat{n}_2 \right\}.$$

where \hat{n} is along the direction of the thrust axis, and $\hat{n}_i = \vec{p}_i / E_{\text{BB}}$, and \vec{p}_i is the momentum of particle i . The event thrust may be constructed in terms of an optimal transport problem between the collider event \mathcal{E} and $\mathcal{P}_2^{\text{BB}}$.² A common definition of the thrust for an event with M massless particles and total energy E_{total} is given by

$$\begin{aligned} t(\mathcal{E}) &= 2 \min_{\hat{n}} \sum_{i=1}^M \frac{|\vec{p}_i| (1 - |\vec{n}_i \cdot \hat{n}|)}{E_{\text{total}}} \\ &= 2 \min_{\hat{n}} \sum_{i=1}^M \frac{E_i}{E_{\text{total}}} \min(1 - \hat{n}_i \cdot \hat{n}, 1 + \hat{n}_i \cdot \hat{n}). \end{aligned} \quad (3)$$

² When computing the transverse thrust, the two energies do not have to be equal.

From Eq. (3), it is clear that thrust can be formulated as the transportation cost to move particle i to either \hat{n} or $-\hat{n}$, with an angular measure of

$$\theta_{ij}^2 = 2n_i^\mu n_{j\mu} = 2(1 - |\vec{n}_i \cdot \hat{n}|)$$

and a normalised energy weight

$$f_{ij} = \frac{|\vec{p}_i|}{E_{\text{total}}}.$$

The minimisation over \hat{n} is equivalent to finding the thrust axis of the event. This expression is identified as the EMD between \mathcal{E} and the closest event $\mathcal{E}' \in \mathcal{P}_2^{\text{BB}}$:

$$t(\mathcal{E}) = \text{EMD}(\mathcal{E}, \mathcal{E}'),$$

with $\beta = 2$ in the notation of Eq. (1). The transverse thrust is obtained by making a transverse projection of the events and considering only the ring of back-to-back particle geometries (or, ‘dipole-like geometries’) made by the subset of $\mathcal{P}_2^{\text{BB}}$ which exists in the transverse plane (illustrated in Figure 1).

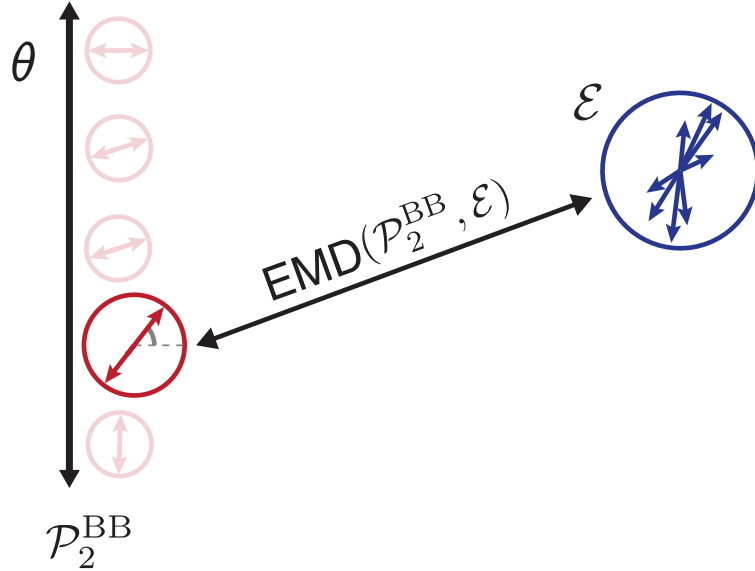


Figure 1: A representation of the EMD as the minimum distance of an event \mathcal{E} to a manifold of two-particle back-to-back events $\mathcal{P}_2^{\text{BB}}$. The angle θ represents the degree of freedom corresponding to the relative azimuthal orientation of the reference event from $\mathcal{P}_2^{\text{BB}}$ and the collider event \mathcal{E} . The arrow indicates, schematically, the EMD describing the minimum cost to transport \mathcal{E} to $\mathcal{P}_2^{\text{BB}}$.

Similarly, choosing $\beta = 1$ instead yields the event sphericity, while considering the larger manifold of all two-particle configurations \mathcal{P}_2 yields the event broadening [85]. The smallest distances between the sets of N -particle manifolds (which do not necessarily conserve momentum) and \mathcal{E} are equivalent to the event N -jettinesses [86].³

Following the example of these event isotropy variables, other event shapes could be constructed to probe different aspects of QCD radiation in collider events. The development of other observables with potentially model- or search-specific applications, e.g. those with non-jetty geometries [52, 88], may be a promising area for further study.

³ Analogously, performing such a calculation within a jet instead of an event results in the N -subjettiness [87].

2 Event isotropies

The ‘event isotropy’ \mathcal{I} [35] builds upon the set of event shapes defined as distances from finite-particle configurations. This observable is defined as a Wasserstein distance between a collider event \mathcal{E} and a (quasi-)uniform radiation pattern \mathcal{U} , determined using the Energy-Mover’s Distance (Section 1.1):

$$\mathcal{I}(\mathcal{E}) = \text{EMD}(\mathcal{E}, \mathcal{U}),$$

The total energy in each reference event \mathcal{U} is defined to be the same as that for the collider event \mathcal{E} it is compared with, so that the EMD is computed with normalised energy transfer ($f_{ij} \rightarrow f_{ij}/E_{\text{total}}$). This ensures that the event isotropy \mathcal{I} is bounded on $\mathcal{I} \in [0, 1]$ and is dimensionless. The least isotropic events take values approaching $\mathcal{I} = 1$. By construction, perfectly (and only perfectly) isotropic events take a value of $\mathcal{I} = 0$, meaning there is zero distance between radiation patterns. Event isotropies can therefore differentiate between quasi-isotropic events better than the existing observables C -parameter and D -parameter [89], which respectively take extreme values for events with symmetric radiation along three perpendicular axes and events that are planar.

Event isotropy observables are defined on sets of massless input particles with no net transverse momentum. In this study, the input particles are the event’s reconstructed anti- k_t jets at either detector level or particle level (Section 4.1). While these objects are massive, only their transverse momentum (p_T) and angular kinematic information (rapidity, y , and azimuthal angle, ϕ) are used for the isotropy calculation. The recoil term is added to \mathcal{E} before computing the isotropy, following the description in Ref. [35], to ensure the resulting distribution of \mathcal{I} is bounded. This quantity is computed as the negative four-vector sum of all jets inputted to the EMD calculation for a given event.

Different choices of the reference event \mathcal{U} can be made, possessing alternative geometrical symmetries. Observables with both one-dimensional ‘ring-like’ and two-dimensional ‘cylindrical’ symmetries are studied in this analysis. In practice, any reference geometry must be constructed using a user-defined finite number of particles, N , for the EMD to be computed using numerical methods. This parameter should be chosen such that it is large enough to maintain approximately continuous symmetries while balancing this against the computational expense, since the complexity of optimal transport problems with n particles scales naively as $O(n^3 \log^2 n)$. The minimal choice of N that prevented discretisation effects was used in this analysis to facilitate this analysis of the large Run 2 LHC dataset.

Three event-shape observables are considered in this analysis. Both a quasi-uniform ring-like geometry with $N = 128$ points ($\mathcal{I}_{\text{Ring}}^{N=128}$), and the special case of a ring-like geometry with $N = 2$ ($\mathcal{I}_{\text{Ring}}^{N=2}$) are studied. This $N = 2$ observable is similar to transverse thrust, but with balanced energy as mentioned earlier. These two cases are studied to more directly compare the behaviours of the isotropy observables because they are defined on sets with zero net transverse momentum, unlike thrust. A quasi-uniform cylindrical geometry with $N = 16$ azimuthal segments is also considered ($\mathcal{I}_{\text{Cyl}}^{N=16}$), resulting in a square reference grid of 352 points in the event rapidity–azimuth plane of $y \in [-4.5, 4.5]$ and $\phi \in [0, 2\pi]$ (matching the acceptance region of $R = 0.4$ jets in ATLAS, described in Section 4.1). All EMDs are calculated with $\beta = 2$, so the case of $\mathcal{I}_{\text{Ring}}^{N=2}$ is similar to the transverse thrust. This choice of squared distances yields larger penalties for large displacements relative to small ones. This is motivated by the study of jets rather than particles, to reduce differences between these two pictures of the event. The squared distance measure is also computed more efficiently. Every observable is separately normalised by the distance between the reference geometry (cylinder, ring, or dipole) and the maximally distant particle configuration with zero net transverse momentum such that the observable is defined on a range of $[0, 1]$. These observables are

summarised in Table 1, along with their corresponding ground measures, following the implementations in Ref. [35]. The quasi-uniform reference geometries are illustrated in Figure 2, and a schematic illustration of the three event-shape observables studied in this analysis is provided in Figure 3.

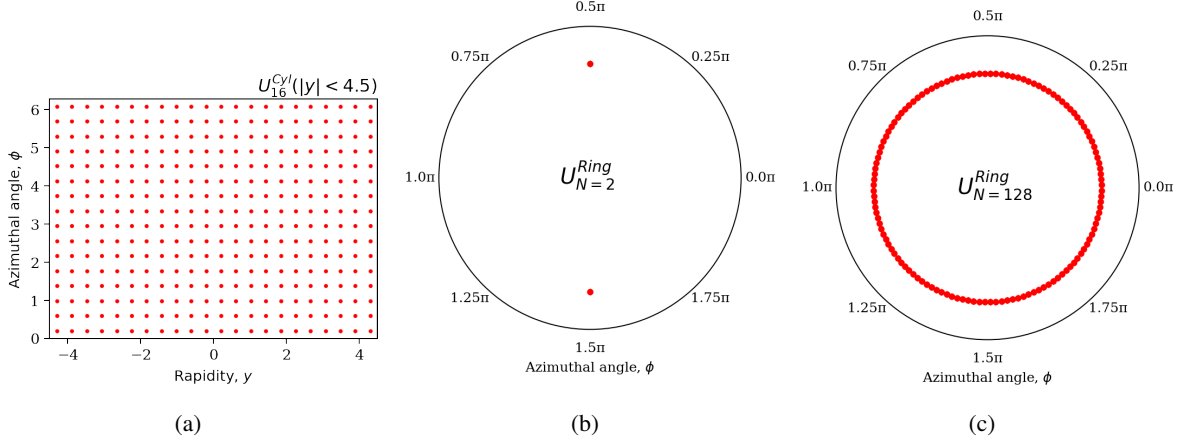


Figure 2: Reference geometries with (a) cylindrical and ring-like symmetry with (b) 2 and (c) 128 reference points. The radius at which the points in the ring-like geometry are located is arbitrary.

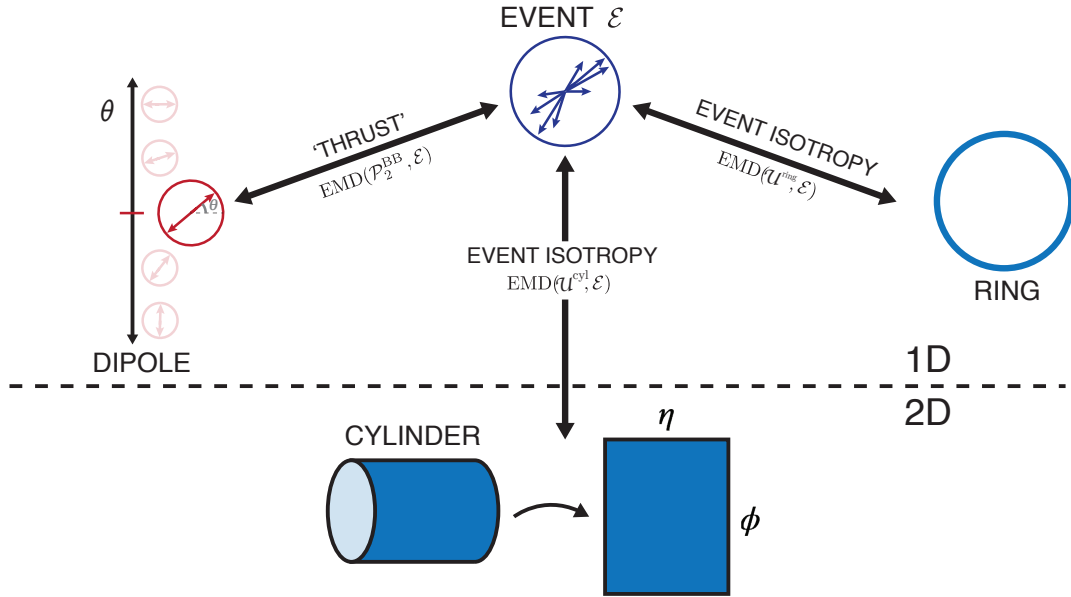


Figure 3: Schematic illustrating the three observables measured in this analysis in terms of the Energy-Mover's Distance from a collider event, \mathcal{E} : $\mathcal{I}_{\text{Ring}}^{N=2}$, $\mathcal{I}_{\text{Cyl}}^{N=16}$, and $1 - \mathcal{I}_{\text{Ring}}^{N=128}$.

Different ground measures θ_{ij} are chosen for the different reference geometries. For the cylindrical case, the ground measure is taken to be the squared rapidity–azimuth distance between particles, where y_i and ϕ_i are the rapidity and azimuth of each input particle, y_{ij} and ϕ_{ij} are their differences between initial position i and new position j , and $y_{\text{max}} = 4.5$ is the maximum rapidity acceptance the cylinder. For the ring geometry (both the isotropic and dipole configurations), the ground measure is taken to be the transversely projected

Table 1: The different geometries used to define event isotropy, with their corresponding ground measures, and default quasi-uniform configurations, adapted from Ref. [35] (where the dipole geometry was not considered explicitly). Details of the normalisation of these observables can be found in Ref. [35].

Geometry	Ground Measure	\mathcal{U}
Cylinder	$\theta_{ij}^{\text{cyl}} = \frac{12}{\pi^2 + 16y_{\text{max}}^2} (y_{ij}^2 + \phi_{ij}^2)$	$\mathcal{U}_N^{\text{cyl}} (y < y_{\text{max}})$
Ring	$\theta_{ij}^{\text{ring}} = \frac{\pi}{\pi-2} (1 - \cos \phi_{ij})$	$\mathcal{U}_N^{\text{ring}}$
Ring (Dipole)	$\theta_{ij}^{\text{ring}} = \frac{1}{1-\frac{1}{\sqrt{3}}} (1 - \cos \phi_{ij})$	$\mathcal{U}_2^{\text{ring}}$

opening angle ϕ between particles i and j . In all isotropy calculations, the reference geometry is oriented with respect to each event such that the overall EMD is minimised. For large N , this is easily accomplished by azimuthally rotating the reference geometry such that a particle in the reference event is aligned with the leading jet in each event. For the case of $\mathcal{I}_{\text{Ring}}^{N=2}$, this minimisation is particularly important and the solution is non-trivial, akin to the computation of the thrust axis. The relative azimuthal angle between $\mathcal{U}_{N=2}^{\text{ring}}$ and collider events that minimises the EMD is therefore found numerically using a function minimiser [90].

To display the results of this analysis most clearly, all presented observables follow the historical convention that the least isotropic (‘dijet-like’) topology is near values of 0, and the most isotropic topology is near values of 1. Therefore, the results of this measurement are presented in terms of $1 - \mathcal{I}_{\text{Ring}}^{N=128}$, $1 - \mathcal{I}_{\text{Cyl}}^{N=16}$ and $\mathcal{I}_{\text{Ring}}^{N=2}$. Figure 4 shows the distributions of these observables at particle level and detector level for the PYTHIA sample of simulated events described in Section 3.3, in events with $N_{\text{jet}} \geq 2$ and $H_{\text{T}2} = (p_{\text{T},1} + p_{\text{T},2}) \geq 500$ GeV (Section 4.2, for details about the binning see Section 4.3). For the ring-like geometries shown in Figures 4(a) and 4(b), it is clear that most multijet events passing this selection at the LHC are dijet-like and well-balanced, but significant tails extend into the isotropic regions. The behaviour of $\mathcal{I}_{\text{Cyl}}^{N=16}$, shown in Figure 4(c), is more complex and exhibits a ‘bulk’ area with tails toward both isotropic topologies (large jet multiplicities, events with both central and forward jets) and non-isotropic topologies (jets only in one detector region, particularly the forward region on only one side of the event).

To better understand the differences between the shapes of $\mathcal{I}_{\text{Ring}}^{N=2}$ and $1 - \mathcal{I}_{\text{Ring}}^{N=128}$, it is informative to consider these observables in exclusive bins of jet multiplicity, N_{jet} . These distributions are shown in Figure 5, demonstrating the improved performance of $1 - \mathcal{I}_{\text{Ring}}^{N=128}$ relative to other event-shape observables in terms of selecting isotropic multijet events. For $\mathcal{I}_{\text{Ring}}^{N=2}$, each exclusive jet-multiplicity bin is distributed across the entire range of the event shape. Three-jet events produce extremal values of $\mathcal{I}_{\text{Ring}}^{N=2}$ most often, but such values may also be produced by events with other jet multiplicities. The $1 - \mathcal{I}_{\text{Ring}}^{N=128}$ observable has distinct endpoints for each exclusive jet-multiplicity bin, and the event shape distribution is dominated by events with increasing jet multiplicities as its value increases. As jet multiplicities are sequentially ordered in this case, the higher cross-section for lower jet multiplicities results in a flatter distribution at lower values of $1 - \mathcal{I}_{\text{Ring}}^{N=128}$ than for $\mathcal{I}_{\text{Ring}}^{N=2}$, where the cross-section falls more steeply for values near 0.

Even though there is a calculable EMD between the reference configurations themselves, the choice of ground measure used to define event isotropy observables results in a non-trivial relationship between

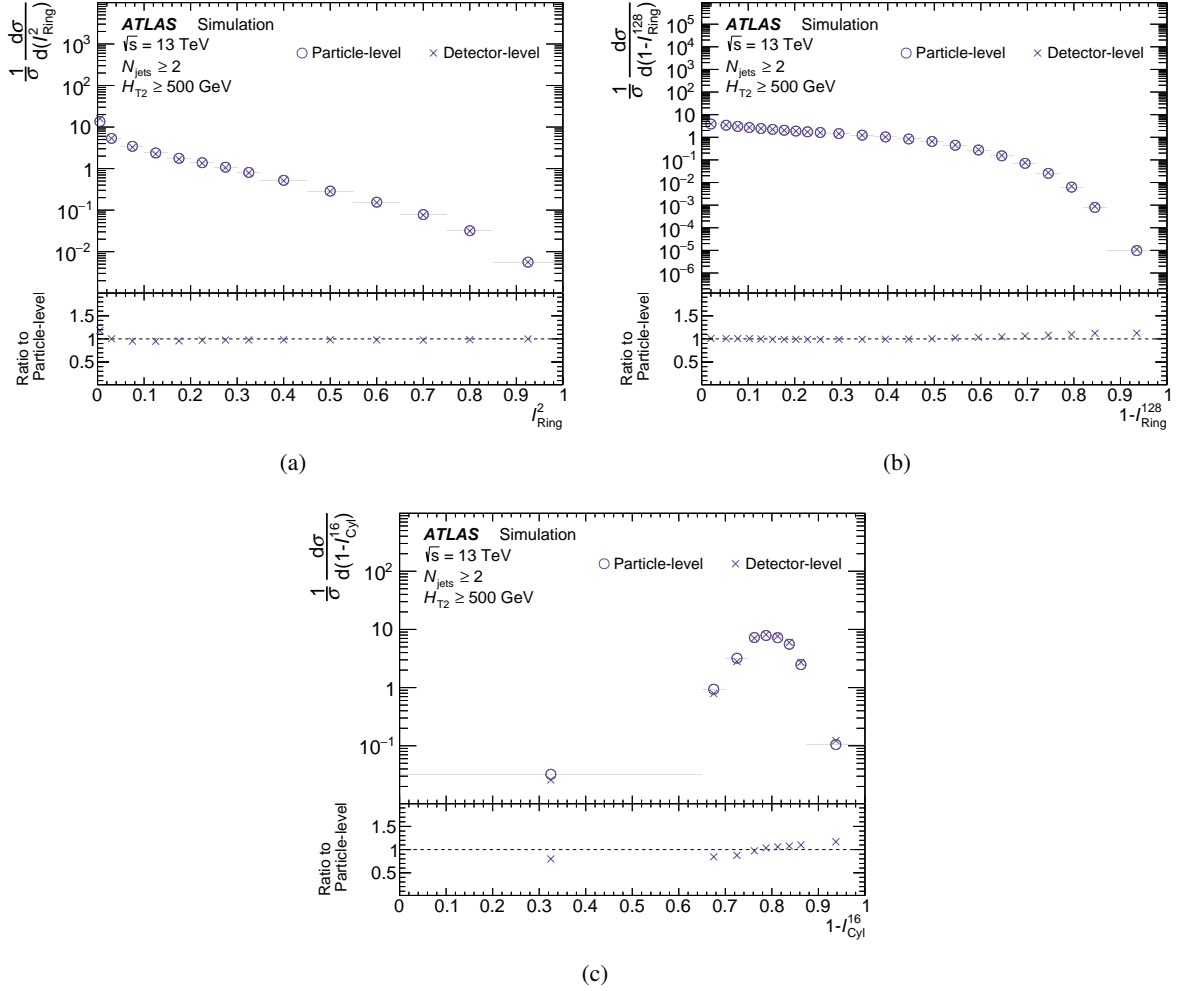


Figure 4: Isotropy observables at particle level (open circles) and detector level (crosses), for events with $H_{T2} \geq 500$ GeV and $N_{\text{jet}} \geq 2$. The event isotropy observables (a) $\mathcal{I}_{\text{Ring}}^{N=2}$, (b) $1 - \mathcal{I}_{\text{Ring}}^{N=128}$ and (c) $1 - \mathcal{I}_{\text{Cyl}}^{N=16}$ are shown. The lower panel of each figure displays the ratios of detector-level to particle-level distributions. The plots are produced using simulated events generated with PYTHIA 8.230.

$1 - \mathcal{I}_{\text{Ring}}^{N=128}$ and $\mathcal{I}_{\text{Ring}}^{N=2}$. This choice is also the reason that the two observables obtain their extreme values from different types of events. The correlations between the studied event-isotropy observables are illustrated at particle level in Figure 6. This correspondence was discussed in Ref. [35], and results from the choice of ground measure and EMD angular exponent $\beta = 2$, which causes the triangle inequality to be violated for these observables:

$$0 \leq \text{EMD}(\mathcal{E}, \mathcal{E}'') \not\leq \text{EMD}(\mathcal{E}, \mathcal{E}') + \text{EMD}(\mathcal{E}', \mathcal{E}'').$$

In fact, EMDs with this ground measure belong to a generalised class of ground measures known as p -Wasserstein metrics [36, 37] (here, with $p = \beta$) that instead satisfy a generalised version of the triangle inequality:

$$\text{EMD}(\mathcal{E}, \mathcal{E}'')^{1/\beta} \leq \text{EMD}(\mathcal{E}, \mathcal{E}')^{1/\beta} + \text{EMD}(\mathcal{E}', \mathcal{E}'')^{1/\beta}.$$

where the parameter β is the exponent related to angular weighting in Equation 1 (taken here as $\beta = 2$). The

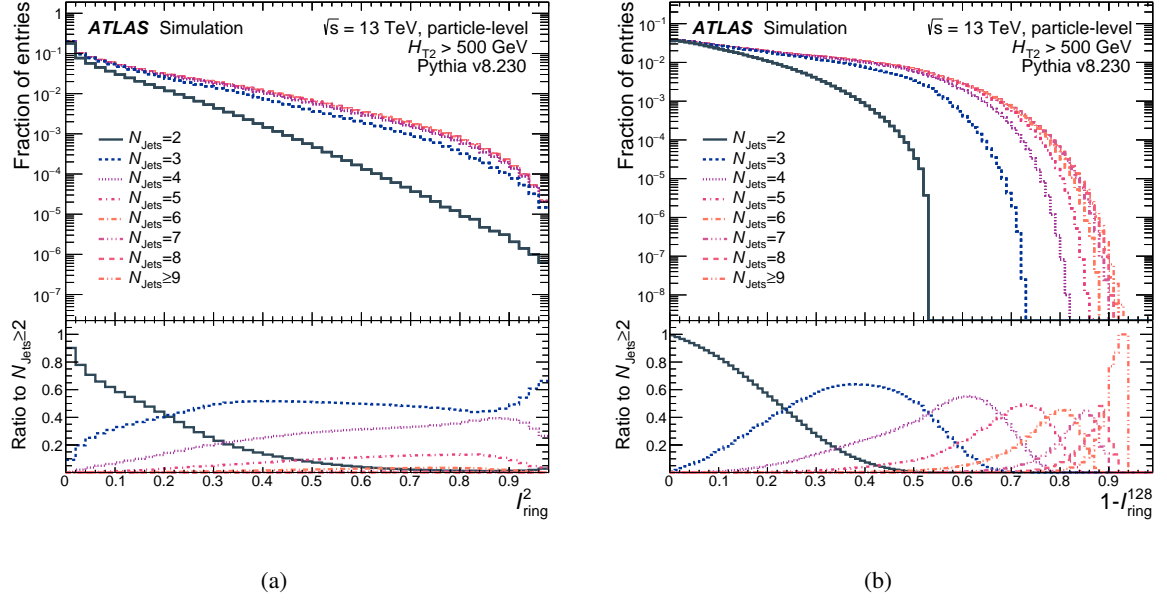


Figure 5: Stacked histograms show the normalised (a) $\mathcal{I}_{\text{Ring}}^{N=2}$ and (b) $1 - \mathcal{I}_{\text{Ring}}^{N=128}$ distributions in separate bins of N_{jet} , for particle-level PYTHIA dijet events with $N_{\text{jet}} \geq 2$ and $H_{T2} > 500$ GeV. The lower panel of each figure shows the ratio of each N_{jet} bin to the inclusive distribution of the observable.

non-trivial relationship between these observables motivates measurements of multiple reference-particle configurations with the same dimensionality – i.e. measuring both $1 - \mathcal{I}_{\text{Ring}}^{N=128}$ and $\mathcal{I}_{\text{Ring}}^{N=2}$.

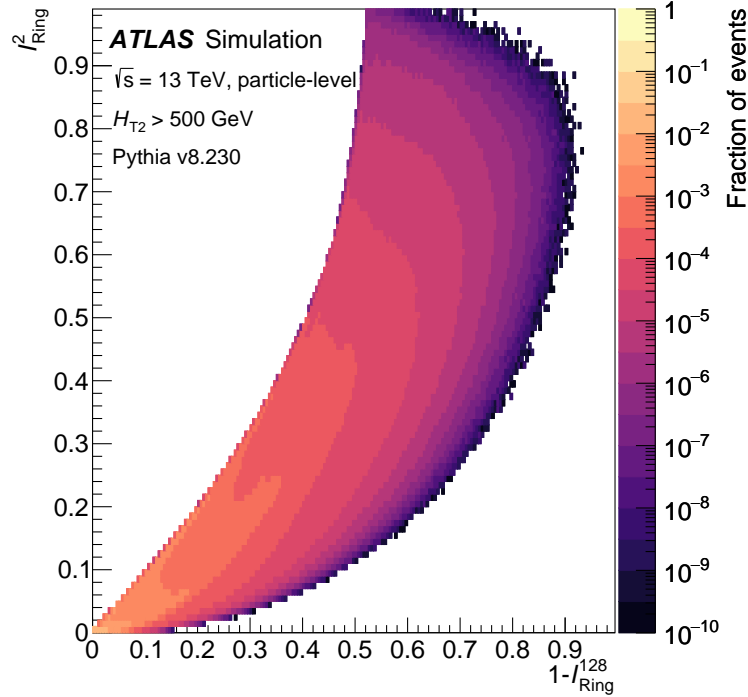


Figure 6: The correlation between $\mathcal{I}_{\text{Ring}}^{N=2}$ and $1 - \mathcal{I}_{\text{Ring}}^{N=128}$ is illustrated as a two-dimensional histogram, for events with $N_{\text{jet}} \geq 2$ and $H_{T2} > 500$ GeV.

3 The ATLAS detector, data and simulation

3.1 The ATLAS detector

The ATLAS detector [91] at the LHC covers nearly the entire solid angle around the collision point.⁴ It consists of an inner tracking detector surrounded by a thin superconducting solenoid, electromagnetic and hadron calorimeters, and a muon spectrometer incorporating three large superconducting air-core toroidal magnets.

The inner-detector system is immersed in a 2 T axial magnetic field and provides charged-particle tracking in the range $|\eta| < 2.5$. The high-granularity silicon pixel detector covers the vertex region and typically provides four measurements per track, the first hit normally being in the insertable B-layer installed before Run 2 [92, 93]. It is followed by the silicon microstrip tracker, which usually provides eight measurements per track. These silicon detectors are complemented by the transition radiation tracker (TRT), which enables radially extended track reconstruction up to $|\eta| = 2.0$. The TRT also provides electron identification

⁴ ATLAS uses a right-handed coordinate system with its origin at the nominal interaction point (IP) in the centre of the detector and the z-axis along the beam pipe. The x-axis points from the IP to the centre of the LHC ring, and the y-axis points upwards. Cylindrical coordinates (r, ϕ) are used in the transverse plane, ϕ being the azimuthal angle around the z-axis. The pseudorapidity is defined in terms of the polar angle θ as $\eta = -\ln \tan(\theta/2)$. Angular distance is measured in units of $\Delta R \equiv \sqrt{(\Delta y)^2 + (\Delta \phi)^2}$, where $y = (1/2)[(E + p_z)/(E - p_z)]$ is the object's rapidity defined by its energy and longitudinal momentum.

information based on the fraction of hits (typically 30 in total) above a higher energy-deposit threshold corresponding to transition radiation.

The calorimeter system covers the pseudorapidity range $|\eta| < 4.9$. Within the region $|\eta| < 3.2$, electromagnetic calorimetry is provided by barrel and endcap high-granularity lead/liquid-argon (LAr) calorimeters, with an additional thin LAr presampler covering $|\eta| < 1.8$ to correct for energy loss in material upstream of the calorimeters. Hadron calorimetry is provided by the steel/scintillator-tile calorimeter, segmented into three barrel structures within $|\eta| < 1.7$, and two copper/LAr hadron endcap calorimeters. The solid angle coverage is completed with forward copper/LAr and tungsten/LAr calorimeter modules optimised for electromagnetic and hadronic energy measurements respectively.

The muon spectrometer comprises separate trigger and high-precision tracking chambers measuring the deflection of muons in a magnetic field generated by the superconducting air-core toroidal magnets. The field integral of the toroids ranges between 2.0 and 6.0 Tm across most of the detector. Three layers of precision chambers, each consisting of layers of monitored drift tubes, cover the region $|\eta| < 2.7$, complemented by cathode-strip chambers in the forward region, where the background is highest. The muon trigger system covers the range $|\eta| < 2.4$ with resistive-plate chambers in the barrel, and thin-gap chambers in the endcap regions.

Interesting events are selected by the first-level trigger system implemented in custom hardware, followed by selections made by algorithms implemented in software in the high-level trigger [94]. The first-level trigger accepts events from the 40 MHz bunch crossings at a rate below 100 kHz, which the high-level trigger further reduces to record events to disk at about 1 kHz.

An extensive software suite [95] is used in data simulation, in the reconstruction and analysis of real and simulated data, in detector operations, and in the trigger and data acquisition systems of the experiment.

3.2 Data

This analysis is performed using data from LHC pp collisions with $\sqrt{s} = 13$ TeV, collected during 2015–2018 with the ATLAS detector. The total integrated luminosity of this dataset is 140 fb^{-1} . The uncertainty in the combined 2015–2018 integrated luminosity is 0.83% [96], obtained using the LUCID-2 detector [97] for the primary luminosity measurements, complemented by measurements using the inner detector and calorimeters. Due to the high instantaneous luminosity and the large total inelastic proton–proton (pp) cross section, there are, on average, 33.7 simultaneous (‘pile-up’) collisions in each bunch crossing. Data are required to satisfy certain quality requirements [73] to be included in the analysis.

3.3 Simulation

Samples of Monte Carlo (MC) simulated dijet and multijet events are used in this analysis. Since the jet production cross-section is much larger than the cross-section for electroweak processes, the dijet and multijet samples are sufficient to describe the data.

PYTHIA 8.230 [98, 99] is used as the nominal MC generator for this analysis, and is also referred to here as the ‘nominal’ simulation. Samples of $2 \rightarrow 2$ dijet events were simulated using the A14 tune [28], the Lund string hadronisation model and the NNPDF2.3LO [100] leading-order (LO) parton distribution function (PDF) set. The PYTHIA parton shower (PS) algorithm uses a dipole-style p_T -ordered evolution, and its

renormalisation and factorisation scales were set to the geometric mean of the squared transverse masses of the outgoing particles. EVTGEN [101] was used to model decays of heavy-flavour hadrons.

Two sets of SHERPA 2.2.5 [102] dijet events were used with the default AHADIC cluster hadronisation model [103] or with the SHERPA interface to the Lund string hadronisation model as implemented in PYTHIA 6.4, and its decay tables. These samples include LO matrix element calculations for $2 \rightarrow 2$ processes, and use the SHERPA parton shower algorithm based on Catani–Seymour dipole subtraction [104]. The CT14_{NNLO} next-to-next-to-leading-order (NNLO) PDF [105] set is used for matrix element calculations and CT10 is used for multi-parton interactions (MPI) [106].

Two sets of HERWIG 7.1.3 [107–109] multijet events were generated with the MMHT2014_{NLO} PDF set [110], default cluster hadronisation model and either the default angle-ordered PS or alternative dipole PS [103]. These samples model $2 \rightarrow 2$ matrix elements with NLO accuracy and $2 \rightarrow 3$ matrix elements with LO accuracy. Both parton shower models were matched to the matrix element calculation using the MC@NLO matching scheme [111, 112]. The p_T of the leading jet is taken as the renormalisation scale.

Two additional samples of dijet events with NLO matrix element accuracy were produced with POWHEG v2 [113–115] using the dijet process implemented in POWHEG Box v2 [116], matched to either the PYTHIA 8 or angle-ordered HERWIG 7 parton showers configured as for the corresponding samples described above. The renormalisation and factorisation scales in these samples were set to the p_T of the underlying Born-level configuration. For the PYTHIA PS, the default Lund string hadronisation model was used with the NNPDF3.0_{NLO} PDF set [117] and A14 tune. For the HERWIG sample, the NNPDF3.0_{NLO} PDF set [117] was also used along with the default HERWIG cluster-based hadronisation model. These samples are referred to as the ‘POWHEG+PYTHIA’ and ‘POWHEG+HERWIG’ samples.

All generated events were passed through a full detector simulation [118] based on GEANT4 [119] and overlaid with simulated minimum-bias interactions generated using PYTHIA 8 with the A3 tune [120] and NNPDF2.3_{LO} PDF set [100] to represent pile-up interactions. The distribution of the average number of pile-up interactions in simulation is reweighted during data analysis to match that observed in Run 2 data.

Additional details of the MC samples used in this measurement may be found in Ref. [75].

4 Methodology

4.1 Jets

All jets in this analysis are reconstructed using the anti- k_t algorithm [76] as implemented in FASTJET [121], using a jet radius parameter $R = 0.4$. The acceptance of jets at detector level has been increased relative to other recent event-shape measurements by ATLAS [68]. In particular, jets with lower transverse momentum and jets in the forward detector region have been included.

‘Particle-level’ jets are reconstructed in MC events without detector simulation. All detector-stable particles with a lifetime τ in the laboratory frame such that $c\tau > 10$ mm are used, except those particles that are expected to leave no or negligible energy depositions in the calorimeter, (i.e. neutrinos or muons). Particle-level jets are required to have a $p_T > 60$ GeV and a rapidity y satisfying $|y| < 4.5$ to enter this analysis.

Detector-level jets are reconstructed from particle-flow objects [122] that combine measurements from the ATLAS inner detector and calorimeter systems to improve the jet energy resolution (JER) and improve the

jet reconstruction efficiency, especially at low jet p_T . These jets are ‘cleaned’ to remove those originating from detector noise, cosmic rays and beam-induced processes by following the methodology described in Ref. [123], updated for particle-flow jets but utilising the same observables. In particular, the leading jet in each event is required to satisfy the ‘BadTight’ jet cleaning criteria if it is within the inner detector acceptance ($|y| < 2.4$). Detector-level jets are required to have a $p_T > 60$ GeV and a rapidity y satisfying $|y| < 4.5$ to be retained for study.

The likelihood that a particle-flow jet originates from a pile-up interaction following these kinematic selections is sufficiently low that no additional pile-up jet rejection is applied [124, 125].

4.2 Event selection

All detector-level events are required to have at least one vertex reconstructed from two or more inner-detector tracks with $p_T > 500$ MeV, and to pass the data quality requirements described in Ref. [73]. Events are required to have at least two selected jets ($N_{\text{jet}} \geq 2$) and to satisfy $H_{T2} \geq 400$ GeV to be included in the analysis. Data were collected using a set of single-jet triggers [126], whose thresholds varied depending on the data-taking period during Run 2. The H_{T2} requirement is applied to ensure that the measurement is performed in a fiducial region where the single-jet triggers are fully efficient for the analysis selection.

Since the acceptance of the standard jet triggers decreases with increasing jet rapidity, they are combined with a dedicated set of forward-jet triggers. Specific combinations of one central- and one forward-jet trigger are used to select events in ranges of H_{T2} where the combination is efficient. Some triggers are prescaled during data-taking, so events in data are reweighted by the appropriate prescale factor to recover a smoothly falling jet p_T spectrum. The prescale factors applied to central- and forward-jet triggers differ, so they are logically combined using the ‘inclusion method’ of Ref. [127].

4.3 Binning

In this analysis, the shape of the event isotropy observables $\mathcal{I}_{\text{Cyl}}^{N=16}$, $\mathcal{I}_{\text{Ring}}^{N=2}$ and $\mathcal{I}_{\text{Ring}}^{N=128}$ is measured in inclusive bins of N_{jet} and H_{T2} . The inclusive jet-multiplicity bins range from $N_{\text{jet}} \geq 2$ to $N_{\text{jet}} \geq 5$, and the inclusive bins of H_{T2} are $H_{T2} \geq 500$ GeV, $H_{T2} \geq 1000$ GeV and $H_{T2} \geq 1500$ GeV. Events with $N_{\text{jet}} \geq 2$ and $H_{T2} \in [400, 500]$ GeV are included in the measurement only during the unfolding procedure (Section 4.4), to mitigate the impact of migrations into the lowest H_{T2} bin of the measurement. The detector resolution for events in the $H_{T2} \in [400, 500]$ GeV region was found to be worse than that for events in higher H_{T2} bins, and so this bin was not included in measured region.

The final results (Section 6) are normalised such that their integral is equal to unity for each set of minimum N_{jet} and H_{T2} requirements applied. Information about the relative normalisation of the various bins studied is thus lost, in exchange for a more precise measurement of the distribution shapes.

4.4 Unfolding

All data presented in Section 6 are unfolded using an Iterative Bayesian Unfolding (IBU) procedure [128] to remove effects arising from the finite efficiency, acceptance and resolution of the ATLAS detector. This unfolding algorithm was implemented using the RooUNFOLD [129] toolkit. Four iterations of the unfolding procedure are used for all observables because this minimises the total uncertainty of the measurement.

Unfolding for the multi-differential measurements of event isotropy in inclusive bins of N_{jet} and H_{T2} is performed simultaneously, to allow the unfolding procedure to account for migrations between all analysis bins.

5 Systematic uncertainties

Many sources of systematic uncertainty are accounted for in this analysis; they are described in the following Sections 5.1–5.4. For each systematic uncertainty, a varied response matrix is constructed and used in place of the nominal one during the unfolding procedure.

5.1 Unfolding methodology: statistical uncertainties and non-closure

Statistical uncertainties arising from the finite Monte Carlo and data sample sizes used for this measurement are estimated during the unfolding procedure with Poissonian pseudo-experiments. For the Monte Carlo simulation, pseudo-experiments are used to vary the response matrix used for the unfolding procedure. The input MC prior is then unfolded with the varied response matrix; the efficiencies and acceptances are allowed to vary during this process. For the data statistical uncertainty, pseudo-experiments are generated to vary the input data spectrum for the unfolding procedure and are then unfolded using the nominal PYTHIA response matrix. Five-hundred pseudo-experiments are generated in both cases; using larger numbers of pseudo-experiments does not significantly alter the results. The 68% inter-quantile range of the output distributions generated as a result of these variations is taken as the corresponding statistical uncertainty.

The non-closure uncertainty in the unfolding procedure is evaluated using a data-driven reweighting procedure. The detector-level PYTHIA spectrum is reweighted to match the observed data spectrum and then unfolded with the nominal PYTHIA response matrix. The difference between this unfolded spectrum and the nominal PYTHIA particle-level spectrum is taken as a systematic uncertainty.

5.2 Choice of nominal Monte Carlo generator

In order to unfold a distribution, one relies on some nominal Monte Carlo simulation to construct the response matrix applied to data. No particular MC model matches the data perfectly, so different results will be obtained if a different MC model is used in the unfolding procedure. To account for the uncertainty related to the choice of nominal MC model, the unfolding procedure is repeated with the nominal PYTHIA prior but using an alternative MC simulation for the event sample. The alternative sample used to evaluate this uncertainty is the HERWIG sample with an angle-ordered parton shower algorithm, which varies many aspects of the simulation with respect to the nominal PYTHIA sample (Section 3.3). Despite the numerous differences between these two simulated samples, they provide competitive descriptions of the measured data, and the HERWIG sample was also considered as a plausible choice for the nominal Monte Carlo model.

The effects of changing the MC model on the analysis efficiencies, acceptance and unfolding response matrix are considered individually. An envelope of the observed differences between the final results following each of these three changes is constructed to conservatively estimate the uncertainty due to the choice of nominal MC generator.

5.3 Jet energy scale and resolution

Systematic uncertainties in the $R = 0.4$ jet energy scale (JES) and resolution (JER) are evaluated using a series of *in situ* measurements and simulation-based techniques, thoroughly documented in Ref. [74]. The source of the largest single experimental uncertainty throughout the analysis is related to the jet energy resolution measurement, made using the p_T balance of dijet events.

Other relevant uncertainties arise from differences in the gluon-initiated jet energy response between PYTHIA and HERWIG ('jet-flavour response' in Ref. [74]), and from the relative *in situ* JES calibration. For all JES/JER variations, the isotropy calculation is repeated with the varied set of jets.

The JES/JER uncertainties can potentially result in asymmetric variations, so they are left unsymmetrised in the presentation of the final results.

5.4 Other experimental uncertainties

Other uncertainties related to experimental effects are accounted for in this analysis. They are typically small, but can occasionally be significant in certain measurement bins.

An uncertainty in the absolute luminosity measurement is applied as a 0.83% variation to the normalisation of the nominal PYTHIA MC simulation. Due to the normalisation applied in this measurement, this systematic uncertainty cancels out by construction.

The uncertainty due to the mismodelling of pile-up events is negligible in all of the final results.

During certain Run 2 data-taking periods, specific tile modules in the hadron calorimeter were disabled due to technical problems. Some of these modules are also disabled in the simulated events corresponding to a given data-taking period, while other modules that were temporarily disabled during data-taking were not disabled in the simulation. No additional correction is applied to the p_T of jets which may have deposited energy in disabled tile modules. The impact of the disabled tile modules on the unfolded distributions is evaluated by repeating the measurement while vetoing events with jets directed at disabled modules in either data or the nominal PYTHIA sample. Differences between these 'vetoed-event' results and the nominal set are taken as a source of systematic uncertainty.

6 Results

A representative selection of the measured distributions are presented in this section. The systematic uncertainties are shown in a summarised format for clarity. Uncertainties arising from similar sources are grouped as follows:

- **Stat.:** statistical uncertainties related to both data and MC sample size in the unfolding procedure (Section 5.1).
- **Unfolding:** the data-driven non-closure uncertainty in the unfolding procedure (Section 5.1).
- **MC model:** uncertainty related to the choice of MC models (Section 5.2), obtained by using the HERWIG sample with angle-ordered parton showers rather than the nominal PYTHIA MC sample when performing the unfolding procedure.

- **JES+JER:** all uncertainties originating from the jet energy scale and jet energy resolution (Section 5.3) – the jet energy resolution uncertainty dominates this category in nearly all cases.
- **Exp. conditions:** uncertainties related to the experimental conditions, such as those originating from pile-up reweighting and disabled tile modules (Section 5.4).

The unfolded data are compared with predictions from several state-of-the-art Monte Carlo models (Section 3.3). Good agreement is often observed between the leading-order and next-to-leading-order Monte Carlo generators throughout the non-isotropic region of a given distribution (i.e. for dijet-like events); poorer agreement is seen as particle configurations become more isotropic.

Figure 7 shows the most inclusive measurement of $\mathcal{I}_{\text{Ring}}^{N=2}$, in events with $N_{\text{jet}} \geq 2$ and $H_{\text{T}2} \geq 500$ GeV. Events with minimal values of this observable are balanced dijet events (e.g. Figure 8(a)), while events with maximal values are symmetric trijet systems (e.g. Figure 8(b)). The NLO POWHEG+PYTHIA and POWHEG+HERWIG predictions overestimate the cross-section at intermediate values of $\mathcal{I}_{\text{Ring}}^{N=2}$, and underestimate the cross-section at low values. The NLO HERWIG predictions with angle-ordered parton showers are closest to the data for small values; their agreement is slightly poorer for isotropic events. The HERWIG sample with the dipole PS model appears to slightly overestimate the cross-section of extremely well-balanced events, but agrees with the angle-ordered model throughout the rest of the distribution. Overall, the data are best described in the isotropic region by the MC predictions with NLO matrix element calculations. Leading-order PYTHIA and SHERPA predictions describe the back-to-back and intermediate range of the distribution well, but underestimate the cross-section for the most isotropic events (for values above ~ 0.6). No significant differences are observed between the cluster and Lund string hadronisation models for the SHERPA samples. The dominant systematic uncertainties of the measured distribution are related either to the jet energy resolution or to the choice of MC model used in the unfolding for isotropic events. The total uncertainty of the measured distribution is below 5% except in the most isotropic bin, where the uncertainty due to the choice of MC model becomes large.

The $1 - \mathcal{I}_{\text{Ring}}^{N=128}$ distribution is shown in Figure 9, also for events with $N_{\text{jet}} \geq 2$ and $H_{\text{T}2} \geq 500$ GeV. Balanced dijet events (e.g. Figure 8(a)) produce the smallest values of this observable, while multijet events with isotropic energy arrangements (e.g. Figure 8(c)) produce the largest values. The increased dynamic range of this observable is evident, as the measured cross-section spans approximately six orders of magnitude. The quality of the modelling description for this observable differs from that of $\mathcal{I}_{\text{Ring}}^{N=2}$ due to the different isotropic patterns it selects. In particular, the POWHEG+PYTHIA and POWHEG+HERWIG predictions are found to strongly disagree with those of the other MC generators, overestimating the measured cross-section for isotropic events while all other predictions underestimate it. Large differences are also found between the HERWIG angle-ordered and dipole shower models: the dipole model predicts relatively more dijet-like events than the angle-ordered model, and correspondingly fewer isotropic events. No notable differences are seen between the SHERPA hadronisation models, which together are found to come the closest to describing the measured data for larger values of $1 - \mathcal{I}_{\text{Ring}}^{N=128}$. The JES/JER systematic uncertainties are the most relevant source of uncertainty for most of the unfolded distribution, occasionally matched by the uncertainty related to the choice of nominal MC model for the unfolding procedure. For the most isotropic events, statistical uncertainties become non-negligible, and the systematic uncertainty related to the effect of the hadron calorimeter’s disabled tile modules during Run 2 data-taking also becomes large. The total uncertainty of this distribution is under 5% until $1 - \mathcal{I}_{\text{Ring}}^{N=128} \sim 0.6$, where it grows to be larger than 10%–15% for the most isotropic events.

The most inclusive measurement of the two-dimensional isotropy observable $1 - \mathcal{I}_{\text{Cyl}}^{N=16}$, for events with $N_{\text{jet}} \geq 2$ and $H_{\text{T}2} \geq 500$ GeV, is shown in Figure 10. This distribution exhibits different characteristics

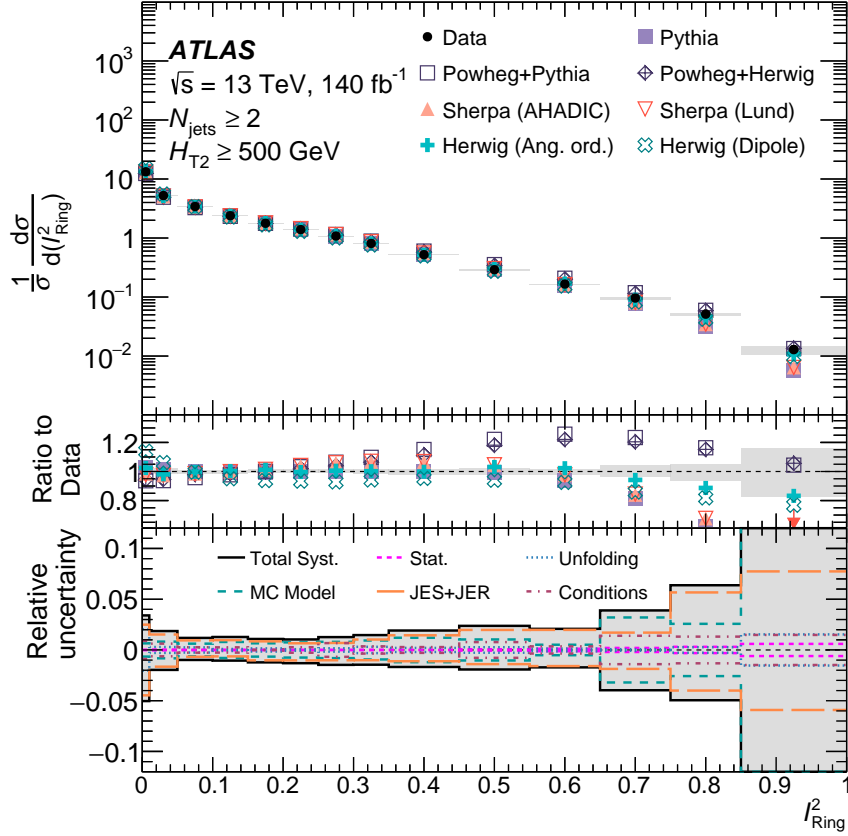


Figure 7: The shape-normalized $\mathcal{I}_{\text{Ring}}^{N=2}$ cross-section in data (closed circles), compared with predictions from several Monte Carlo generators. Events with $H_{T2} \geq 500$ GeV and $N_{\text{jet}} \geq 2$ are included. The middle panel displays the ratios of different event generator predictions to the unfolded data. Event generator predictions are displayed as different marker styles. The grey band in the upper and middle panels indicates the total uncertainty of the measurement. If the ratio of a prediction to the unfolded data is outside the range of values displayed in the middle panel, an arrow is drawn at the edge of the panel as an indicator. The lower panel summarises the various sources of systematic uncertainty in the measurement. Systematic uncertainties are summarized in groups, with different line styles. The total uncertainty is shown as a solid black line. Some uncertainty bands take values outside the range displayed in the figure: the range is selected for maximum clarity in the bulk of the distribution.

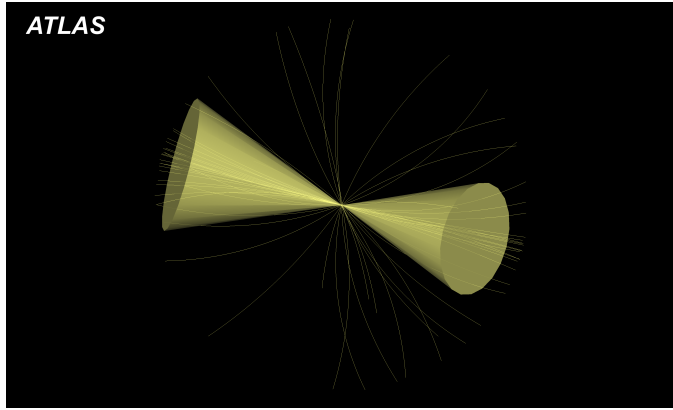
than the ring-like geometries. Events with dijet systems in the forward region on one side of ATLAS (e.g. Figure 11(a)) produce the smallest values of this observable; the highest values are produced by multijet events that evenly cover the rapidity–azimuth plane with activity in both the central and forward regions (e.g. Figure 11(b)). None of the MC predictions accurately describe this observable, although the best descriptions occur near the peak of the distribution around $1 - \mathcal{I}_{\text{Cyl}}^{N=16} \sim 0.8$. The HERWIG angle-ordered and dipole parton shower models predict distributions that have a peak at respectively larger and smaller values than that observed in the measured data. This results in large differences between their respective ratios to the unfolded data. As a result, they surround the data points across the entire distribution except for the highest-value bin. The predictions from the PYTHIA, POWHEG+PYTHIA and POWHEG+HERWIG samples are consistent except at low values, where the PYTHIA sample overestimates the observed cross-section. Once again, no sensitivity to the hadronisation models implemented in SHERPA is observed. The precision of the measurement in this N_{jet} and H_{T2} bin is everywhere better than 10%, and is dominated throughout

by the jet energy resolution component of the JES/JER error band.

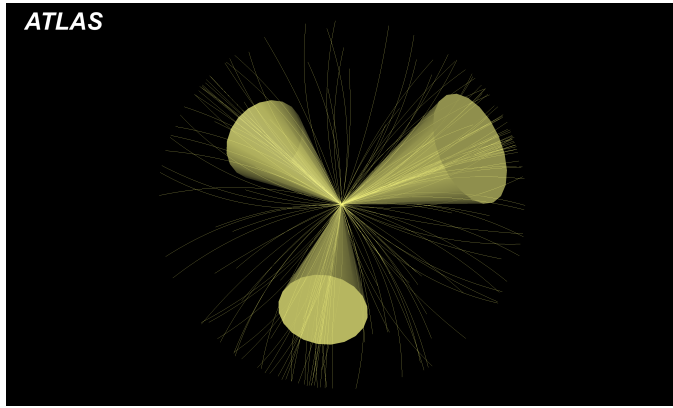
Figures 12–14 present measurements of event isotropy observables with $H_{T2} \geq 500$ GeV and an increasing minimum N_{jet} requirement. Intuitively, the average value of each observable becomes larger as the minimum jet multiplicity is increased, indicating a more isotropic topology. Binning in N_{jet} can elicit larger differences between the MC predictions, particularly between the angle-ordered and dipole HERWIG parton shower models and the PYTHIA, POWHEG+PYTHIA and POWHEG+HERWIG predictions for back-to-back events. Even at larger minimum jet multiplicities, the NLO MC predictions are found to maintain the quality of their description of the rate of balanced trijet events at large values of $\mathcal{I}_{\text{Ring}}^{N=2}$. The HERWIG sample with the dipole PS model is observed to increasingly underestimate the cross-section of back-to-back events in the $\mathcal{I}_{\text{Ring}}^{N=2}$ distribution as the jet multiplicity increases, while the angle-ordered PS model instead overestimates this region. The differences between these models for the $1 - \mathcal{I}_{\text{Cyl}}^{N=16}$ distributions are also enhanced by increasing the minimum jet multiplicity.

The largest uncertainties in these measured distributions are again typically due to the JES/JER systematic uncertainties, although changing the MC model used in the unfolding procedure can result in larger uncertainties for larger jet-multiplicity values (and so, for larger values of $1 - \mathcal{I}_{\text{Ring}}^{N=128}$). In the tails of distributions, the statistical uncertainties and those related to disabled tile modules can become sizeable, but never dominant for the $H_{T2} \geq 500$ GeV bin. Overall, each observable is measured less precisely as the minimum N_{jet} requirement is increased. The $\mathcal{I}_{\text{Ring}}^{N=2}$ distributions tend to be measured with a precision better than 10%, except in the lowest and highest bins. For $1 - \mathcal{I}_{\text{Ring}}^{N=128}$, the uncertainty for low values is less than 5% for $N_{\text{jet}} \geq 2, 3$ but increases in this region for larger jet multiplicities. In the $N_{\text{jet}} \geq 5$ selection, the uncertainty in this region approaches 50%.

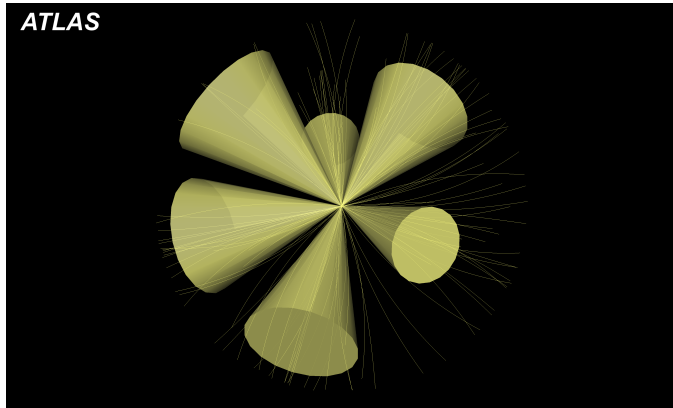
Finally, cross-sections measured differentially with respect to the event isotropy observables are presented in inclusive bins of both N_{jet} and H_{T2} for the ring-like isotropies in Figure 15 and for the cylindrical isotropy in Figure 16. In these figures, events with $N_{\text{jet}} \geq 5$ are shown in three inclusive H_{T2} bins. The trends observed are also generally observable for other jet multiplicities. There are no significant trends in MC modelling that evolve as a function of H_{T2} . Events are noted to very gradually become more collimated and dijet-like as the energy scale of the events increases. The MC predictions' description of the measured data often improves as H_{T2} increases, but trends in modelling are similar to those observed in the other measured distributions. For these triple-differential measurements, the uncertainty that dominates depends on the bin. At low energy scales, it is typically related to the choice of nominal MC model used in the unfolding procedure. In the higher H_{T2} bins, the impact of the JES/JER uncertainty on the steeply falling H_{T2} spectrum compounds as the energy scale is increased beyond the region where the measurement is normalized, resulting in degraded precision at high energies.



(a)



(b)



(c)

Figure 8: Displays of three events in the Run 2 dataset that are examples of extreme values of the ring-like event-isotropy observables studied in this analysis. The event displays show an image of the event in the transverse plane, with the beamline running perpendicularly into the images at their centres. Anti- k_t $R = 0.4$ particle-flow jets passing a p_T requirement of 60 GeV are illustrated as cones in these displays, with a length corresponding to their logarithmically rescaled p_T . Charged-particle tracks in the inner detector are also shown, as curved lines. The events are (a) event 1921189174 from run 349268, which has small values of both $\mathcal{I}_{\text{Ring}}^{N=2}$ and $1 - \mathcal{I}_{\text{Ring}}^{N=128}$, (b) event 1126942872 from run 305811, which has a large value of $\mathcal{I}_{\text{Ring}}^{N=2}$ and a moderate value of $1 - \mathcal{I}_{\text{Ring}}^{N=128}$, and (c) event 2132056011 from run 349268, which has a large value of $1 - \mathcal{I}_{\text{Ring}}^{N=128}$ and a moderate value of $\mathcal{I}_{\text{Ring}}^{N=2}$.

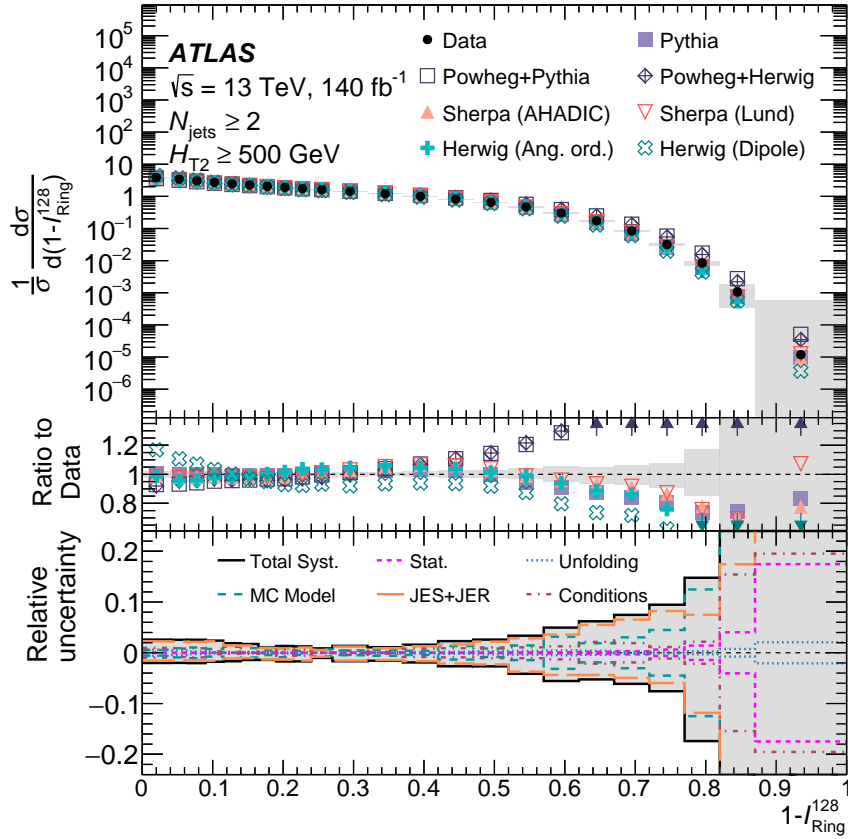


Figure 9: The shape-normalized $J_{\text{Ring}}^{N=128}$ cross-section in data (closed circles), compared with predictions from several Monte Carlo generators. Events with $H_{T2} \geq 500 \text{ GeV}$ and $N_{\text{jet}} \geq 2$ are included. The middle panel displays the ratios of different event generator predictions to the unfolded data. Event generator predictions are displayed as different marker styles. The grey band in the upper and middle panels indicates the total uncertainty of the measurement. If the ratio of a prediction to the unfolded data is outside the range of values displayed in the middle panel, an arrow is drawn at the edge of the panel as an indicator. The lower panel summarises the various sources of systematic uncertainty in the measurement. Systematic uncertainties are summarized in groups, with different line styles. The total uncertainty is shown as a solid black line. Some uncertainty bands take values outside the range displayed in the figure: the range is selected for maximum clarity in the bulk of the distribution.

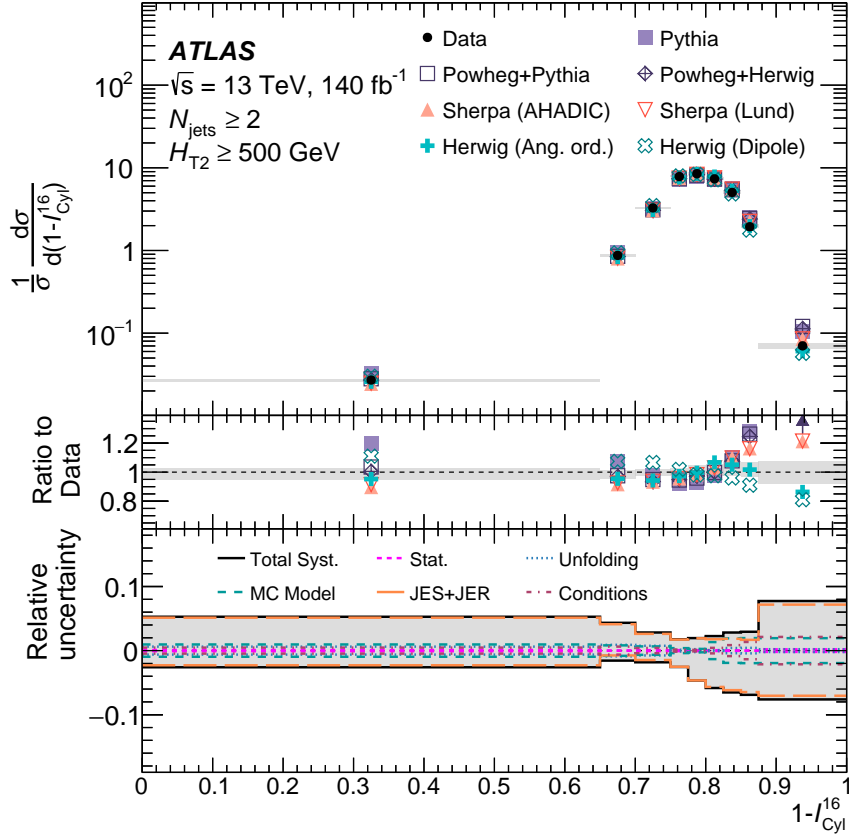
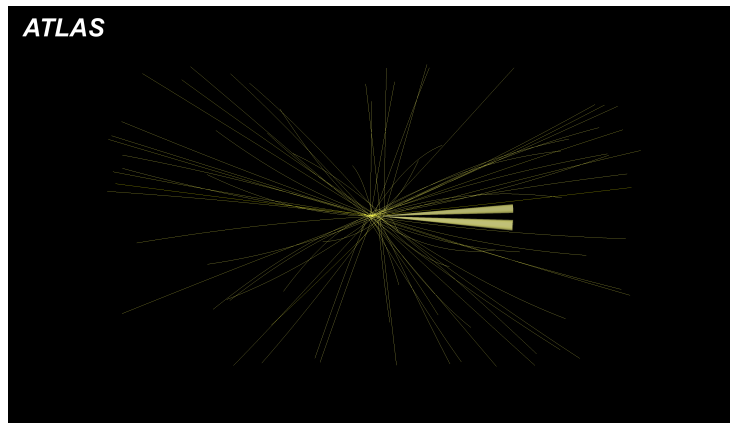
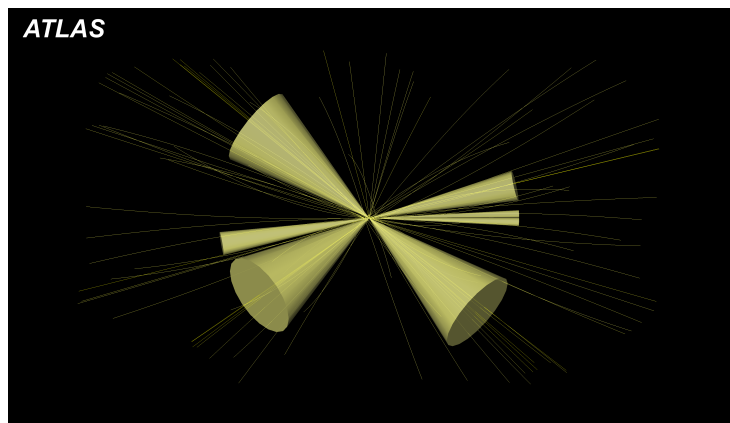


Figure 10: The shape-normalized $\mathcal{I}_{\text{Cyl}}^{N=16}$ cross-section in data (closed circles), compared with predictions from several Monte Carlo generators. Events with $H_{T2} \geq 500$ GeV and $N_{\text{jet}} \geq 2$ are included. The middle panel displays the ratios of different event generator predictions to the unfolded data. Event generator predictions are displayed as different marker styles. The grey band in the upper and middle panels indicates the total uncertainty of the measurement. If the ratio of a prediction to the unfolded data is outside the range of values displayed in the middle panel, an arrow is drawn at the edge of the panel as an indicator. The lower panel summarises the various sources of systematic uncertainty in the measurement. Systematic uncertainties are summarized in groups, with different line styles. The total uncertainty is shown as a solid black line.



(a)



(b)

Figure 11: Displays of two events in the Run 2 dataset that are examples of extreme values of the cylindrical event-isotropy observables studied in this analysis. The event displays show an image of the event from the side of the barrel, with the beamline running horizontally across the middle of each image. Anti- k_t $R = 0.4$ particle-flow jets passing a p_T requirement of 60 GeV are illustrated as cones in these displays, with a length corresponding to their logarithmically rescaled p_T . Charged-particle tracks in the inner detector are also shown, as curved lines. The events are (a) event 1095666999 from run 307454, which has a small value of $1 - \mathcal{I}_{\text{Cyl}}^{N=16}$, and (b) event 2433141809 from run 340030, which has a large value of $1 - \mathcal{I}_{\text{Cyl}}^{N=16}$.

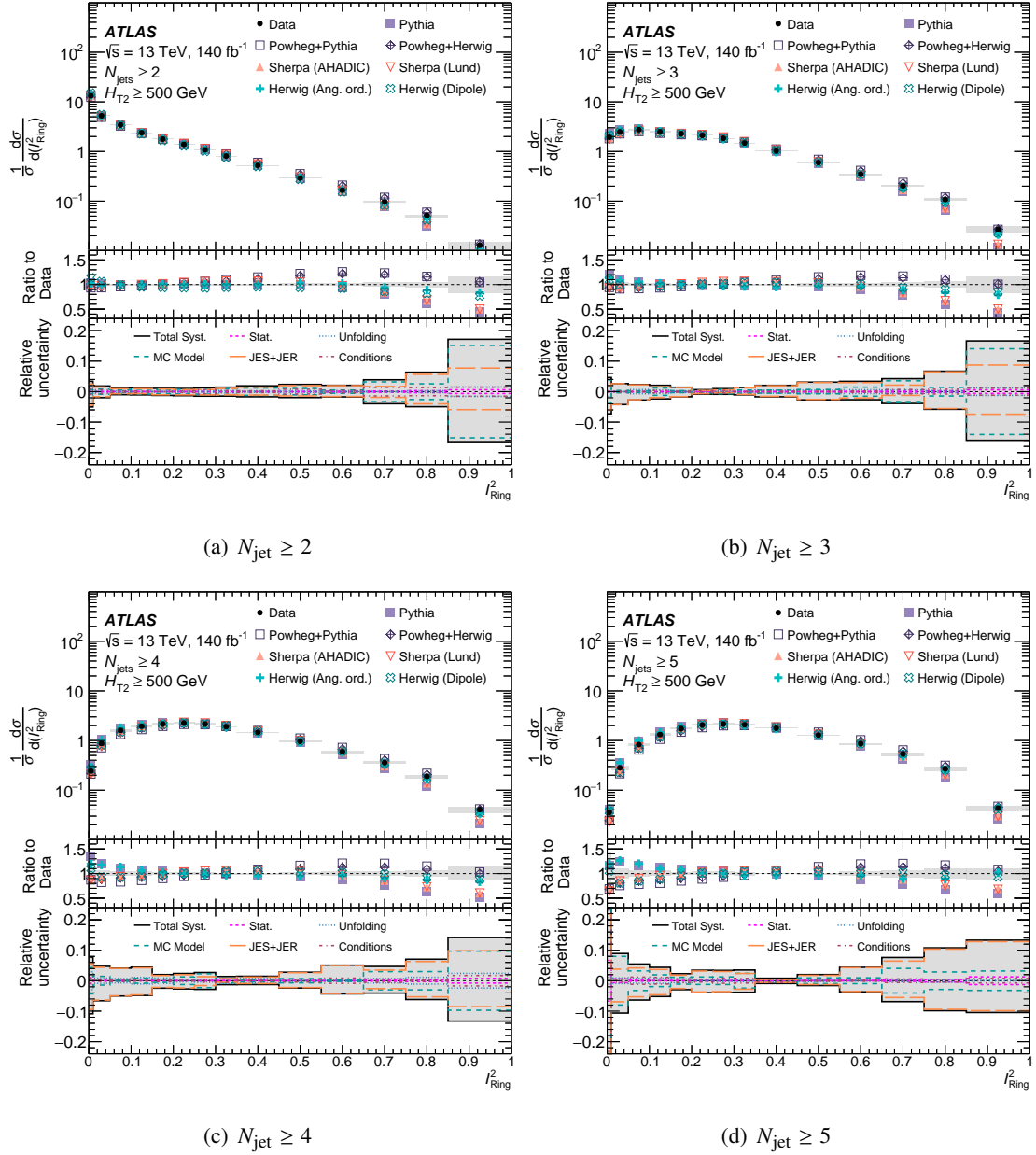


Figure 12: The shape-normalized $I_{\text{Ring}}^{N=2}$ cross-section in data (closed circles), compared with predictions from several Monte Carlo generators. The distribution is presented for events with $H_{T2} \geq 500$ GeV, in several inclusive bins of N_{jet} . The middle panels display the ratios of different event generator predictions to the unfolded data. Event generator predictions are displayed as different marker styles. The grey band in the upper and middle panels indicates the total uncertainty of the measurement. The lower panels summarise the various sources of systematic uncertainty in the measurement. Systematic uncertainties are summarized in groups, with different line styles. The total uncertainty is shown as a solid black line.

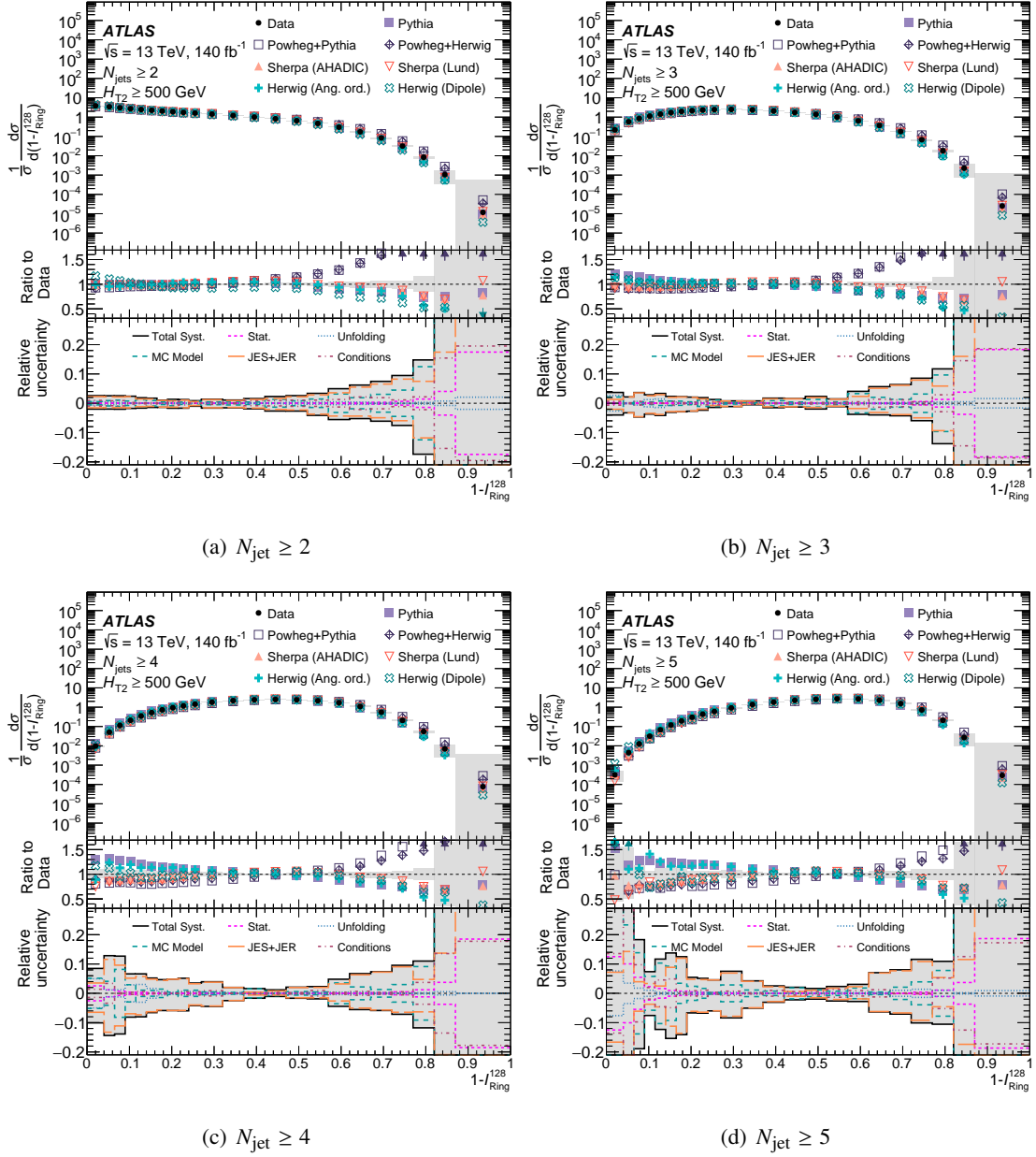


Figure 13: The shape-normalized $\mathcal{I}_{\text{Ring}}^{N=128}$ cross-section in data (closed circles), compared with predictions from several Monte Carlo generators. The distribution is presented for events with $H_{T2} \geq 500$ GeV, in several inclusive bins of N_{jet} . The middle panels display the ratios of different event generator predictions to the unfolded data. The grey band in the upper and middle panels indicates the total uncertainty of the measurement. If the ratio of a prediction to the unfolded data is outside the range of values displayed in the middle panels, an arrow is drawn at the edge of the panel as an indicator. Event generator predictions are displayed as different marker styles. The lower panels summarise the various sources of systematic uncertainty in the measurement. Systematic uncertainties are summarized in groups, with different line styles. The total uncertainty is shown as a solid black line. Some uncertainty bands take values outside the range displayed in the figure: the range is selected for maximum clarity in the bulk of the distribution.

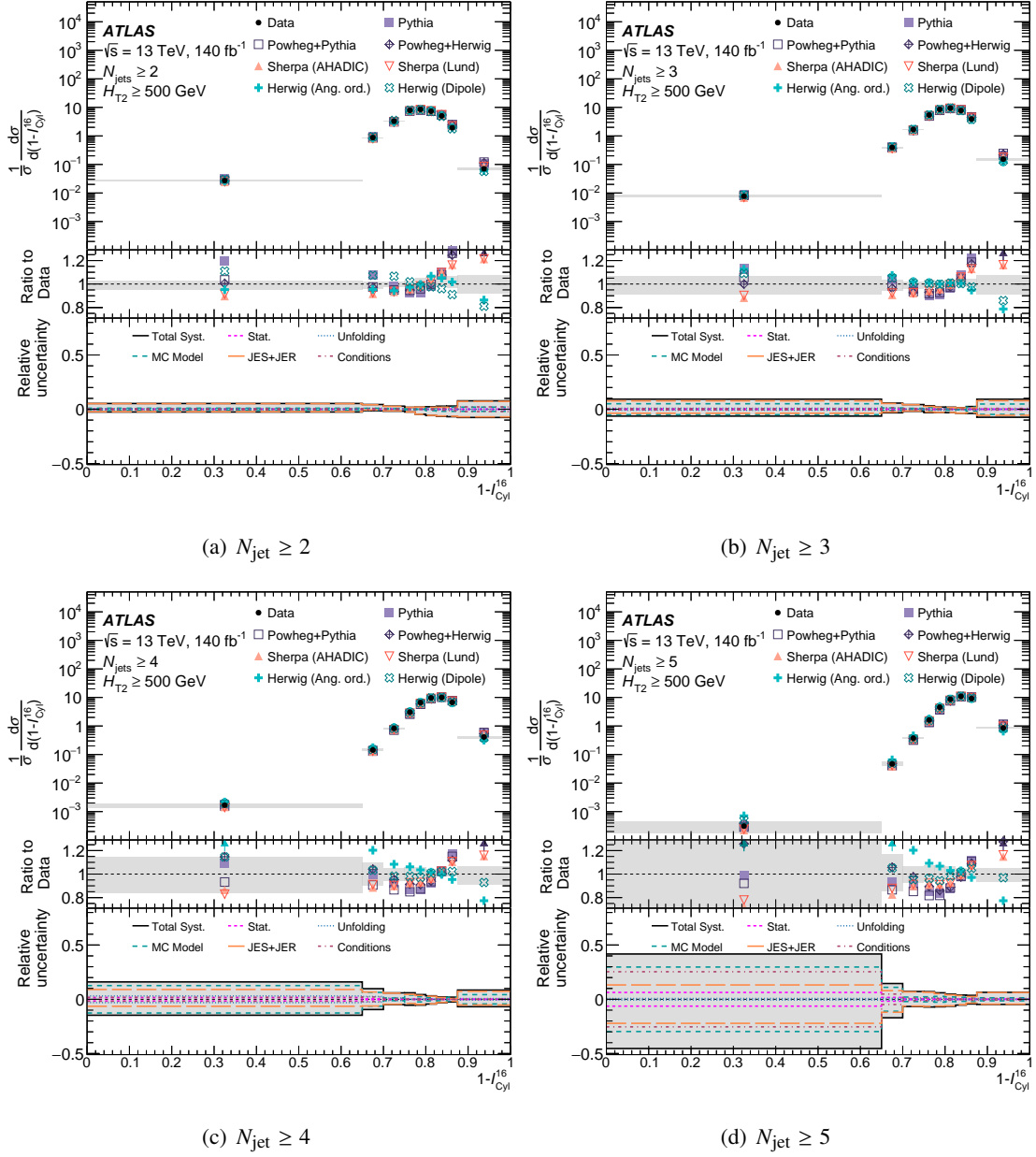
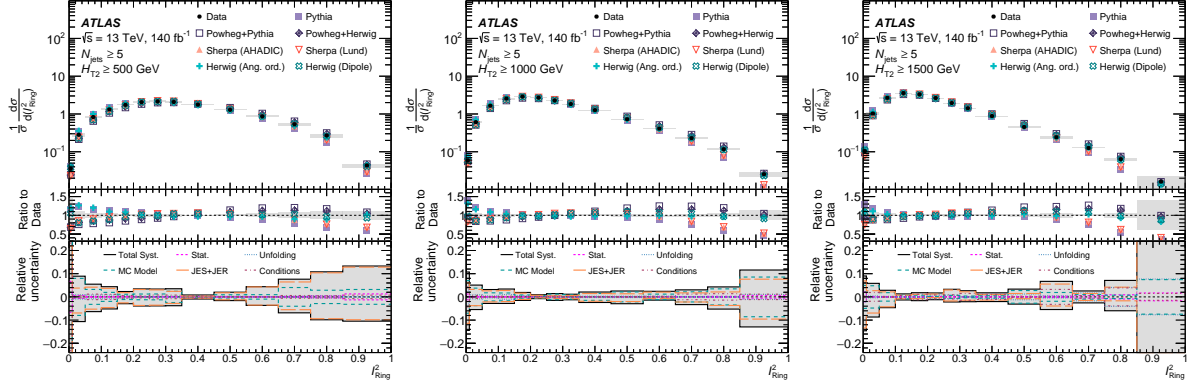
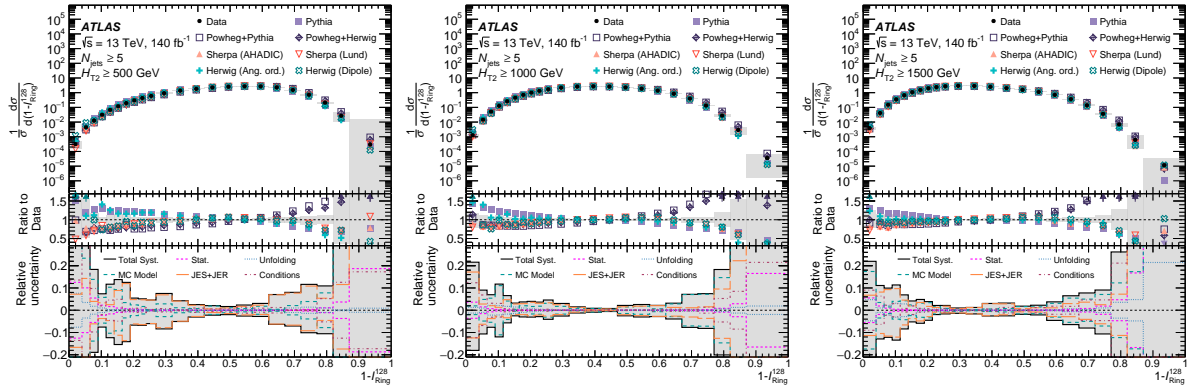


Figure 14: The shape-normalized $I_{\text{Cyl}}^{N=16}$ cross-section in data (closed circles), compared with predictions from several Monte Carlo generators. The distribution is presented for events with $H_{T2} \geq 500$ GeV, in several inclusive bins of N_{jet} . The middle panels display the ratios of different event generator predictions to the unfolded data. Event generator predictions are displayed as different marker styles. The grey band in the upper and middle panels indicates the total uncertainty of the measurement. If the ratio of a prediction to the unfolded data is outside the range of values displayed in the middle panels, an arrow is drawn at the edge of the panel as an indicator. The lower panels summarise the various sources of systematic uncertainty in the measurement. Systematic uncertainties are summarized in groups, with different line styles. The total uncertainty is shown as a solid black line.



(a) $\mathcal{I}_{\text{Ring}}^{N=2}, H_{T2} \geq 500 \text{ GeV}, N_{\text{jet}} \geq 5$ (b) $\mathcal{I}_{\text{Ring}}^{N=2}, H_{T2} \geq 1000 \text{ GeV}, N_{\text{jet}} \geq 5$ (c) $\mathcal{I}_{\text{Ring}}^{N=2}, H_{T2} \geq 1500 \text{ GeV}, N_{\text{jet}} \geq 5$



(d) $\mathcal{I}_{\text{Ring}}^{N=128}, H_{T2} \geq 500 \text{ GeV}, N_{\text{jet}} \geq 5$ (e) $\mathcal{I}_{\text{Ring}}^{N=128}, H_{T2} \geq 1000 \text{ GeV}, N_{\text{jet}} \geq 5$ (f) $\mathcal{I}_{\text{Ring}}^{N=128}, H_{T2} \geq 1500 \text{ GeV}, N_{\text{jet}} \geq 5$

Figure 15: The shape-normalized $\mathcal{I}_{\text{Ring}}^{N=2}$ and $\mathcal{I}_{\text{Ring}}^{N=128}$ cross-sections in data (closed circles), compared with predictions from several Monte Carlo generators. Events with $N_{\text{jet}} \geq 5$ are presented differentially in inclusive bins of H_{T2} . The middle panels display the ratios of different event generator predictions to the unfolded data. Event generator predictions are displayed as different marker styles. The grey band in the upper and middle panels indicates the total uncertainty of the measurement. If the ratio of a prediction to the unfolded data is outside the range of values displayed in the middle panels, an arrow is drawn at the edge of the panel as an indicator. The lower panels summarise the various sources of systematic uncertainty in the measurement. Systematic uncertainties are summarized in groups, with different line styles. The total uncertainty is shown as a solid black line. Some uncertainty bands take values outside the range displayed in the figure: the range is selected for maximum clarity in the bulk of the distribution.

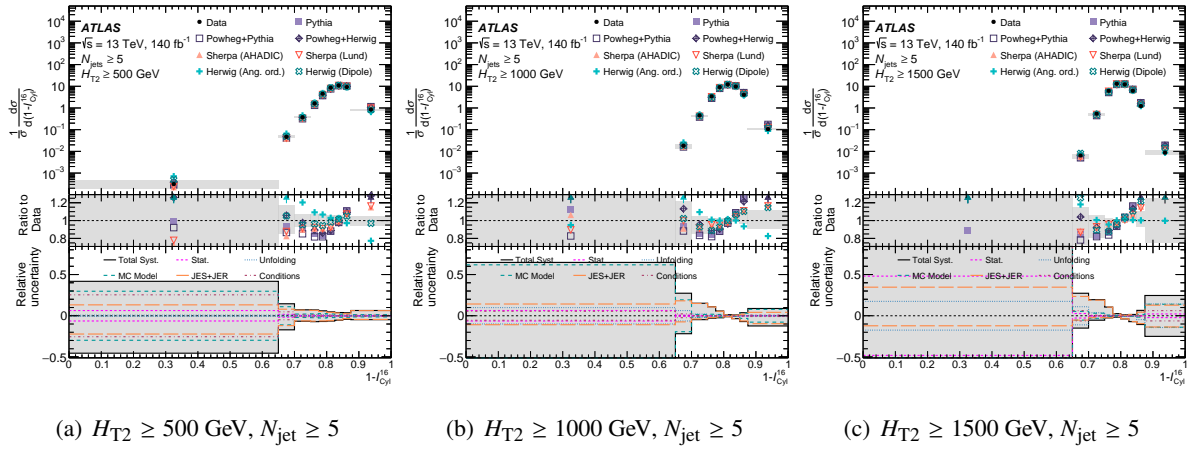


Figure 16: The shape-normalised $I_{\text{Cyl}}^{N=16}$ cross-section in data (closed circles), compared with predictions from several Monte Carlo generators. Events with $N_{\text{jet}} \geq 5$ are presented differentially in inclusive bins of H_{T2} . The middle panels display the ratios of different event generator predictions to the unfolded data. Event generator predictions are displayed as different marker styles. The grey band in the upper and middle panels indicates the total uncertainty of the measurement. If the ratio of a prediction to the unfolded data is outside the range of values displayed in the middle panels, an arrow is drawn at the edge of the panel as an indicator. The lower panels summarise the various sources of systematic uncertainty in the measurement. Systematic uncertainties are summarized in groups, with different line styles. The total uncertainty is shown as a solid black line. Some uncertainty bands take values outside the range displayed in the figure: the range is selected for maximum clarity in the bulk of the distribution.

7 Concluding remarks

A measurement of novel event-shape observables that describe collider events in terms of their *event isotropy* has been performed in 139 fb^{-1} of proton–proton collisions with centre-of-mass energy $\sqrt{s} = 13 \text{ TeV}$, recorded with the ATLAS detector at CERN’s Large Hadron Collider. These event shapes are defined in terms of isotropic reference geometries with cylindrical and circular symmetries, using the Energy-Mover’s Distance to quantify Wasserstein distances between multijet events and the isotropic configurations in terms of optimal transport problems. Event isotropies are shown to have increased sensitivity to isotropic multijet events when compared with other event shapes such as the transverse thrust. They are capable of exposing a remote piece of QCD phase space that is difficult to model and relevant to many searches for physics beyond the Standard Model.

Cross-sections are measured differentially with respect to three event-isotropy observables in inclusive bins of jet multiplicity and H_{T2} . These measurements are corrected for acceptance and detector resolution effects, and normalised relative to the number of events passing the analysis selection in each such bin. This procedure allows the measurement to directly probe the shape of the event isotropies.

The measured data are compared with the predictions of several state-of-the-art Monte Carlo event generators. Agreement between the unfolded data and the simulated events tends to be best in balanced, dijet-like arrangements and deteriorates in more isotropic configurations. For the measurement of $\mathcal{I}_{\text{Ring}}^{N=2}$, an observable that interpolates between balanced dijet and trijet events similarly to the transverse thrust, the predictions of NLO MC generators generally outperform those of LO simulation. In the measurement of $1 - \mathcal{I}_{\text{Ring}}^{N=128}$, which interpolates between balanced dijet events and isotropic multijet configurations in the transverse plane, no single event generator accurately describes the distribution. In particular, the descriptions from the NLO POWHEG+PYTHIA and HERWIG simulations differ in the region sensitive to isotropic configurations. The two-dimensional isotropy $1 - \mathcal{I}_{\text{Cyl}}^{N=16}$ interpolates between forward dijet events and multijet events with activity more evenly covering the rapidity–azimuth plane. This observable is not well-predicted by any MC generator, and elicits large differences between the parton shower models available in HERWIG.

A Rivet routine is available for this measurement [130], and the measured data points have been made publicly available along with other auxiliary information [131] for use in future Monte Carlo tuning campaigns and other studies of QCD.

Acknowledgements

We thank CERN for the very successful operation of the LHC, as well as the support staff from our institutions without whom ATLAS could not be operated efficiently.

We acknowledge the support of ANPCyT, Argentina; YerPhI, Armenia; ARC, Australia; BMFWF and FWF, Austria; ANAS, Azerbaijan; CNPq and FAPESP, Brazil; NSERC, NRC and CFI, Canada; CERN; ANID, Chile; CAS, MOST and NSFC, China; Minciencias, Colombia; MEYS CR, Czech Republic; DNRF and DNSRC, Denmark; IN2P3-CNRS and CEA-DRF/IRFU, France; SRNSFG, Georgia; BMBF, HGF and MPG, Germany; GSRI, Greece; RGC and Hong Kong SAR, China; ISF and Benoziyo Center, Israel; INFN, Italy; MEXT and JSPS, Japan; CNRST, Morocco; NWO, Netherlands; RCN, Norway; MEiN, Poland; FCT, Portugal; MNE/IFA, Romania; MESTD, Serbia; MSSR, Slovakia; ARRS and MIZŠ, Slovenia; DSI/NRF, South Africa; MICINN, Spain; SRC and Wallenberg Foundation, Sweden; SERI, SNSF and Cantons of

Bern and Geneva, Switzerland; MOST, Taiwan; TENMAK, Türkiye; STFC, United Kingdom; DOE and NSF, United States of America. In addition, individual groups and members have received support from BCKDF, CANARIE, Compute Canada and CRC, Canada; PRIMUS 21/SCI/017 and UNCE SCI/013, Czech Republic; COST, ERC, ERDF, Horizon 2020 and Marie Skłodowska-Curie Actions, European Union; Investissements d’Avenir Labex, Investissements d’Avenir Idex and ANR, France; DFG and AvH Foundation, Germany; Herakleitos, Thales and Aristeia programmes co-financed by EU-ESF and the Greek NSRF, Greece; BSF-NSF and MINERVA, Israel; Norwegian Financial Mechanism 2014-2021, Norway; NCN and NAWA, Poland; La Caixa Banking Foundation, CERCA Programme Generalitat de Catalunya and PROMETEO and GenT Programmes Generalitat Valenciana, Spain; Göran Gustafssons Stiftelse, Sweden; The Royal Society and Leverhulme Trust, United Kingdom.

The crucial computing support from all WLCG partners is acknowledged gratefully, in particular from CERN, the ATLAS Tier-1 facilities at TRIUMF (Canada), NDGF (Denmark, Norway, Sweden), CC-IN2P3 (France), KIT/GridKA (Germany), INFN-CNAF (Italy), NL-T1 (Netherlands), PIC (Spain), ASGC (Taiwan), RAL (UK) and BNL (USA), the Tier-2 facilities worldwide and large non-WLCG resource providers. Major contributors of computing resources are listed in Ref. [132].

References

- [1] A. Banfi, G. P. Salam and G. Zanderighi, *Phenomenology of event shapes at hadron colliders*, [JHEP **06** \(2010\) 038](#), arXiv: [1001.4082 \[hep-ph\]](#).
- [2] E. Farhi, *Quantum Chromodynamics Test for Jets*, [Phys. Rev. Lett. **39** \(25 1977\) 1587](#).
- [3] TASSO Collaboration, *Evidence for Planar Events in e^+e^- Annihilation at High-Energies*, [Phys. Lett. B **86** \(1979\) 243](#).
- [4] JADE Collaboration, *Observation of planar three-jet events in e^+e^- annihilation and evidence for gluon bremsstrahlung*, [Phys. Lett. B **91** \(1980\) 142](#), ISSN: 0370-2693.
- [5] TASSO Collaboration, *Jet Production and Fragmentation in e^+e^- Annihilation at 12-GeV to 43-GeV*, [Z. Phys. C **22** \(1984\) 307](#).
- [6] MARK-J Collaboration, *Tests of quantum chromodynamics and a direct measurement of the strong coupling constant α_s at $\sqrt{s} = 30$ GeV*, [Phys. Lett. B **89** \(1979\) 139](#), ISSN: 0370-2693.
- [7] MARK-II Collaboration, *First Measurements of Hadronic Decays of the Z Boson*, [Phys. Rev. Lett. **63** \(1989\) 1558](#).
- [8] L3 Collaboration, *A Test of QCD based on four jet events from Z^0 decays*, [Phys. Lett. B **248** \(1990\) 227](#).
- [9] L3 Collaboration, *Determination of α_s from hadronic event shapes measured on the Z^0 resonance*, [Phys. Lett. B **284** \(1992\) 471](#).
- [10] TASSO Collaboration, *Global Jet Properties at 14-GeV to 44-GeV Center-of-mass Energy in e^+e^- Annihilation*, [Z. Phys. C **47** \(1990\) 187](#).

- [11] SLD Collaboration, *Measurement of $\alpha_s(M(Z)^2)$ from hadronic event observables at the Z^0 resonance*, [Phys. Rev. D **51** \(1995\) 962](#), arXiv: [hep-ex/9501003](#).
- [12] ALEPH Collaboration, *Measurement of α_s from scaling violations in fragmentation functions in e^+e^- annihilation*, [Phys. Lett. B **357** \(1995\) 487](#), [Erratum: [Phys. Lett. B **364** \(1995\) 247](#)].
- [13] S. Kluth, P.A. Movilla Fernandez, S. Bethke, C. Pahl and P. Pfeifenschneider, *A Measurement of the QCD color factors using event shape distributions at $\sqrt{s} = 14$ GeV to 189 GeV*, [Eur. Phys. J. C **21** \(2001\) 199](#), arXiv: [hep-ex/0012044](#) [[hep-ex](#)].
- [14] OPAL Collaboration, *A Simultaneous measurement of the QCD color factors and the strong coupling*, [Eur. Phys. J. C **20** \(2001\) 601](#), arXiv: [hep-ex/0101044](#).
- [15] ALEPH Collaboration, *Studies of QCD at e^+e^- centre-of-mass energies between 91-GeV and 209-GeV*, [Eur. Phys. J. C **35** \(2004\) 457](#).
- [16] DELPHI Collaboration, *A Study of the energy evolution of event shape distributions and their means with the DELPHI detector at LEP*, [Eur. Phys. J. C **29** \(2003\) 285](#), arXiv: [hep-ex/0307048](#).
- [17] M. Dasgupta and G. P. Salam, *Event shapes in e^+e^- annihilation and deep inelastic scattering*, [J. Phys. G **30** \(2004\) R143](#), arXiv: [hep-ph/0312283](#).
- [18] L3 Collaboration, *Studies of hadronic event structure in e^+e^- annihilation from 30-GeV to 209-GeV with the L3 detector*, [Phys. Rept. **399** \(2004\) 71](#), arXiv: [hep-ex/0406049](#).
- [19] OPAL Collaboration, *Measurement of event shape distributions and moments in e^+e^- to hadrons at 91-GeV - 209-GeV and a determination of α_s* , [Eur. Phys. J. C **40** \(2005\) 287](#), arXiv: [hep-ex/0503051](#).
- [20] H1 Collaboration, *Measurement of event shape variables in deep-inelastic scattering at HERA*, [Eur. Phys. J. C **46** \(2006\) 343](#), arXiv: [hep-ex/0512014](#).
- [21] ZEUS Collaboration, *Event shapes in deep inelastic scattering at HERA*, [Nucl. Phys. B **767** \(2007\) 1](#), arXiv: [hep-ex/0604032](#).
- [22] S. Kluth, ‘ $\alpha_s(M(Z^0))$ from Jade Event Shapes’, *44th Rencontres de Moriond on QCD and High Energy Interactions*, 2009 295, arXiv: [0905.4891](#) [[hep-ex](#)].
- [23] OPAL Collaboration, *Determination of α_s using OPAL hadronic event shapes at $\sqrt{s} = 91 - 209$ GeV and resummed NNLO calculations*, [Eur. Phys. J. C **71** \(2011\) 1733](#), arXiv: [1101.1470](#) [[hep-ex](#)].
- [24] OPAL Collaboration, *Measurement of α_s with radiative hadronic events*, [Eur. Phys. J. C **53** \(2008\) 21](#), arXiv: [0902.1128](#) [[hep-ex](#)].
- [25] M. Tanabashi et al., *Review of Particle Physics*, [Phys. Rev. D **98** \(2018\) 030001](#).
- [26] P. Nason and G. Zanderighi, *Fits of α_s using power corrections in the three-jet region*, (2023), arXiv: [2301.03607](#) [[hep-ph](#)].
- [27] P. Skands, S. Carrazza and J. Rojo, *Tuning PYTHIA 8.1: the Monash 2013 Tune*, [Eur. Phys. J. C **74** \(2014\) 3024](#), arXiv: [1404.5630](#) [[hep-ph](#)].

- [28] ATLAS Collaboration, *ATLAS Pythia 8 tunes to 7 TeV data*, ATL-PHYS-PUB-2014-021, 2014, URL: <https://cds.cern.ch/record/1966419>.
- [29] CMS Collaboration, *Extraction and validation of a new set of CMS PYTHIA8 tunes from underlying-event measurements*, *Eur. Phys. J. C* **80** (2020) 4, arXiv: [1903.12179](https://arxiv.org/abs/1903.12179) [[hep-ex](#)].
- [30] L. A. Anchordoqui et al., *Searching for the layered structure of space at the LHC*, *Phys. Rev. D* **83** (2011) 114046, arXiv: [1012.1870](https://arxiv.org/abs/1012.1870) [[hep-ph](#)].
- [31] F. Krauss, S. Kuttimalai and T. Plehn, *LHC multijet events as a probe for anomalous dimension-six gluon interactions*, *Phys. Rev. D* **95** (2017) 035024, arXiv: [1611.00767](https://arxiv.org/abs/1611.00767) [[hep-ph](#)].
- [32] R. Goldouzian and M. D. Hildreth, *LHC dijet angular distributions as a probe for the dimension-six triple gluon vertex*, *Phys. Lett. B* **811** (2020) 135889, arXiv: [2001.02736](https://arxiv.org/abs/2001.02736) [[hep-ph](#)].
- [33] A. Buckley, J. M. Butterworth, L. Corpe, D. Huang and P. Sun, *New sensitivity of current LHC measurements to vector-like quarks*, *SciPost Phys.* **9** (2020) 069, arXiv: [2006.07172](https://arxiv.org/abs/2006.07172) [[hep-ph](#)].
- [34] A. Buckley et al., *Testing new physics models with global comparisons to collider measurements: the Contur toolkit*, *SciPost Phys. Core* **4** (2021) 013, arXiv: [2102.04377](https://arxiv.org/abs/2102.04377) [[hep-ph](#)].
- [35] C. Cesarotti and J. Thaler, *A Robust Measure of Event Isotropy at Colliders*, *JHEP* **08** (2020) 084, arXiv: [2004.06125](https://arxiv.org/abs/2004.06125) [[hep-ph](#)].
- [36] L. N. Wasserstein, *Markov processes over denumerable products of spaces describing large systems of automata*, *Problems of Information Transmission* **5** (1969) 47.
- [37] R. L. Dobrushin, *Prescribing a system of random variables by conditional distributions*, *Theory of Probability & Its Applications* **15** (1970) 458.
- [38] S. Brandt, C. Peyrou, R. Sosnowski and A. Wroblewski, *The principal axis of jets — an attempt to analyse high-energy collisions as two-body processes*, *Phys. Lett.* **12** (1964) 57, ISSN: 0031-9163, URL: <http://www.sciencedirect.com/science/article/pii/003191636491176X>.
- [39] A. De Rújula, J. Ellis, E. Floratos and M. Gaillard, *QCD predictions for hadronic final states in e^+e^- annihilation*, *Nucl. Phys. B* **138** (1978) 387, ISSN: 0550-3213, URL: <https://www.sciencedirect.com/science/article/pii/0550321378903887>.
- [40] J. D. Bjorken and S. J. Brodsky, *Statistical Model for Electron-Positron Annihilation into Hadrons*, *Phys. Rev. D* **1** (1970) 1416, URL: <https://link.aps.org/doi/10.1103/PhysRevD.1.1416>.
- [41] J. R. Ellis, M. K. Gaillard and G. G. Ross, *Search for Gluons in e^+e^- Annihilation*, *Nucl. Phys. B* **111** (1976) 253, [Erratum: *Nucl.Phys.B* 130, 516 (1977)].
- [42] H. Georgi and M. Machacek, *Simple Quantum-Chromodynamics Prediction of Jet Structure in e^+e^- Annihilation*, *Phys. Rev. Lett.* **39** (20 1977) 1237, URL: <https://link.aps.org/doi/10.1103/PhysRevLett.39.1237>.

- [43] P. T. Komiske, E. M. Metodiev and J. Thaler, *Metric Space of Collider Events*, [*Phys. Rev. Lett.* **123** \(2019\) 041801](#), arXiv: [1902.02346 \[hep-ph\]](#).
- [44] P. T. Komiske, E. M. Metodiev and J. Thaler, *The Hidden Geometry of Particle Collisions*, [*JHEP* **07** \(2020\) 006](#), arXiv: [2004.04159 \[hep-ph\]](#).
- [45] C. Cesarotti, M. Reece and M. J. Strassler, *The efficacy of event isotropy as an event shape observable*, [*JHEP* **07** \(2021\) 215](#), arXiv: [2011.06599 \[hep-ph\]](#).
- [46] ATLAS Collaboration, *Probing the CP nature of the top-Higgs Yukawa coupling in $t\bar{t}H$ and tH events with $H \rightarrow b\bar{b}$ decays using the ATLAS detector at the LHC*, (2023), arXiv: [2303.05974 \[hep-ex\]](#).
- [47] CMS Collaboration, *Search for CP violation in ttH and tH production in multilepton channels in proton–proton collisions at $\sqrt{s} = 13$ TeV*, (2022), arXiv: [2208.02686 \[hep-ex\]](#).
- [48] ATLAS Collaboration, *Observation of four-top-quark production in the multilepton final state with the ATLAS detector*, (2023), arXiv: [2303.15061 \[hep-ex\]](#).
- [49] CMS Collaboration, *Observation of four top quark production in proton–proton collisions at $\sqrt{s} = 13$ TeV*, (2023), arXiv: [2305.13439 \[hep-ex\]](#).
- [50] V. V. Khoze, F. Krauss and M. Schott, *Large Effects from Small QCD Instantons: Making Soft Bombs at Hadron Colliders*, [*JHEP* **04** \(2020\) 201](#), arXiv: [1911.09726 \[hep-ph\]](#).
- [51] S. Amoroso, D. Kar and M. Schott, *How to discover QCD Instantons at the LHC*, [*Eur. Phys. J. C* **81** \(2021\) 624](#), arXiv: [2012.09120 \[hep-ph\]](#).
- [52] S. Knapen, S. Pagan Griso, M. Papucci and D. J. Robinson, *Triggering Soft Bombs at the LHC*, [*JHEP* **08** \(2017\) 076](#), arXiv: [1612.00850 \[hep-ph\]](#).
- [53] C. Cesarotti, M. Reece and M. J. Strassler, *Spheres To Jets: Tuning Event Shapes with 5d Simplified Models*, [*JHEP* **05** \(2021\) 096](#), arXiv: [2009.08981 \[hep-ph\]](#).
- [54] N. Arkani-Hamed, S. Dimopoulos and G. R. Dvali, *The Hierarchy problem and new dimensions at a millimeter*, [*Phys. Lett. B* **429** \(1998\) 263](#), arXiv: [hep-ph/9803315](#).
- [55] I. Antoniadis, N. Arkani-Hamed, S. Dimopoulos and G. R. Dvali, *New dimensions at a millimeter to a Fermi and superstrings at a TeV*, [*Phys. Lett. B* **436** \(1998\) 257](#), arXiv: [hep-ph/9804398](#).
- [56] N. Arkani-Hamed, S. Dimopoulos and G. R. Dvali, *Phenomenology, astrophysics and cosmology of theories with submillimeter dimensions and TeV scale quantum gravity*, [*Phys. Rev. D* **59** \(1999\) 086004](#), arXiv: [hep-ph/9807344](#).
- [57] L. Randall and R. Sundrum, *A Large mass hierarchy from a small extra dimension*, [*Phys. Rev. Lett.* **83** \(1999\) 3370](#), arXiv: [hep-ph/9905221](#).
- [58] L. Randall and R. Sundrum, *An Alternative to compactification*, [*Phys. Rev. Lett.* **83** \(1999\) 4690](#), arXiv: [hep-th/9906064](#).

- [59] S. B. Giddings and S. D. Thomas, *High-energy colliders as black hole factories: The End of short distance physics*, [Phys. Rev. D **65** \(2002\) 056010](#), arXiv: [hep-ph/0106219](#).
- [60] L. A. Anchordoqui, H. Goldberg and A. D. Shapere, *Phenomenology of Randall-Sundrum black holes*, [Phys. Rev. D **66** \(2002\) 024033](#), arXiv: [hep-ph/0204228](#).
- [61] G. L. Landsberg, *Black Holes at Future Colliders and Beyond*, [J. Phys. G **32** \(2006\) R337](#), arXiv: [hep-ph/0607297](#).
- [62] P. Meade and L. Randall, *Black Holes and Quantum Gravity at the LHC*, [JHEP **05** \(2008\) 003](#), arXiv: [0708.3017 \[hep-ph\]](#).
- [63] S. Dimopoulos and G. L. Landsberg, *Black holes at the LHC*, [Phys. Rev. Lett. **87** \(2001\) 161602](#), arXiv: [hep-ph/0106295](#).
- [64] CMS Collaboration, *First Measurement of Hadronic Event Shapes in pp Collisions at $\sqrt{s} = 7$ TeV*, [Phys. Lett. B **699** \(2011\) 48](#), arXiv: [1102.0068 \[hep-ex\]](#).
- [65] ATLAS Collaboration, *Measurement of charged-particle event shape variables in inclusive $\sqrt{s} = 7$ TeV proton-proton interactions with the ATLAS detector*, [Phys. Rev. D **88** \(2013\) 032004](#), arXiv: [1207.6915 \[hep-ex\]](#).
- [66] ATLAS Collaboration, *Measurement of event shapes at large momentum transfer with the ATLAS detector in pp collisions at $\sqrt{s} = 7$ TeV*, [Eur. Phys. J. C **72** \(2012\) 2211](#), arXiv: [1206.2135 \[hep-ex\]](#).
- [67] CMS Collaboration, *Event shape variables measured using multijet final states in proton-proton collisions at $\sqrt{s} = 13$ TeV*, [JHEP **12** \(2018\) 117](#), arXiv: [1811.00588 \[hep-ex\]](#).
- [68] ATLAS Collaboration, *Measurement of hadronic event shapes in high- p_T multijet final states at $\sqrt{s} = 13$ TeV with the ATLAS detector*, [JHEP **01** \(2021\) 188](#), arXiv: [2007.12600 \[hep-ex\]](#), Erratum: [JHEP **12** \(2021\) 053](#).
- [69] CMS Collaboration, *Event shapes and azimuthal correlations in $Z + jets$ events in pp collisions at $\sqrt{s} = 7$ TeV*, [Phys. Lett. B **722** \(2013\) 238](#), arXiv: [1301.1646 \[hep-ex\]](#).
- [70] ATLAS Collaboration, *Measurement of event-shape observables in $Z \rightarrow \ell^+ \ell^-$ events in pp collisions at $\sqrt{s} = 7$ TeV with the ATLAS detector at the LHC*, [Eur. Phys. J. C **76** \(2016\) 375](#), arXiv: [1602.08980 \[hep-ex\]](#).
- [71] CDF Collaboration, *Measurement of QCD jet broadening in $p\bar{p}$ collisions at $\sqrt{s} = 1.8$ TeV*, [Phys. Rev. D **44** \(1991\) 601](#).
- [72] M. V. Sorin, *Measurement of the dijet transverse thrust distribution in proton - anti-proton collisions*, PhD thesis: Buenos Aires U., 2003.
- [73] ATLAS Collaboration, *ATLAS data quality operations and performance for 2015–2018 data-taking*, [JINST **15** \(2020\) P04003](#), arXiv: [1911.04632 \[physics.ins-det\]](#).
- [74] ATLAS Collaboration, *Jet energy scale and resolution measured in proton-proton collisions at $\sqrt{s} = 13$ TeV with the ATLAS detector*, [Eur. Phys. J. C **81** \(2020\) 689](#), arXiv: [2007.02645 \[hep-ex\]](#).

- [75] ATLAS Collaboration, *Multijet simulation for 13 TeV ATLAS Analyses*, ATL-PHYS-PUB-2019-017, 2019, URL: <https://cds.cern.ch/record/2672252>.
- [76] M. Cacciari, G. P. Salam and G. Soyez, *The anti- k_t jet clustering algorithm*, *JHEP* **04** (2008) 063, arXiv: [0802.1189](https://arxiv.org/abs/0802.1189) [[hep-ph](#)].
- [77] O. Pele and B. Taskar, ‘The Tangent Earth Mover’s Distance’, *Geometric Science of Information*, ed. by F. Nielsen and F. Barbaresco, Berlin, Heidelberg: Springer Berlin Heidelberg, 2013 397, ISBN: 978-3-642-40020-9, URL: https://doi.org/10.1007/978-3-642-40020-9_43.
- [78] S. Peleg, M. Werman and H. Rom, *A unified approach to the change of resolution: space and gray-level*, *IEEE Transactions on Pattern Analysis and Machine Intelligence* **11** (1989) 739.
- [79] Y. Rubner, C. Tomasi and L. J. Guibas, ‘A Metric for Distributions with Applications to Image Databases’, *Proceedings of the Sixth International Conference on Computer Vision, ICCV ’98*, Washington, DC, USA: IEEE Computer Society, 1998 59, ISBN: 81-7319-221-9, URL: <https://doi.org/10.1109/ICCV.1998.710701>.
- [80] Y. Rubner, C. Tomasi and L. J. Guibas, *The Earth Mover’s Distance as a Metric for Image Retrieval*, *International Journal of Computer Vision* **40** (2000) 99, ISSN: 1573-1405, URL: <https://doi.org/10.1023/A:1026543900054>.
- [81] O. Pele and M. Werman, ‘A Linear Time Histogram Metric for Improved SIFT Matching’, *Computer Vision – ECCV 2008*, ed. by D. Forsyth, P. Torr and A. Zisserman, Berlin, Heidelberg: Springer Berlin Heidelberg, 2008 495, ISBN: 978-3-540-88690-7, URL: https://doi.org/10.1007/978-3-540-88690-7_37.
- [82] C. Cesarotti, *CARICESAROTTI/EVENT_ISOTROPY: Zenodo Release*, version v1.0.0, 2020, URL: <https://doi.org/10.5281/zenodo.4939331>.
- [83] R. Flamary et al., *POT: Python Optimal Transport*, *Journal of Machine Learning Research* **22** (2021) 1, URL: <http://jmlr.org/papers/v22/20-451.html>.
- [84] N. Bonneel, M. van de Panne, S. Paris and W. Heidrich, *Displacement Interpolation Using Lagrangian Mass Transport*, *ACM Trans. Graph.* **30** (2011) 1, ISSN: 0730-0301, URL: <https://doi.org/10.1145/2070781.2024192>.
- [85] S. Catani, G. Turnock and B. R. Webber, *Jet broadening measures in e^+e^- annihilation*, *Phys. Lett. B* **295** (1992) 269.
- [86] I. W. Stewart, F. J. Tackmann and W. J. Waalewijn, *N -Jettiness: An Inclusive Event Shape to Veto Jets*, *Phys. Rev. Lett.* **105** (2010) 092002, arXiv: [1004.2489](https://arxiv.org/abs/1004.2489) [[hep-ph](#)].
- [87] J. Thaler and K. Van Tilburg, *Identifying Boosted Objects with N -subjettiness*, *JHEP* **03** (2011) 015, arXiv: [1011.2268](https://arxiv.org/abs/1011.2268) [[hep-ph](#)].
- [88] M. J. Strassler, *Why Unparticle Models with Mass Gaps are Examples of Hidden Valleys*, (2008), arXiv: [0801.0629](https://arxiv.org/abs/0801.0629) [[hep-ph](#)].
- [89] R. Ellis, D. Ross and A. Terrano, *The perturbative calculation of jet structure in e^+e^- annihilation*, *Nucl. Phys B* **178** (1981) 421, ISSN: 0550-3213, URL: <http://www.sciencedirect.com/science/article/pii/0550321381901656>.

- [90] P. Virtanen et al., *SciPy 1.0: Fundamental Algorithms for Scientific Computing in Python*, *Nature Methods* **17** (2020) 261.
- [91] ATLAS Collaboration, *The ATLAS Experiment at the CERN Large Hadron Collider*, *JINST* **3** (2008) S08003.
- [92] ATLAS Collaboration, *ATLAS Insertable B-Layer: Technical Design Report*, ATLAS-TDR-19; CERN-LHCC-2010-013, 2010, URL: <https://cds.cern.ch/record/1291633>, Addendum: ATLAS-TDR-19-ADD-1; CERN-LHCC-2012-009, 2012, URL: <https://cds.cern.ch/record/1451888>.
- [93] B. Abbott et al., *Production and integration of the ATLAS Insertable B-Layer*, *JINST* **13** (2018) T05008, arXiv: [1803.00844](https://arxiv.org/abs/1803.00844) [[physics.ins-det](#)].
- [94] ATLAS Collaboration, *Performance of the ATLAS trigger system in 2015*, *Eur. Phys. J. C* **77** (2017) 317, arXiv: [1611.09661](https://arxiv.org/abs/1611.09661) [[hep-ex](#)].
- [95] ATLAS Collaboration, *The ATLAS Collaboration Software and Firmware*, ATL-SOFT-PUB-2021-001, 2021, URL: <https://cds.cern.ch/record/2767187>.
- [96] ATLAS Collaboration, *Luminosity determination in pp collisions at $\sqrt{s} = 13$ TeV using the ATLAS detector at the LHC*, (2022), arXiv: [2212.09379](https://arxiv.org/abs/2212.09379) [[hep-ex](#)].
- [97] G. Avoni et al., *The new LUCID-2 detector for luminosity measurement and monitoring in ATLAS*, *JINST* **13** (2018) P07017.
- [98] T. Sjöstrand et al., *An introduction to PYTHIA 8.2*, *Comput. Phys. Commun.* **191** (2015) 159, arXiv: [1410.3012](https://arxiv.org/abs/1410.3012) [[hep-ph](#)].
- [99] T. Sjöstrand, S. Mrenna and P. Z. Skands, *PYTHIA 6.4 physics and manual*, *JHEP* **05** (2006) 026, arXiv: [hep-ph/0603175](https://arxiv.org/abs/hep-ph/0603175).
- [100] NNPDF Collaboration, R. D. Ball et al., *Parton distributions with LHC data*, *Nucl. Phys. B* **867** (2013) 244, arXiv: [1207.1303](https://arxiv.org/abs/1207.1303) [[hep-ph](#)].
- [101] D. J. Lange, *The EvtGen particle decay simulation package*, *Nucl. Instrum. Meth. A* **462** (2001) 152.
- [102] T. Gleisberg et al., *Event generation with SHERPA 1.1*, *JHEP* **02** (2009) 007, arXiv: [0811.4622](https://arxiv.org/abs/0811.4622) [[hep-ph](#)].
- [103] B. R. Webber, *A QCD model for jet fragmentation including soft gluon interference*, *Nucl. Phys. B* **238** (1984) 492.
- [104] S. Schumann and F. Krauss, *A parton shower algorithm based on Catani–Seymour dipole factorisation*, *JHEP* **03** (2008) 038, arXiv: [0709.1027](https://arxiv.org/abs/0709.1027) [[hep-ph](#)].
- [105] S. Dulat et al., *New parton distribution functions from a global analysis of quantum chromodynamics*, *Phys. Rev. D* **93** (2016) 033006, arXiv: [1506.07443](https://arxiv.org/abs/1506.07443) [[hep-ph](#)].
- [106] H.-L. Lai et al., *New parton distributions for collider physics*, *Phys. Rev. D* **82** (2010) 074024, arXiv: [1007.2241](https://arxiv.org/abs/1007.2241) [[hep-ph](#)].
- [107] M. Bähr et al., *Herwig++ physics and manual*, *Eur. Phys. J. C* **58** (2008) 639, arXiv: [0803.0883](https://arxiv.org/abs/0803.0883) [[hep-ph](#)].

- [108] J. Bellm et al., *Herwig 7.0/Herwig++ 3.0 release note*, *Eur. Phys. J. C* **76** (2016) 196, arXiv: [1512.01178 \[hep-ph\]](#).
- [109] J. Bellm et al., *Herwig 7.1 Release Note*, (2017), arXiv: [1705.06919 \[hep-ph\]](#).
- [110] L. A. Harland-Lang, A. D. Martin, P. Motylinski and R. S. Thorne, *Parton distributions in the LHC era: MMHT 2014 PDFs*, *Eur. Phys. J. C* **75** (2015) 204, arXiv: [1412.3989 \[hep-ph\]](#).
- [111] L. Lönnblad, *Correcting the Colour-Dipole Cascade Model with Fixed Order Matrix Elements*, *JHEP* **05** (2002) 046, arXiv: [hep-ph/0112284](#).
- [112] L. Lönnblad and S. Prestel, *Matching tree-level matrix elements with interleaved showers*, *JHEP* **03** (2012) 019, arXiv: [1109.4829 \[hep-ph\]](#).
- [113] P. Nason, *A new method for combining NLO QCD with shower Monte Carlo algorithms*, *JHEP* **11** (2004) 040, arXiv: [hep-ph/0409146](#).
- [114] S. Frixione, P. Nason and C. Oleari, *Matching NLO QCD computations with parton shower simulations: the POWHEG method*, *JHEP* **11** (2007) 070, arXiv: [0709.2092 \[hep-ph\]](#).
- [115] S. Alioli, K. Hamilton, P. Nason, C. Oleari and E. Re, *Jet pair production in POWHEG*, *JHEP* **04** (2011) 081, arXiv: [1012.3380 \[hep-ph\]](#).
- [116] S. Alioli, P. Nason, C. Oleari and E. Re, *A general framework for implementing NLO calculations in shower Monte Carlo programs: the POWHEG BOX*, *JHEP* **06** (2010) 043, arXiv: [1002.2581 \[hep-ph\]](#).
- [117] The NNPDF Collaboration, R. D. Ball et al., *Parton distributions for the LHC run II*, *JHEP* **04** (2015) 040, arXiv: [1410.8849 \[hep-ph\]](#).
- [118] ATLAS Collaboration, *The ATLAS Simulation Infrastructure*, *Eur. Phys. J. C* **70** (2010) 823, arXiv: [1005.4568 \[physics.ins-det\]](#).
- [119] S. Agostinelli et al., *GEANT4 – a simulation toolkit*, *Nucl. Instrum. Meth. A* **506** (2003) 250.
- [120] ATLAS Collaboration, *The Pythia 8 A3 tune description of ATLAS minimum bias and inelastic measurements incorporating the Donnachie–Landshoff diffractive model*, ATL-PHYS-PUB-2016-017, 2016, URL: <https://cds.cern.ch/record/2206965>.
- [121] M. Cacciari, G. P. Salam and G. Soyez, *FastJet user manual*, *Eur. Phys. J. C* **72** (2012) 1896, arXiv: [1111.6097 \[hep-ph\]](#).
- [122] ATLAS Collaboration, *Jet reconstruction and performance using particle flow with the ATLAS Detector*, *Eur. Phys. J. C* **77** (2017) 466, arXiv: [1703.10485 \[hep-ex\]](#).
- [123] ATLAS Collaboration, *Selection of jets produced in 13 TeV proton–proton collisions with the ATLAS detector*, ATLAS-CONF-2015-029, 2015, URL: <https://cds.cern.ch/record/2037702>.
- [124] ATLAS Collaboration, *Performance of pile-up mitigation techniques for jets in pp collisions at $\sqrt{s} = 8$ TeV using the ATLAS detector*, *Eur. Phys. J. C* **76** (2016) 581, arXiv: [1510.03823 \[hep-ex\]](#).

- [125] ATLAS Collaboration, *Identification and rejection of pile-up jets at high pseudorapidity with the ATLAS detector*, *Eur. Phys. J. C* **77** (2017) 580, arXiv: [1705.02211 \[hep-ex\]](#),
Erratum: *Eur. Phys. J. C* **77** (2017) 712.
- [126] ATLAS Collaboration, *The performance of the jet trigger for the ATLAS detector during 2011 data taking*, *Eur. Phys. J. C* **76** (2016) 526, arXiv: [1606.07759 \[hep-ex\]](#).
- [127] V. Lendermann et al., *Combining Triggers in HEP Data Analysis*, *Nucl. Instrum. Meth. A* **604** (2009) 707, arXiv: [0901.4118 \[hep-ex\]](#).
- [128] G. D'Agostini, *A multidimensional unfolding method based on Bayes' theorem*, *Nucl. Instrum. Meth. A* **362** (1995) 487, ISSN: 0168-9002.
- [129] T. Adye, 'Unfolding algorithms and tests using RooUnfold', *Proceedings, 2011 Workshop on Statistical Issues Related to Discovery Claims in Search Experiments and Unfolding (PHYSTAT 2011)* (CERN, Geneva, Switzerland, 17th–20th Jan. 2011) 313, arXiv: [1105.1160 \[physics.data-an\]](#).
- [130] A. Buckley et al., *Rivet user manual*, *Comput. Phys. Commun.* **184** (2013) 2803, arXiv: [1003.0694 \[hep-ph\]](#).
- [131] *Event Isotropies*, HEPData (collection), <https://doi.org/10.17182/hepdata.110164>, 2021.
- [132] ATLAS Collaboration, *ATLAS Computing Acknowledgements*, ATL-SOFT-PUB-2021-003, 2021, URL: <https://cds.cern.ch/record/2776662>.

The ATLAS Collaboration

G. Aad ¹⁰², B. Abbott ¹²⁰, D.C. Abbott ¹⁰³, K. Abeling ⁵⁵, S.H. Abidi ²⁹, A. Aboulhorma ^{35e}, H. Abramowicz ¹⁵¹, H. Abreu ¹⁵⁰, Y. Abulaiti ¹¹⁷, A.C. Abusleme Hoffman ^{137a}, B.S. Acharya ^{69a,69b,r}, C. Adam Bourdarios ⁴, L. Adamczyk ^{85a}, L. Adamek ¹⁵⁵, S.V. Addepalli ²⁶, J. Adelman ¹¹⁵, A. Adiguzel ^{21c}, S. Adorni ⁵⁶, T. Adye ¹³⁴, A.A. Affolder ¹³⁶, Y. Afik ³⁶, M.N. Agaras ¹³, J. Agarwala ^{73a,73b}, A. Aggarwal ¹⁰⁰, C. Agheorghiesei ^{27c}, J.A. Aguilar-Saavedra ^{130f}, A. Ahmad ³⁶, F. Ahmadov ^{38,ad}, W.S. Ahmed ¹⁰⁴, S. Ahuja ⁹⁵, X. Ai ⁴⁸, G. Aielli ^{76a,76b}, M. Ait Tamlihat ^{35e}, B. Aitbenkikh ^{35a}, I. Aizenberg ¹⁶⁹, M. Akbiyik ¹⁰⁰, T.P.A. Åkesson ⁹⁸, A.V. Akimov ³⁷, K. Al Houry ⁴¹, G.L. Alberghi ^{23b}, J. Albert ¹⁶⁵, P. Albicocco ⁵³, S. Alderweireldt ⁵², M. Aleksa ³⁶, I.N. Aleksandrov ³⁸, C. Alexa ^{27b}, T. Alexopoulos ¹⁰, A. Alfonsi ¹¹⁴, F. Alfonsi ^{23b}, M. Alhroob ¹²⁰, B. Ali ¹³², S. Ali ¹⁴⁸, M. Aliev ³⁷, G. Alimonti ^{71a}, W. Alkakh ⁵⁵, C. Allaire ⁶⁶, B.M.M. Allbrooke ¹⁴⁶, C.A. Allendes Flores ^{137f}, P.P. Allport ²⁰, A. Aloisio ^{72a,72b}, F. Alonso ⁹⁰, C. Alpigiani ¹³⁸, M. Alvarez Estevez ⁹⁹, M.G. Alviggi ^{72a,72b}, M. Aly ¹⁰¹, Y. Amaral Coutinho ^{82b}, A. Ambler ¹⁰⁴, C. Amelung ³⁶, M. Amerl ¹, C.G. Ames ¹⁰⁹, D. Amidei ¹⁰⁶, S.P. Amor Dos Santos ^{130a}, K.R. Amos ¹⁶³, V. Ananiev ¹²⁵, C. Anastopoulos ¹³⁹, T. Andeen ¹¹, J.K. Anders ³⁶, S.Y. Andrean ^{47a,47b}, A. Andreazza ^{71a,71b}, S. Angelidakis ⁹, A. Angerami ^{41,ag}, A.V. Anisenkov ³⁷, A. Annovi ^{74a}, C. Antel ⁵⁶, M.T. Anthony ¹³⁹, E. Antipov ¹²¹, M. Antonelli ⁵³, D.J.A. Antrim ^{17a}, F. Anulli ^{75a}, M. Aoki ⁸³, T. Aoki ¹⁵³, J.A. Aparisi Pozo ¹⁶³, M.A. Aparo ¹⁴⁶, L. Aperio Bella ⁴⁸, C. Appelt ¹⁸, N. Aranzabal ³⁶, V. Araujo Ferraz ^{82a}, C. Arcangeletti ⁵³, A.T.H. Arce ⁵¹, E. Arena ⁹², J-F. Arguin ¹⁰⁸, S. Argyropoulos ⁵⁴, J.-H. Arling ⁴⁸, A.J. Armbruster ³⁶, O. Arnaez ¹⁵⁵, H. Arnold ¹¹⁴, Z.P. Arrubarrena Tame ¹⁰⁹, G. Artoni ^{75a,75b}, H. Asada ¹¹¹, K. Asai ¹¹⁸, S. Asai ¹⁵³, N.A. Asbah ⁶¹, J. Assahsah ^{35d}, K. Assamagan ²⁹, R. Astalos ^{28a}, R.J. Atkin ^{33a}, M. Atkinson ¹⁶², N.B. Atlay ¹⁸, H. Atmani ^{62b}, P.A. Atmasiddha ¹⁰⁶, K. Augsten ¹³², S. Auricchio ^{72a,72b}, A.D. Auriol ²⁰, V.A. Austrup ¹⁷¹, G. Avner ¹⁵⁰, G. Avolio ³⁶, K. Axiotis ⁵⁶, M.K. Ayoub ^{14c}, G. Azuelos ^{108,al}, D. Babal ^{28a}, H. Bachacou ¹³⁵, K. Bachas ^{152,u}, A. Bachiu ³⁴, F. Backman ^{47a,47b}, A. Badea ⁶¹, P. Bagnaia ^{75a,75b}, M. Bahmani ¹⁸, A.J. Bailey ¹⁶³, V.R. Bailey ¹⁶², J.T. Baines ¹³⁴, C. Bakalis ¹⁰, O.K. Baker ¹⁷², P.J. Bakker ¹¹⁴, E. Bakos ¹⁵, D. Bakshi Gupta ⁸, S. Balaji ¹⁴⁷, R. Balasubramanian ¹¹⁴, E.M. Baldin ³⁷, P. Balek ¹³³, E. Ballabene ^{71a,71b}, F. Balli ¹³⁵, L.M. Baltes ^{63a}, W.K. Balunas ³², J. Balz ¹⁰⁰, E. Banas ⁸⁶, M. Bandieramonte ¹²⁹, A. Bandyopadhyay ²⁴, S. Bansal ²⁴, L. Barak ¹⁵¹, E.L. Barberio ¹⁰⁵, D. Barberis ^{57b,57a}, M. Barbero ¹⁰², G. Barbour ⁹⁶, K.N. Barends ^{33a}, T. Barillari ¹¹⁰, M-S. Barisits ³⁶, T. Barklow ¹⁴³, R.M. Barnett ^{17a}, P. Baron ¹²², D.A. Baron Moreno ¹⁰¹, A. Baroncelli ^{62a}, G. Barone ²⁹, A.J. Barr ¹²⁶, L. Barranco Navarro ^{47a,47b}, F. Barreiro ⁹⁹, J. Barreiro Guimarães da Costa ^{14a}, U. Barron ¹⁵¹, M.G. Barros Teixeira ^{130a}, S. Barsov ³⁷, F. Bartels ^{63a}, R. Bartoldus ¹⁴³, A.E. Barton ⁹¹, P. Bartos ^{28a}, A. Basalae ⁴⁸, A. Basan ¹⁰⁰, M. Baselga ⁴⁹, I. Bashta ^{77a,77b}, A. Bassalat ^{66,b}, M.J. Basso ¹⁵⁵, C.R. Basson ¹⁰¹, R.L. Bates ⁵⁹, S. Batlamous ^{35e}, J.R. Batley ³², B. Batool ¹⁴¹, M. Battaglia ¹³⁶, D. Battulga ¹⁸, M. Baucé ^{75a,75b}, P. Bauer ²⁴, A. Bayirli ^{21a}, J.B. Beacham ⁵¹, T. Beau ¹²⁷, P.H. Beauchemin ¹⁵⁸, F. Becherer ⁵⁴, P. Bechtel ²⁴, H.P. Beck ^{19,t}, K. Becker ¹⁶⁷, A.J. Beddall ^{21d}, V.A. Bednyakov ³⁸, C.P. Bee ¹⁴⁵, L.J. Beemster ¹⁵, T.A. Beermann ³⁶, M. Begalli ^{82d}, M. Begel ²⁹, A. Behera ¹⁴⁵, J.K. Behr ⁴⁸, C. Beirao Da Cruz E Silva ³⁶, J.F. Beirer ^{55,36}, F. Beisiegel ²⁴, M. Belfkir ¹⁵⁹, G. Bella ¹⁵¹, L. Bellagamba ^{23b}, A. Bellerive ³⁴, P. Bellos ²⁰, K. Beloborodov ³⁷, K. Belotskiy ³⁷, N.L. Belyaev ³⁷, D. Benckekroun ^{35a}, F. Bendebba ^{35a}, Y. Benhammou ¹⁵¹, D.P. Benjamin ²⁹,

M. Benoit [ID²⁹](#), J.R. Bensinger [ID²⁶](#), S. Bentvelsen [ID¹¹⁴](#), L. Beresford [ID³⁶](#), M. Beretta [ID⁵³](#),
E. Bergeaas Kuutmann [ID¹⁶¹](#), N. Berger [ID⁴](#), B. Bergmann [ID¹³²](#), J. Beringer [ID^{17a}](#), S. Berlendis [ID⁷](#),
G. Bernardi [ID⁵](#), C. Bernius [ID¹⁴³](#), F.U. Bernlochner [ID²⁴](#), T. Berry [ID⁹⁵](#), P. Berta [ID¹³³](#), A. Berthold [ID⁵⁰](#),
I.A. Bertram [ID⁹¹](#), S. Bethke [ID¹¹⁰](#), A. Betti [ID^{75a,75b}](#), A.J. Bevan [ID⁹⁴](#), M. Bhamjee [ID^{33c}](#), S. Bhatta [ID¹⁴⁵](#),
D.S. Bhattacharya [ID¹⁶⁶](#), P. Bhattarai [ID²⁶](#), V.S. Bhopatkar [ID¹²¹](#), R. Bi [ID^{29,ao}](#), R.M. Bianchi [ID¹²⁹](#),
O. Biebel [ID¹⁰⁹](#), R. Bielski [ID¹²³](#), M. Biglietti [ID^{77a}](#), T.R.V. Billoud [ID¹³²](#), M. Bindi [ID⁵⁵](#), A. Bingul [ID^{21b}](#),
C. Bini [ID^{75a,75b}](#), A. Biondini [ID⁹²](#), C.J. Birch-sykes [ID¹⁰¹](#), G.A. Bird [ID^{20,134}](#), M. Birman [ID¹⁶⁹](#),
M. Biros [ID¹³³](#), T. Bisanz [ID³⁶](#), E. Bisceglie [ID^{43b,43a}](#), D. Biswas [ID^{170,n}](#), A. Bitadze [ID¹⁰¹](#), K. Bjørke [ID¹²⁵](#),
I. Bloch [ID⁴⁸](#), C. Blocker [ID²⁶](#), A. Blue [ID⁵⁹](#), U. Blumenschein [ID⁹⁴](#), J. Blumenthal [ID¹⁰⁰](#), G.J. Bobbink [ID¹¹⁴](#),
V.S. Bobrovnikov [ID³⁷](#), M. Boehler [ID⁵⁴](#), D. Bogavac [ID³⁶](#), A.G. Bogdanchikov [ID³⁷](#), C. Bohm [ID^{47a}](#),
V. Boisvert [ID⁹⁵](#), P. Bokan [ID⁴⁸](#), T. Bold [ID^{85a}](#), M. Bomben [ID⁵](#), M. Bona [ID⁹⁴](#), M. Boonekamp [ID¹³⁵](#),
C.D. Booth [ID⁹⁵](#), A.G. Borbély [ID⁵⁹](#), H.M. Borecka-Bielska [ID¹⁰⁸](#), L.S. Borgna [ID⁹⁶](#), G. Borissov [ID⁹¹](#),
D. Bortoletto [ID¹²⁶](#), D. Boscherini [ID^{23b}](#), M. Bosman [ID¹³](#), J.D. Bossio Sola [ID³⁶](#), K. Bouaouda [ID^{35a}](#),
N. Bouchhar [ID¹⁶³](#), J. Boudreau [ID¹²⁹](#), E.V. Bouhova-Thacker [ID⁹¹](#), D. Boumediene [ID⁴⁰](#), R. Bouquet [ID⁵](#),
A. Boveia [ID¹¹⁹](#), J. Boyd [ID³⁶](#), D. Boye [ID²⁹](#), I.R. Boyko [ID³⁸](#), J. Bracinik [ID²⁰](#), N. Brahimi [ID^{62d}](#),
G. Brandt [ID¹⁷¹](#), O. Brandt [ID³²](#), F. Braren [ID⁴⁸](#), B. Brau [ID¹⁰³](#), J.E. Brau [ID¹²³](#), K. Brendlinger [ID⁴⁸](#),
R. Brenner [ID¹⁶⁹](#), L. Brenner [ID¹¹⁴](#), R. Brenner [ID¹⁶¹](#), S. Bressler [ID¹⁶⁹](#), D. Britton [ID⁵⁹](#), D. Britzger [ID¹¹⁰](#),
I. Brock [ID²⁴](#), G. Brooijmans [ID⁴¹](#), W.K. Brooks [ID^{137f}](#), E. Brost [ID²⁹](#), T.L. Bruckler [ID¹²⁶](#),
P.A. Bruckman de Renstrom [ID⁸⁶](#), B. Brüers [ID⁴⁸](#), D. Bruncko [ID^{28b,*}](#), A. Bruni [ID^{23b}](#), G. Bruni [ID^{23b}](#),
M. Bruschi [ID^{23b}](#), N. Bruscinò [ID^{75a,75b}](#), T. Buanes [ID¹⁶](#), Q. Buat [ID¹³⁸](#), P. Buchholz [ID¹⁴¹](#),
A.G. Buckley [ID⁵⁹](#), I.A. Budagov [ID^{38,*}](#), M.K. Bugge [ID¹²⁵](#), O. Bulekov [ID³⁷](#), B.A. Bullard [ID¹⁴³](#),
S. Burdin [ID⁹²](#), C.D. Burgard [ID⁴⁹](#), A.M. Burger [ID⁴⁰](#), B. Burghgrave [ID⁸](#), J.T.P. Burr [ID³²](#), C.D. Burton [ID¹¹](#),
J.C. Burzynski [ID¹⁴²](#), E.L. Busch [ID⁴¹](#), V. Büscher [ID¹⁰⁰](#), P.J. Bussey [ID⁵⁹](#), J.M. Butler [ID²⁵](#), C.M. Buttar [ID⁵⁹](#),
J.M. Butterworth [ID⁹⁶](#), W. Buttinger [ID¹³⁴](#), C.J. Buxo Vazquez [ID¹⁰⁷](#), A.R. Buzykaev [ID³⁷](#), G. Cabras [ID^{23b}](#),
S. Cabrera Urbán [ID¹⁶³](#), D. Caforio [ID⁵⁸](#), H. Cai [ID¹²⁹](#), Y. Cai [ID^{14a,14d}](#), V.M.M. Cairo [ID³⁶](#), O. Cakir [ID^{3a}](#),
N. Calace [ID³⁶](#), P. Calafiura [ID^{17a}](#), G. Calderini [ID¹²⁷](#), P. Calfayan [ID⁶⁸](#), G. Callea [ID⁵⁹](#), L.P. Caloba [ID^{82b}](#),
D. Calvet [ID⁴⁰](#), S. Calvet [ID⁴⁰](#), T.P. Calvet [ID¹⁰²](#), M. Calvetti [ID^{74a,74b}](#), R. Camacho Toro [ID¹²⁷](#),
S. Camarda [ID³⁶](#), D. Camarero Munoz [ID²⁶](#), P. Camarri [ID^{76a,76b}](#), M.T. Camerlingo [ID^{72a,72b}](#),
D. Cameron [ID¹²⁵](#), C. Camincher [ID¹⁶⁵](#), M. Campanelli [ID⁹⁶](#), A. Camplani [ID⁴²](#), V. Canale [ID^{72a,72b}](#),
A. Canesse [ID¹⁰⁴](#), M. Cano Bret [ID⁸⁰](#), J. Cantero [ID¹⁶³](#), Y. Cao [ID¹⁶²](#), F. Capocasa [ID²⁶](#), M. Capua [ID^{43b,43a}](#),
A. Carbone [ID^{71a,71b}](#), R. Cardarelli [ID^{76a}](#), J.C.J. Cardenas [ID⁸](#), F. Cardillo [ID¹⁶³](#), T. Carli [ID³⁶](#),
G. Carlino [ID^{72a}](#), J.I. Carlotto [ID¹³](#), B.T. Carlson [ID^{129,v}](#), E.M. Carlson [ID^{165,156a}](#), L. Carminati [ID^{71a,71b}](#),
M. Carnesale [ID^{75a,75b}](#), S. Caron [ID¹¹³](#), E. Carquin [ID^{137f}](#), S. Carrá [ID^{71a,71b}](#), G. Carratta [ID^{23b,23a}](#),
F. Carrio Argos [ID^{33g}](#), J.W.S. Carter [ID¹⁵⁵](#), T.M. Carter [ID⁵²](#), M.P. Casado [ID^{13,k}](#), A.F. Casha [ID¹⁵⁵](#),
E.G. Castiglia [ID¹⁷²](#), F.L. Castillo [ID^{63a}](#), L. Castillo Garcia [ID¹³](#), V. Castillo Gimenez [ID¹⁶³](#),
N.F. Castro [ID^{130a,130e}](#), A. Catinaccio [ID³⁶](#), J.R. Catmore [ID¹²⁵](#), V. Cavaliere [ID²⁹](#), N. Cavalli [ID^{23b,23a}](#),
V. Cavasinni [ID^{74a,74b}](#), E. Celebi [ID^{21a}](#), F. Celli [ID¹²⁶](#), M.S. Centonze [ID^{70a,70b}](#), K. Cerny [ID¹²²](#),
A.S. Cerqueira [ID^{82a}](#), A. Cerri [ID¹⁴⁶](#), L. Cerrito [ID^{76a,76b}](#), F. Cerutti [ID^{17a}](#), A. Cervelli [ID^{23b}](#), C. Cesarotti [ID^g](#),
S.A. Cetin [ID^{21d}](#), Z. Chadi [ID^{35a}](#), D. Chakraborty [ID¹¹⁵](#), M. Chala [ID^{130f}](#), J. Chan [ID¹⁷⁰](#), W.Y. Chan [ID¹⁵³](#),
J.D. Chapman [ID³²](#), B. Chargeishvili [ID^{149b}](#), D.G. Charlton [ID²⁰](#), T.P. Charman [ID⁹⁴](#), M. Chatterjee [ID¹⁹](#),
S. Chekanov [ID⁶](#), S.V. Chekulaev [ID^{156a}](#), G.A. Chelkov [ID^{38,a}](#), A. Chen [ID¹⁰⁶](#), B. Chen [ID¹⁵¹](#), B. Chen [ID¹⁶⁵](#),
H. Chen [ID^{14c}](#), H. Chen [ID²⁹](#), J. Chen [ID^{62c}](#), J. Chen [ID¹⁴²](#), S. Chen [ID¹⁵³](#), S.J. Chen [ID^{14c}](#), X. Chen [ID^{62c}](#),
X. Chen [ID^{14b,ak}](#), Y. Chen [ID^{62a}](#), C.L. Cheng [ID¹⁷⁰](#), H.C. Cheng [ID^{64a}](#), S. Cheong [ID¹⁴³](#), A. Cheplakov [ID³⁸](#),
E. Cheremushkina [ID⁴⁸](#), E. Cherepanova [ID¹¹⁴](#), R. Cherkaoui El Moursli [ID^{35e}](#), E. Cheu [ID⁷](#), K. Cheung [ID⁶⁵](#),
L. Chevalier [ID¹³⁵](#), V. Chiarella [ID⁵³](#), G. Chiarelli [ID^{74a}](#), N. Chiedde [ID¹⁰²](#), G. Chiodini [ID^{70a}](#),
A.S. Chisholm [ID²⁰](#), A. Chitan [ID^{27b}](#), M. Chitishvili [ID¹⁶³](#), Y.H. Chiu [ID¹⁶⁵](#), M.V. Chizhov [ID³⁸](#), K. Choi [ID¹¹](#),
A.R. Chomont [ID^{75a,75b}](#), Y. Chou [ID¹⁰³](#), E.Y.S. Chow [ID¹¹⁴](#), T. Chowdhury [ID^{33g}](#), L.D. Christopher [ID^{33g}](#),

K.L. Chu^{64a}, M.C. Chu^{64a}, X. Chu^{14a,14d}, J. Chudoba¹³¹, J.J. Chwastowski⁸⁶, D. Cieri¹¹⁰,
 K.M. Ciesla^{85a}, V. Cindro⁹³, A. Ciocio^{17a}, F. Cirotto^{72a,72b}, Z.H. Citron^{169,o}, M. Citterio^{71a},
 D.A. Ciubotaru^{27b}, B.M. Ciungu¹⁵⁵, A. Clark⁵⁶, P.J. Clark⁵², J.M. Clavijo Columbie⁴⁸,
 S.E. Clawson¹⁰¹, C. Clement^{47a,47b}, J. Clercx⁴⁸, L. Clissa^{23b,23a}, Y. Coadou¹⁰²,
 M. Cobal^{69a,69c}, A. Coccaro^{57b}, R.F. Coelho Barrue^{130a}, R. Coelho Lopes De Sa¹⁰³,
 S. Coelli^{71a}, H. Cohen¹⁵¹, A.E.C. Coimbra^{71a,71b}, B. Cole⁴¹, J. Collot⁶⁰,
 P. Conde Muiño^{130a,130g}, M.P. Connell^{33c}, S.H. Connell^{33c}, I.A. Connelly⁵⁹, E.I. Conroy¹²⁶,
 F. Conventi^{72a,am}, H.G. Cooke²⁰, A.M. Cooper-Sarkar¹²⁶, F. Cormier¹⁶⁴, L.D. Corpe³⁶,
 M. Corradi^{75a,75b}, E.E. Corrigan⁹⁸, F. Corriveau^{104,ab}, A. Cortes-Gonzalez¹⁸, M.J. Costa¹⁶³,
 F. Costanza⁴, D. Costanzo¹³⁹, B.M. Cote¹¹⁹, G. Cowan⁹⁵, J.W. Cowley³², K. Cranmer¹¹⁷,
 S. Crépe-Renaudin⁶⁰, F. Crescioli¹²⁷, M. Cristinziani¹⁴¹, M. Cristoforetti^{78a,78b,d}, V. Croft¹⁵⁸,
 G. Crosetti^{43b,43a}, A. Cueto³⁶, T. Cuhadar Donszelmann¹⁶⁰, H. Cui^{14a,14d}, Z. Cui⁷,
 W.R. Cunningham⁵⁹, F. Curcio^{43b,43a}, P. Czodrowski³⁶, M.M. Czurylo^{63b},
 M.J. Da Cunha Sargedas De Sousa^{62a}, J.V. Da Fonseca Pinto^{82b}, C. Da Via¹⁰¹, W. Dabrowski^{85a},
 T. Dado⁴⁹, S. Dahbi^{33g}, T. Dai¹⁰⁶, C. Dallapiccola¹⁰³, M. Dam⁴², G. D'amen²⁹,
 V. D'Amico¹⁰⁹, J. Damp¹⁰⁰, J.R. Dandoy¹²⁸, M.F. Daneri³⁰, M. Danninger¹⁴², V. Dao³⁶,
 G. Darbo^{57b}, S. Darmora⁶, S.J. Das^{29,ao}, S. D'Auria^{71a,71b}, C. David^{156b}, T. Davidek¹³³,
 D.R. Davis⁵¹, B. Davis-Purcell³⁴, I. Dawson⁹⁴, K. De⁸, R. De Asmundis^{72a},
 M. De Beurs¹¹⁴, N. De Biase⁴⁸, S. De Castro^{23b,23a}, N. De Groot¹¹³, P. de Jong¹¹⁴,
 H. De la Torre¹⁰⁷, A. De Maria^{14c}, A. De Salvo^{75a}, U. De Sanctis^{76a,76b}, A. De Santo¹⁴⁶,
 J.B. De Vivie De Regie⁶⁰, D.V. Dedovich³⁸, J. Degens¹¹⁴, A.M. Deiana⁴⁴, F. Del Corso^{23b,23a},
 J. Del Peso⁹⁹, F. Del Rio^{63a}, F. Deliot¹³⁵, C.M. Delitzsch⁴⁹, M. Della Pietra^{72a,72b},
 D. Della Volpe⁵⁶, A. Dell'Acqua³⁶, L. Dell'Asta^{71a,71b}, M. Delmastro⁴, P.A. Delsart⁶⁰,
 S. Demers¹⁷², M. Demichev³⁸, S.P. Denisov³⁷, L. D'Eramo¹¹⁵, D. Derendarz⁸⁶,
 F. Derue¹²⁷, P. Dervan⁹², K. Desch²⁴, K. Dette¹⁵⁵, C. Deutsch²⁴, F.A. Di Bello^{57b,57a},
 A. Di Ciaccio^{76a,76b}, L. Di Ciaccio⁴, A. Di Domenico^{75a,75b}, C. Di Donato^{72a,72b},
 A. Di Girolamo³⁶, G. Di Gregorio⁵, A. Di Luca^{78a,78b}, B. Di Micco^{77a,77b}, R. Di Nardo^{77a,77b},
 C. Diaconu¹⁰², F.A. Dias¹¹⁴, T. Dias Do Vale¹⁴², M.A. Diaz^{137a,137b}, F.G. Diaz Capriles²⁴,
 M. Didenko¹⁶³, E.B. Diehl¹⁰⁶, L. Diehl⁵⁴, S. Díez Cornell⁴⁸, C. Díez Pardos¹⁴¹,
 C. Dimitriadi^{24,161}, A. Dimitrievska^{17a}, J. Dingfelder²⁴, I-M. Dinu^{27b}, S.J. Dittmeier^{63b},
 F. Dittus³⁶, F. Djama¹⁰², T. Djobava^{149b}, J.I. Djuvsland¹⁶, C. Doglioni^{101,98}, J. Dolejsi¹³³,
 Z. Dolezal¹³³, M. Donadelli^{82c}, B. Dong¹⁰⁷, J. Donini⁴⁰, A. D'Onofrio^{77a,77b},
 M. D'Onofrio⁹², J. Dopke¹³⁴, A. Doria^{72a}, M.T. Dova⁹⁰, A.T. Doyle⁵⁹, M.A. Draguet¹²⁶,
 E. Drechsler¹⁴², E. Dreyer¹⁶⁹, I. Drivas-koulouris¹⁰, A.S. Drobac¹⁵⁸, M. Drozdova⁵⁶,
 D. Du^{62a}, T.A. du Pree¹¹⁴, F. Dubinin³⁷, M. Dubovsky^{28a}, E. Duchovni¹⁶⁹, G. Duckeck¹⁰⁹,
 O.A. Ducu^{27b}, D. Duda¹¹⁰, A. Dudarev³⁶, M. D'uffizi¹⁰¹, L. Dufлот⁶⁶, M. Dührssen³⁶,
 C. Dülsen¹⁷¹, A.E. Dumitriu^{27b}, M. Dunford^{63a}, S. Dungs⁴⁹, K. Dunne^{47a,47b},
 A. Duperrin¹⁰², H. Duran Yildiz^{3a}, M. Düren⁵⁸, A. Durglishvili^{149b}, B.L. Dwyer¹¹⁵,
 G.I. Dyckes^{17a}, M. Dyndal^{85a}, S. Dysch¹⁰¹, B.S. Dziedzic⁸⁶, Z.O. Earnshaw¹⁴⁶,
 B. Eckerova^{28a}, S. Eggebrecht⁵⁵, M.G. Eggleston⁵¹, E. Egidio Purcino De Souza¹²⁷,
 L.F. Ehrke⁵⁶, G. Eigen¹⁶, K. Einsweiler^{17a}, T. Ekelof¹⁶¹, P.A. Ekman⁹⁸, Y. El Ghazali^{35b},
 H. El Jarrari^{35e,148}, A. El Moussaouy^{35a}, V. Ellajosyula¹⁶¹, M. Ellert¹⁶¹, F. Ellinghaus¹⁷¹,
 A.A. Elliot⁹⁴, N. Ellis³⁶, J. Elmsheuser²⁹, M. Elsing³⁶, D. Emelianov¹³⁴, A. Emerman⁴¹,
 Y. Enari¹⁵³, I. Ene^{17a}, S. Epari¹³, J. Erdmann^{49,ai}, A. Ereditato¹⁹, P.A. Erland⁸⁶,
 M. Errenst¹⁷¹, M. Escalier⁶⁶, C. Escobar¹⁶³, E. Etzion¹⁵¹, G. Evans^{130a}, H. Evans⁶⁸,
 M.O. Evans¹⁴⁶, A. Ezhilov³⁷, S. Ezzarqtouni^{35a}, F. Fabbri⁵⁹, L. Fabbri^{23b,23a}, G. Facini⁹⁶,
 V. Fadeyev¹³⁶, R.M. Fakhrutdinov³⁷, S. Falciano^{75a}, L.F. Falda Ulhoa Coelho³⁶, P.J. Falke²⁴,

S. Falke ³⁶, J. Faltova ¹³³, Y. Fan ^{14a}, Y. Fang ^{14a,14d}, G. Fanourakis ⁴⁶, M. Fanti ^{71a,71b},
 M. Faraj ^{69a,69b}, Z. Farazpay ⁹⁷, A. Farbin ⁸, A. Farilla ^{77a}, T. Farooque ¹⁰⁷, S.M. Farrington ⁵²,
 F. Fassi ^{35e}, D. Fassouliotis ⁹, M. Faucci Giannelli ^{76a,76b}, W.J. Fawcett ³², L. Fayard ⁶⁶,
 P. Federicova ¹³¹, O.L. Fedin ^{37,a}, G. Fedotov ³⁷, M. Feickert ¹⁷⁰, L. Feligioni ¹⁰², A. Fell ¹³⁹,
 D.E. Fellers ¹²³, C. Feng ^{62b}, M. Feng ^{14b}, Z. Feng ¹¹⁴, M.J. Fenton ¹⁶⁰, A.B. Fenyuk ³⁷,
 L. Ferencz ⁴⁸, R.A.M. Ferguson ⁹¹, J. Ferrando ⁴⁸, A. Ferrari ¹⁶¹, P. Ferrari ^{114,113},
 R. Ferrari ^{73a}, D. Ferrere ⁵⁶, C. Ferretti ¹⁰⁶, F. Fiedler ¹⁰⁰, A. Filipčič ⁹³, E.K. Filmer ¹,
 F. Filthaut ¹¹³, M.C.N. Fiolhais ^{130a,130c,c}, L. Fiorini ¹⁶³, F. Fischer ¹⁴¹, W.C. Fisher ¹⁰⁷,
 T. Fitschen ¹⁰¹, I. Fleck ¹⁴¹, P. Fleischmann ¹⁰⁶, T. Flick ¹⁷¹, L. Flores ¹²⁸, M. Flores ^{33d,ah},
 L.R. Flores Castillo ^{64a}, F.M. Follega ^{78a,78b}, N. Fomin ¹⁶, J.H. Foo ¹⁵⁵, B.C. Forland ⁶⁸,
 A. Formica ¹³⁵, A.C. Forti ¹⁰¹, E. Fortin ¹⁰², A.W. Fortman ⁶¹, M.G. Foti ^{17a}, L. Fountas ^{9,1},
 D. Fournier ⁶⁶, H. Fox ⁹¹, P. Francavilla ^{74a,74b}, S. Francescato ⁶¹, S. Franchellucci ⁵⁶,
 M. Franchini ^{23b,23a}, S. Franchino ^{63a}, D. Francis ³⁶, L. Franco ¹¹³, L. Franconi ¹⁹, M. Franklin ⁶¹,
 G. Frattari ²⁶, A.C. Freegard ⁹⁴, P.M. Freeman ²⁰, W.S. Freund ^{82b}, N. Fritzsche ⁵⁰, A. Froch ⁵⁴,
 D. Froidevaux ³⁶, J.A. Frost ¹²⁶, Y. Fu ^{62a}, M. Fujimoto ¹¹⁸, E. Fullana Torregrosa ^{163,*},
 J. Fuster ¹⁶³, A. Gabrielli ^{23b,23a}, A. Gabrielli ¹⁵⁵, P. Gadow ⁴⁸, G. Gagliardi ^{57b,57a},
 L.G. Gagnon ^{17a}, G.E. Gallardo ¹²⁶, E.J. Gallas ¹²⁶, B.J. Gallop ¹³⁴, R. Gamboa Goni ⁹⁴,
 K.K. Gan ¹¹⁹, S. Ganguly ¹⁵³, J. Gao ^{62a}, Y. Gao ⁵², F.M. Garay Walls ^{137a,137b}, B. Garcia ^{29,ao},
 C. García ¹⁶³, J.E. García Navarro ¹⁶³, M. Garcia-Sciveres ^{17a}, R.W. Gardner ³⁹, D. Garg ⁸⁰,
 R.B. Garg ^{143,s}, C.A. Garner ¹⁵⁵, V. Garonne ²⁹, S.J. Gasiorowski ¹³⁸, P. Gaspar ^{82b},
 G. Gaudio ^{73a}, V. Gautam ¹³, P. Gauzzi ^{75a,75b}, I.L. Gavrilenko ³⁷, A. Gavrilyuk ³⁷, C. Gay ¹⁶⁴,
 G. Gaycken ⁴⁸, E.N. Gazis ¹⁰, A.A. Geanta ^{27b,27e}, C.M. Gee ¹³⁶, J. Geisen ⁹⁸, C. Gemme ^{57b},
 M.H. Genest ⁶⁰, S. Gentile ^{75a,75b}, S. George ⁹⁵, W.F. George ²⁰, T. Gerialis ⁴⁶, L.O. Gerlach ⁵⁵,
 P. Gessinger-Befurt ³⁶, M. Ghasemi Bostanabad ¹⁶⁵, M. Ghneimat ¹⁴¹, K. Ghorbanian ⁹⁴,
 A. Ghosal ¹⁴¹, A. Ghosh ¹⁶⁰, A. Ghosh ⁷, B. Giacobbe ^{23b}, S. Giagu ^{75a,75b}, P. Giannetti ^{74a},
 A. Giannini ^{62a}, S.M. Gibson ⁹⁵, M. Gignac ¹³⁶, D.T. Gil ^{85b}, A.K. Gilbert ^{85a}, B.J. Gilbert ⁴¹,
 D. Gillberg ³⁴, G. Gilles ¹¹⁴, N.E.K. Gillwald ⁴⁸, L. Ginabat ¹²⁷, D.M. Gingrich ^{2,al},
 M.P. Giordani ^{69a,69c}, P.F. Giraud ¹³⁵, G. Giugliarelli ^{69a,69c}, D. Giugni ^{71a}, F. Giuli ³⁶,
 I. Gkialas ^{9,1}, L.K. Gladilin ³⁷, C. Glasman ⁹⁹, G.R. Gledhill ¹²³, M. Glisic ¹²³, I. Gnesi ^{43b,h},
 Y. Go ^{29,ao}, M. Goblirsch-Kolb ²⁶, B. Gocke ⁴⁹, D. Godin ¹⁰⁸, B. Gokturk ^{21a}, S. Goldfarb ¹⁰⁵,
 T. Golling ⁵⁶, M.G.D. Gololo ^{33g}, D. Golubkov ³⁷, J.P. Gombas ¹⁰⁷, A. Gomes ^{130a,130b},
 G. Gomes Da Silva ¹⁴¹, A.J. Gomez Delegido ¹⁶³, R. Goncalves Gama ⁵⁵, R. Gonçalves ^{130a,130c},
 G. Gonella ¹²³, L. Gonella ²⁰, A. Gongadze ³⁸, F. Gonnella ²⁰, J.L. Gonski ⁴¹,
 R.Y. González Andana ⁵², S. González de la Hoz ¹⁶³, S. Gonzalez Fernandez ¹³,
 R. Gonzalez Lopez ⁹², C. Gonzalez Renteria ^{17a}, R. Gonzalez Suarez ¹⁶¹, S. Gonzalez-Sevilla ⁵⁶,
 G.R. Gonzalvo Rodriguez ¹⁶³, L. Goossens ³⁶, N.A. Gorasia ²⁰, P.A. Gorbounov ³⁷, B. Gorini ³⁶,
 E. Gorini ^{70a,70b}, A. Gorišek ⁹³, A.T. Goshaw ⁵¹, M.I. Gostkin ³⁸, S. Goswami ¹²¹,
 C.A. Gottardo ³⁶, M. Goughri ^{35b}, V. Goumarre ⁴⁸, A.G. Goussiou ¹³⁸, N. Govender ^{33c},
 C. Goy ⁴, I. Grabowska-Bold ^{85a}, K. Graham ³⁴, E. Gramstad ¹²⁵, S. Grancagnolo ¹⁸,
 M. Grandi ¹⁴⁶, V. Gratchev ^{37,*}, P.M. Gravila ^{27f}, F.G. Gravili ^{70a,70b}, H.M. Gray ^{17a},
 M. Greco ^{70a,70b}, C. Grefe ²⁴, I.M. Gregor ⁴⁸, P. Grenier ¹⁴³, C. Grieco ¹³, A.A. Grillo ¹³⁶,
 K. Grimm ^{31,p}, S. Grinstein ^{13,x}, J.-F. Grivaz ⁶⁶, E. Gross ¹⁶⁹, J. Grosse-Knetter ⁵⁵, C. Grud ¹⁰⁶,
 A. Grummer ¹¹², J.C. Grundy ¹²⁶, L. Guan ¹⁰⁶, W. Guan ¹⁷⁰, C. Gubbels ¹⁶⁴,
 J.G.R. Guerrero Rojas ¹⁶³, G. Guerrieri ^{69a,69b}, F. Guescini ¹¹⁰, R. Gugel ¹⁰⁰, J.A.M. Guhit ¹⁰⁶,
 A. Guida ⁴⁸, T. Guillemin ⁴, E. Guilloton ^{167,134}, S. Guindon ³⁶, F. Guo ^{14a,14d}, J. Guo ^{62c},
 L. Guo ⁶⁶, Y. Guo ¹⁰⁶, R. Gupta ⁴⁸, S. Gurbuz ²⁴, S.S. Gurdasani ⁵⁴, G. Gustavino ³⁶,
 M. Guth ⁵⁶, P. Gutierrez ¹²⁰, L.F. Gutierrez Zagazeta ¹²⁸, C. Gutschow ⁹⁶, C. Guyot ¹³⁵,

C. Gwenlan ^{id126}, C.B. Gwilliam ^{id92}, E.S. Haaland ^{id125}, A. Haas ^{id117}, M. Habedank ^{id48},
 C. Haber ^{id17a}, H.K. Hadavand ^{id8}, A. Hadeif ^{id100}, S. Hadzic ^{id110}, E.H. Haines ^{id96}, M. Haleem ^{id166},
 J. Haley ^{id121}, J.J. Hall ^{id139}, G.D. Hallewell ^{id102}, L. Halser ^{id19}, K. Hamano ^{id165}, H. Hamdaoui ^{id35e},
 M. Hamer ^{id24}, G.N. Hamity ^{id52}, J. Han ^{id62b}, K. Han ^{id62a}, L. Han ^{id14c}, L. Han ^{id62a}, S. Han ^{id17a},
 Y.F. Han ^{id155}, K. Hanagaki ^{id83}, M. Hance ^{id136}, D.A. Hangal ^{id41.ag}, H. Hanif ^{id142}, M.D. Hank ^{id39},
 R. Hankache ^{id101}, J.B. Hansen ^{id42}, J.D. Hansen ^{id42}, P.H. Hansen ^{id42}, K. Hara ^{id157}, D. Harada ^{id56},
 T. Harenberg ^{id171}, S. Harkusha ^{id37}, Y.T. Harris ^{id126}, N.M. Harrison ^{id119}, P.F. Harrison ^{id167},
 N.M. Hartman ^{id143}, N.M. Hartmann ^{id109}, Y. Hasegawa ^{id140}, A. Hasib ^{id52}, S. Haug ^{id19},
 R. Hauser ^{id107}, M. Havranek ^{id132}, C.M. Hawkes ^{id20}, R.J. Hawkins ^{id36}, S. Hayashida ^{id111},
 D. Hayden ^{id107}, C. Hayes ^{id106}, R.L. Hayes ^{id164}, C.P. Hays ^{id126}, J.M. Hays ^{id94}, H.S. Hayward ^{id92},
 F. He ^{id62a}, Y. He ^{id154}, Y. He ^{id127}, M.P. Heath ^{id52}, V. Hedberg ^{id98}, A.L. Heggelund ^{id125},
 N.D. Hehir ^{id94}, C. Heidegger ^{id54}, K.K. Heidegger ^{id54}, W.D. Heidorn ^{id81}, J. Heilman ^{id34},
 S. Heim ^{id48}, T. Heim ^{id17a}, J.G. Heinlein ^{id128}, J.J. Heinrich ^{id123}, L. Heinrich ^{id110.aj}, J. Hejbal ^{id131},
 L. Helary ^{id48}, A. Held ^{id170}, S. Hellesund ^{id125}, C.M. Helling ^{id164}, S. Hellman ^{id47a.47b}, C. Helsens ^{id36},
 R.C.W. Henderson ^{id91}, L. Henkelmann ^{id32}, A.M. Henriques Correia ^{id36}, H. Herde ^{id98},
 Y. Hernández Jiménez ^{id145}, L.M. Herrmann ^{id24}, M.G. Herrmann ^{id109}, T. Herrmann ^{id50}, G. Herten ^{id54},
 R. Hertenberger ^{id109}, L. Hervás ^{id36}, N.P. Hessey ^{id156a}, H. Hibi ^{id84}, E. Higón-Rodríguez ^{id163},
 S.J. Hillier ^{id20}, I. Hinchliffe ^{id17a}, F. Hinterkeuser ^{id24}, M. Hirose ^{id124}, S. Hirose ^{id157},
 D. Hirschbuehl ^{id171}, T.G. Hitchings ^{id101}, B. Hiti ^{id93}, J. Hobbs ^{id145}, R. Hobincu ^{id27e}, N. Hod ^{id169},
 M.C. Hodgkinson ^{id139}, B.H. Hodgkinson ^{id32}, A. Hoecker ^{id36}, J. Hofer ^{id48}, D. Hohn ^{id54}, T. Holm ^{id24},
 M. Holzbock ^{id110}, L.B.A.H. Hommels ^{id32}, B.P. Honan ^{id101}, J. Hong ^{id62c}, T.M. Hong ^{id129},
 J.C. Honig ^{id54}, A. Hönle ^{id110}, B.H. Hooberman ^{id162}, W.H. Hopkins ^{id6}, Y. Horii ^{id111}, S. Hou ^{id148},
 A.S. Howard ^{id93}, J. Howarth ^{id59}, J. Hoya ^{id6}, M. Hrabovsky ^{id122}, A. Hrynevich ^{id48}, T. Hryn'ova ^{id4},
 P.J. Hsu ^{id65}, S.-C. Hsu ^{id138}, Q. Hu ^{id41}, Y.F. Hu ^{id14a.14d.an}, D.P. Huang ^{id96}, S. Huang ^{id64b},
 X. Huang ^{id14c}, Y. Huang ^{id62a}, Y. Huang ^{id14a}, Z. Huang ^{id101}, Z. Hubacek ^{id132}, M. Huebner ^{id24},
 F. Huegging ^{id24}, T.B. Huffman ^{id126}, M. Huhtinen ^{id36}, S.K. Huiberts ^{id16}, R. Hulsken ^{id104},
 N. Huseynov ^{id12.a}, J. Huston ^{id107}, J. Huth ^{id61}, R. Hyneman ^{id143}, S. Hyrych ^{id28a}, G. Iacobucci ^{id56},
 G. Iakovidis ^{id29}, I. Ibragimov ^{id141}, L. Iconomidou-Fayard ^{id66}, P. Iengo ^{id72a.72b}, R. Iguchi ^{id153},
 T. Iizawa ^{id56}, Y. Ikegami ^{id83}, A. Ilg ^{id19}, N. Ilic ^{id155}, H. Imam ^{id35a}, T. Ingebretsen Carlson ^{id47a.47b},
 G. Introzzi ^{id73a.73b}, M. Iodice ^{id77a}, V. Ippolito ^{id75a.75b}, M. Ishino ^{id153}, W. Islam ^{id170}, C. Issever ^{id18.48},
 S. Istin ^{id21a.aq}, H. Ito ^{id168}, J.M. Iturbe Ponce ^{id64a}, R. Iuppa ^{id78a.78b}, A. Ivina ^{id169}, J.M. Izen ^{id45},
 V. Izzo ^{id72a}, P. Jacka ^{id131.132}, P. Jackson ^{id1}, R.M. Jacobs ^{id48}, B.P. Jaeger ^{id142}, C.S. Jagfeld ^{id109},
 P. Jain ^{id54}, G. Jäkel ^{id171}, K. Jakobs ^{id54}, T. Jakoubek ^{id169}, J. Jamieson ^{id59}, K.W. Janas ^{id85a},
 G. Jarlskog ^{id98}, A.E. Jaspán ^{id92}, M. Javurkova ^{id103}, F. Jeanneau ^{id135}, L. Jeanty ^{id123},
 J. Jejelava ^{id149a.ae}, P. Jenni ^{id54.i}, C.E. Jessiman ^{id34}, S. Jézéquel ^{id4}, J. Jia ^{id145}, X. Jia ^{id61},
 X. Jia ^{id14a.14d}, Z. Jia ^{id14c}, Y. Jiang ^{id62a}, S. Jiggins ^{id52}, J. Jimenez Pena ^{id110}, S. Jin ^{id14c}, A. Jinaru ^{id27b},
 O. Jinnouchi ^{id154}, P. Johansson ^{id139}, K.A. Johns ^{id7}, J.W. Johnson ^{id136}, D.M. Jones ^{id32}, E. Jones ^{id167},
 P. Jones ^{id32}, R.W.L. Jones ^{id91}, T.J. Jones ^{id92}, R. Joshi ^{id119}, J. Jovicevic ^{id15}, X. Ju ^{id17a},
 J.J. Junggeburth ^{id36}, T. Junkermann ^{id63a}, A. Juste Rozas ^{id13.x}, S. Kabana ^{id137e}, A. Kaczmarzka ^{id86},
 M. Kado ^{id75a.75b}, H. Kagan ^{id119}, M. Kagan ^{id143}, A. Kahn ^{id41}, A. Kahn ^{id128}, C. Kahra ^{id100}, T. Kaji ^{id168},
 E. Kajomovitz ^{id150}, N. Kakati ^{id169}, C.W. Kalderon ^{id29}, A. Kamenshchikov ^{id155}, S. Kanayama ^{id154},
 N.J. Kang ^{id136}, D. Kar ^{id33g}, K. Karava ^{id126}, M.J. Kareem ^{id156b}, E. Karentzos ^{id54}, I. Karkanas ^{id152.f},
 S.N. Karpov ^{id38}, Z.M. Karpova ^{id38}, V. Kartvelishvili ^{id91}, A.N. Karyukhin ^{id37}, E. Kasimi ^{id152.f},
 C. Kato ^{id62d}, J. Katzy ^{id48}, S. Kaur ^{id34}, K. Kawade ^{id140}, K. Kawagoe ^{id89}, T. Kawamoto ^{id135},
 G. Kawamura ^{id55}, E.F. Kay ^{id165}, F.I. Kaya ^{id158}, S. Kazakos ^{id13}, V.F. Kazanin ^{id37}, Y. Ke ^{id145},
 J.M. Keaveney ^{id33a}, R. Keeler ^{id165}, G.V. Kehris ^{id61}, J.S. Keller ^{id34}, A.S. Kelly ^{id96}, D. Kelsey ^{id146},
 J.J. Kempster ^{id20}, K.E. Kennedy ^{id41}, P.D. Kennedy ^{id100}, O. Kepka ^{id131}, B.P. Kerridge ^{id167},

S. Kersten ¹⁷¹, B.P. Kerševan ⁹³, S. Keshri ⁶⁶, L. Keszeghova ^{28a}, S. Ketabchi Haghighat ¹⁵⁵, M. Khandoga ¹²⁷, A. Khanov ¹²¹, A.G. Kharlamov ³⁷, T. Kharlamova ³⁷, E.E. Khoda ¹³⁸, T.J. Khoo ¹⁸, G. Khoriali ¹⁶⁶, J. Khubua ^{149b}, Y.A.R. Khwaira ⁶⁶, M. Kiehn ³⁶, A. Kilgallon ¹²³, D.W. Kim ^{47a,47b}, E. Kim ¹⁵⁴, Y.K. Kim ³⁹, N. Kimura ⁹⁶, A. Kirchhoff ⁵⁵, D. Kirchmeier ⁵⁰, C. Kirfel ²⁴, J. Kirk ¹³⁴, A.E. Kiryunin ¹¹⁰, T. Kishimoto ¹⁵³, D.P. Kisliuk ¹⁵⁵, C. Kitsaki ¹⁰, O. Kivernyk ²⁴, M. Klassen ^{63a}, C. Klein ³⁴, L. Klein ¹⁶⁶, M.H. Klein ¹⁰⁶, M. Klein ⁹², S.B. Klein ⁵⁶, U. Klein ⁹², P. Klimek ³⁶, A. Klimentov ²⁹, F. Klimpel ¹¹⁰, T. Klioutchnikova ³⁶, P. Kluit ¹¹⁴, S. Kluth ¹¹⁰, E. Kneringer ⁷⁹, T.M. Knight ¹⁵⁵, A. Knue ⁵⁴, D. Kobayashi⁸⁹, R. Kobayashi ⁸⁷, M. Kocian ¹⁴³, P. Kodyš ¹³³, D.M. Koeck ¹⁴⁶, P.T. Koenig ²⁴, T. Koffas ³⁴, M. Kolb ¹³⁵, I. Koletsou ⁴, T. Komarek ¹²², K. Köneke ⁵⁴, A.X.Y. Kong ¹, T. Kono ¹¹⁸, N. Konstantinidis ⁹⁶, B. Konya ⁹⁸, R. Kopeliansky ⁶⁸, S. Koperny ^{85a}, K. Korcyl ⁸⁶, K. Kordas ^{152,f}, G. Koren ¹⁵¹, A. Korn ⁹⁶, S. Korn ⁵⁵, I. Korolkov ¹³, N. Korotkova ³⁷, B. Kortman ¹¹⁴, O. Kortner ¹¹⁰, S. Kortner ¹¹⁰, W.H. Kostecka ¹¹⁵, V.V. Kostyukhin ¹⁴¹, A. Kotsokechagia ¹³⁵, A. Kotwal ⁵¹, A. Koulouris ³⁶, A. Kourkouveli-Charalampidi ^{73a,73b}, C. Kourkoumelis ⁹, E. Kourlitis ⁶, O. Kovanda ¹⁴⁶, R. Kowalewski ¹⁶⁵, W. Kozanecki ¹³⁵, A.S. Kozhin ³⁷, V.A. Kramarenko ³⁷, G. Kramberger ⁹³, P. Kramer ¹⁰⁰, M.W. Krasny ¹²⁷, A. Krasznahorkay ³⁶, J.A. Kremer ¹⁰⁰, T. Kresse ⁵⁰, J. Kretschmar ⁹², K. Kreul ¹⁸, P. Krieger ¹⁵⁵, S. Krishnamurthy ¹⁰³, M. Krivos ¹³³, K. Krizka ^{17a}, K. Kroeninger ⁴⁹, H. Kroha ¹¹⁰, J. Kroll ¹³¹, J. Kroll ¹²⁸, K.S. Krowpman ¹⁰⁷, U. Kruchonak ³⁸, H. Krüger ²⁴, N. Krumnack⁸¹, M.C. Kruse ⁵¹, J.A. Krzysiak ⁸⁶, O. Kuchinskaia ³⁷, S. Kuday ^{3a}, D. Kuechler ⁴⁸, J.T. Kuechler ⁴⁸, S. Kuehn ³⁶, R. Kuesters ⁵⁴, T. Kuhl ⁴⁸, V. Kukhtin ³⁸, Y. Kulchitsky ^{37,a}, S. Kuleshov ^{137d,137b}, M. Kumar ^{33g}, N. Kumari ¹⁰², A. Kupco ¹³¹, T. Kupfer⁴⁹, A. Kupich ³⁷, O. Kuprash ⁵⁴, H. Kurashige ⁸⁴, L.L. Kurchaninov ^{156a}, Y.A. Kurochkin ³⁷, A. Kurova ³⁷, M. Kuze ¹⁵⁴, A.K. Kvam ¹⁰³, J. Kvita ¹²², T. Kwan ¹⁰⁴, K.W. Kwok ^{64a}, N.G. Kyriacou ¹⁰⁶, L.A.O. Laatu ¹⁰², C. Lacasta ¹⁶³, F. Lacava ^{75a,75b}, H. Lacker ¹⁸, D. Lacour ¹²⁷, N.N. Lad ⁹⁶, E. Ladygin ³⁸, B. Laforge ¹²⁷, T. Lagouri ^{137e}, S. Lai ⁵⁵, I.K. Lakomic ^{85a}, N. Lalloue ⁶⁰, J.E. Lambert ¹²⁰, S. Lammers ⁶⁸, W. Lampl ⁷, C. Lampoudis ^{152,f}, A.N. Lancaster ¹¹⁵, E. Lançon ²⁹, U. Landgraf ⁵⁴, M.P.J. Landon ⁹⁴, V.S. Lang ⁵⁴, R.J. Langenberg ¹⁰³, A.J. Lankford ¹⁶⁰, F. Lanni ³⁶, K. Lantzsch ²⁴, A. Lanza ^{73a}, A. Lapertosa ^{57b,57a}, J.F. Laporte ¹³⁵, T. Lari ^{71a}, F. Lasagni Manghi ^{23b}, M. Lassnig ³⁶, V. Latonova ¹³¹, T.S. Lau ^{64a}, A. Laudrain ¹⁰⁰, A. Laurier ³⁴, S.D. Lawlor ⁹⁵, Z. Lawrence ¹⁰¹, M. Lazzaroni ^{71a,71b}, B. Le¹⁰¹, B. Leban ⁹³, A. Lebedev ⁸¹, M. LeBlanc ³⁶, T. LeCompte ⁶, F. Ledroit-Guillon ⁶⁰, A.C.A. Lee⁹⁶, G.R. Lee ¹⁶, L. Lee ⁶¹, S.C. Lee ¹⁴⁸, S. Lee ^{47a,47b}, T.F. Lee ⁹², L.L. Leeuw ^{33c}, H.P. Lefebvre ⁹⁵, M. Lefebvre ¹⁶⁵, C. Leggett ^{17a}, K. Lehmann ¹⁴², G. Lehmann Miotto ³⁶, M. Leigh ⁵⁶, W.A. Leight ¹⁰³, A. Leisos ^{152,w}, M.A.L. Leite ^{82c}, C.E. Leitgeb ⁴⁸, R. Leitner ¹³³, K.J.C. Leney ⁴⁴, T. Lenz ²⁴, S. Leone ^{74a}, C. Leonidopoulos ⁵², A. Leopold ¹⁴⁴, C. Leroy ¹⁰⁸, R. Les ¹⁰⁷, C.G. Lester ³², M. Levchenko ³⁷, J. Levêque ⁴, D. Levin ¹⁰⁶, L.J. Levinson ¹⁶⁹, M.P. Lewicki ⁸⁶, D.J. Lewis ⁴, A. Li ⁵, B. Li ^{62b}, C. Li ^{62a}, C-Q. Li ^{62c}, H. Li ^{62a}, H. Li ^{62b}, H. Li ^{14c}, H. Li ^{62b}, J. Li ^{62c}, K. Li ¹³⁸, L. Li ^{62c}, M. Li ^{14a,14d}, Q.Y. Li ^{62a}, S. Li ^{14a,14d}, S. Li ^{62d,62c,e}, T. Li ^{62b}, X. Li ¹⁰⁴, Z. Li ^{62b}, Z. Li ¹²⁶, Z. Li ¹⁰⁴, Z. Li ⁹², Z. Li ^{14a,14d}, Z. Liang ^{14a}, M. Liberatore ⁴⁸, B. Liberti ^{76a}, K. Lie ^{64c}, J. Lieber Marin ^{82b}, K. Lin ¹⁰⁷, R.A. Linck ⁶⁸, R.E. Lindley ⁷, J.H. Lindon ², A. Linss ⁴⁸, E. Lipeles ¹²⁸, A. Lipniacka ¹⁶, A. Lister ¹⁶⁴, J.D. Little ⁴, B. Liu ^{14a}, B.X. Liu ¹⁴², D. Liu ^{62d,62c}, J.B. Liu ^{62a}, J.K.K. Liu ³², K. Liu ^{62d,62c}, M. Liu ^{62a}, M.Y. Liu ^{62a}, P. Liu ^{14a}, Q. Liu ^{62d,138,62c}, X. Liu ^{62a}, Y. Liu ^{14c,14d}, Y.L. Liu ¹⁰⁶, Y.W. Liu ^{62a}, M. Livan ^{73a,73b}, J. Llorente Merino ¹⁴², S.L. Lloyd ⁹⁴, E.M. Lobodzinska ⁴⁸, P. Loch ⁷, S. Loffredo ^{76a,76b}, T. Lohse ¹⁸, K. Lohwasser ¹³⁹, M. Lokajicek ^{131,*}, J.D. Long ¹⁶², I. Longarini ¹⁶⁰,

L. Longo ^{70a,70b}, R. Longo ¹⁶², I. Lopez Paz ⁶⁷, A. Lopez Solis ⁴⁸, J. Lorenz ¹⁰⁹,
 N. Lorenzo Martinez ⁴, A.M. Lory ¹⁰⁹, X. Lou ^{47a,47b}, X. Lou ^{14a,14d}, A. Lounis ⁶⁶, J. Love ⁶,
 P.A. Love ⁹¹, J.J. Lozano Bahilo ¹⁶³, G. Lu ^{14a,14d}, M. Lu ⁸⁰, S. Lu ¹²⁸, Y.J. Lu ⁶⁵,
 H.J. Lubatti ¹³⁸, C. Luci ^{75a,75b}, F.L. Lucio Alves ^{14c}, A. Lucotte ⁶⁰, F. Luehring ⁶⁸, I. Luise ¹⁴⁵,
 O. Lukianchuk ⁶⁶, O. Lundberg ¹⁴⁴, B. Lund-Jensen ¹⁴⁴, N.A. Luongo ¹²³, M.S. Lutz ¹⁵¹,
 D. Lynn ²⁹, H. Lyons⁹², R. Lysak ¹³¹, E. Lytken ⁹⁸, F. Lyu ^{14a}, V. Lyubushkin ³⁸,
 T. Lyubushkina ³⁸, M.M. Lyukova ¹⁴⁵, H. Ma ²⁹, L.L. Ma ^{62b}, Y. Ma ⁹⁶, D.M. Mac Donell ¹⁶⁵,
 G. Maccarrone ⁵³, J.C. MacDonald ¹³⁹, R. Madar ⁴⁰, W.F. Mader ⁵⁰, J. Maeda ⁸⁴, T. Maeno ²⁹,
 M. Maerker ⁵⁰, H. Maguire ¹³⁹, D.J. Mahon ⁴¹, A. Maio ^{130a,130b,130d}, K. Maj ^{85a},
 O. Majersky ^{28a}, S. Majewski ¹²³, N. Makovec ⁶⁶, V. Maksimovic ¹⁵, B. Malaescu ¹²⁷,
 Pa. Malecki ⁸⁶, V.P. Maleev ³⁷, F. Malek ⁶⁰, D. Malito ^{43b,43a}, U. Mallik ⁸⁰, C. Malone ³²,
 S. Maltezos¹⁰, S. Malyukov³⁸, J. Mamuzic ¹³, G. Mancini ⁵³, G. Manco ^{73a,73b}, J.P. Mandalia ⁹⁴,
 I. Mandić ⁹³, L. Manhaes de Andrade Filho ^{82a}, I.M. Maniatis ¹⁶⁹, J. Manjarres Ramos ⁵⁰,
 D.C. Mankad ¹⁶⁹, A. Mann ¹⁰⁹, B. Mansoulie ¹³⁵, S. Manzoni ³⁶, A. Marantis ^{152,w},
 G. Marchiori ⁵, M. Marcisovsky ¹³¹, C. Marcon ^{71a,71b}, M. Marinescu ²⁰, M. Marjanovic ¹²⁰,
 E.J. Marshall ⁹¹, Z. Marshall ^{17a}, S. Marti-Garcia ¹⁶³, T.A. Martin ¹⁶⁷, V.J. Martin ⁵²,
 B. Martin dit Latour ¹⁶, L. Martinelli ^{75a,75b}, M. Martinez ^{13,x}, P. Martinez Agullo ¹⁶³,
 V.I. Martinez Outschoorn ¹⁰³, P. Martinez Suarez ¹³, S. Martin-Haugh ¹³⁴, V.S. Martoiu ^{27b},
 A.C. Martyniuk ⁹⁶, A. Marzin ³⁶, S.R. Maschek ¹¹⁰, D. Mascione ^{78a,78b}, L. Masetti ¹⁰⁰,
 T. Mashimo ¹⁵³, J. Masik ¹⁰¹, A.L. Maslennikov ³⁷, L. Massa ^{23b}, P. Massarotti ^{72a,72b},
 P. Mastrandrea ^{74a,74b}, A. Mastroberardino ^{43b,43a}, T. Masubuchi ¹⁵³, T. Mathisen ¹⁶¹,
 N. Matsuzawa¹⁵³, J. Maurer ^{27b}, B. Maček ⁹³, D.A. Maximov ³⁷, R. Mazini ¹⁴⁸, I. Maznas ^{152,f},
 M. Mazza ¹⁰⁷, S.M. Mazza ¹³⁶, C. Mc Ginn ²⁹, J.P. Mc Gowan ¹⁰⁴, S.P. Mc Kee ¹⁰⁶,
 E.F. McDonald ¹⁰⁵, A.E. McDougall ¹¹⁴, J.A. Mcfayden ¹⁴⁶, G. Mchedlidze ^{149b},
 R.P. Mckenzie ^{33g}, T.C. Mclachlan ⁴⁸, D.J. Mclaughlin ⁹⁶, K.D. McLean ¹⁶⁵, S.J. McMahon ¹³⁴,
 P.C. McNamara ¹⁰⁵, C.M. Mcpartland ⁹², R.A. McPherson ^{165,ab}, T. Megy ⁴⁰, S. Mehlhase ¹⁰⁹,
 A. Mehta ⁹², B. Meirose ⁴⁵, D. Melini ¹⁵⁰, B.R. Mellado Garcia ^{33g}, A.H. Melo ⁵⁵,
 F. Meloni ⁴⁸, E.D. Mendes Gouveia ^{130a}, A.M. Mendes Jacques Da Costa ²⁰, H.Y. Meng ¹⁵⁵,
 L. Meng ⁹¹, S. Menke ¹¹⁰, M. Mentink ³⁶, E. Meoni ^{43b,43a}, C. Merlassino ¹²⁶,
 L. Merola ^{72a,72b}, C. Meroni ^{71a}, G. Merz¹⁰⁶, O. Meshkov ³⁷, J. Metcalfe ⁶, A.S. Mete ⁶,
 C. Meyer ⁶⁸, J-P. Meyer ¹³⁵, M. Michetti ¹⁸, R.P. Middleton ¹³⁴, L. Mijović ⁵²,
 G. Mikenberg ¹⁶⁹, M. Mikesikova ¹³¹, M. Mikuž ⁹³, H. Mildner ¹³⁹, A. Milic ³⁶,
 C.D. Milke ⁴⁴, D.W. Miller ³⁹, L.S. Miller ³⁴, A. Milov ¹⁶⁹, D.A. Milstead^{47a,47b}, T. Min^{14c},
 A.A. Minaenko ³⁷, I.A. Minashvili ^{149b}, L. Mince ⁵⁹, A.I. Mincer ¹¹⁷, B. Mindur ^{85a},
 M. Mineev ³⁸, Y. Mino ⁸⁷, L.M. Mir ¹³, M. Miralles Lopez ¹⁶³, M. Mironova ¹²⁶,
 M.C. Missio ¹¹³, T. Mitani ¹⁶⁸, A. Mitra ¹⁶⁷, V.A. Mitsou ¹⁶³, O. Miu ¹⁵⁵, P.S. Miyagawa ⁹⁴,
 Y. Miyazaki⁸⁹, A. Mizukami ⁸³, J.U. Mjörnmark ⁹⁸, T. Mkrtchyan ^{63a}, T. Mlinarevic ⁹⁶,
 M. Mlynarikova ³⁶, T. Moa ^{47a,47b}, S. Mobius ⁵⁵, K. Mochizuki ¹⁰⁸, P. Moder ⁴⁸, P. Mogg ¹⁰⁹,
 A.F. Mohammed ^{14a,14d}, S. Mohapatra ⁴¹, G. Mokgatitswane ^{33g}, B. Mondal ¹⁴¹, S. Mondal ¹³²,
 K. Mönig ⁴⁸, E. Monnier ¹⁰², L. Monsonis Romero¹⁶³, J. Montejo Berlingen ³⁶, M. Montella ¹¹⁹,
 F. Monticelli ⁹⁰, N. Morange ⁶⁶, A.L. Moreira De Carvalho ^{130a}, M. Moreno Llácer ¹⁶³,
 C. Moreno Martinez ⁵⁶, P. Morettini ^{57b}, S. Morgenstern ¹⁶⁷, M. Morii ⁶¹, M. Morinaga ¹⁵³,
 A.K. Morley ³⁶, F. Morodei ^{75a,75b}, L. Morvaj ³⁶, P. Moschovakos ³⁶, B. Moser ³⁶,
 M. Mosidze^{149b}, T. Moskalets ⁵⁴, P. Moskvitina ¹¹³, J. Moss ^{31,q}, E.J.W. Moyse ¹⁰³,
 O. Mtintsilana ^{33g}, S. Muanza ¹⁰², J. Mueller ¹²⁹, D. Muenstermann ⁹¹, R. Müller ¹⁹,
 G.A. Mullier ¹⁶¹, J.J. Mullin¹²⁸, D.P. Mungo ¹⁵⁵, J.L. Munoz Martinez ¹³, D. Munoz Perez ¹⁶³,
 F.J. Munoz Sanchez ¹⁰¹, M. Murin ¹⁰¹, W.J. Murray ^{167,134}, A. Murrone ^{71a,71b}, J.M. Muse ¹²⁰,

M. Muškinja ^{17a}, C. Mwewa ²⁹, A.G. Myagkov ^{37,a}, A.J. Myers ⁸, A.A. Myers ¹²⁹, G. Myers ⁶⁸,
M. Myska ¹³², B.P. Nachman ^{17a}, O. Nackenhorst ⁴⁹, A. Nag ⁵⁰, K. Nagai ¹²⁶, K. Nagano ⁸³,
J.L. Nagle ^{29,ao}, E. Nagy ¹⁰², A.M. Nairz ³⁶, Y. Nakahama ⁸³, K. Nakamura ⁸³, H. Nanjo ¹²⁴,
R. Narayan ⁴⁴, E.A. Narayanan ¹¹², I. Naryshkin ³⁷, M. Naseri ³⁴, C. Nass ²⁴, G. Navarro ^{22a},
J. Navarro-Gonzalez ¹⁶³, R. Nayak ¹⁵¹, A. Nayaz ¹⁸, P.Y. Nechaeva ³⁷, F. Nechansky ⁴⁸,
L. Nedic ¹²⁶, T.J. Neep ²⁰, A. Negri ^{73a,73b}, M. Negrini ^{23b}, C. Nellist ¹¹³, C. Nelson ¹⁰⁴,
K. Nelson ¹⁰⁶, S. Nemecek ¹³¹, M. Nessi ^{36,j}, M.S. Neubauer ¹⁶², F. Neuhaus ¹⁰⁰,
J. Neundorff ⁴⁸, R. Newhouse ¹⁶⁴, P.R. Newman ²⁰, C.W. Ng ¹²⁹, Y.S. Ng ¹⁸, Y.W.Y. Ng ⁴⁸,
B. Ngair ^{35e}, H.D.N. Nguyen ¹⁰⁸, R.B. Nickerson ¹²⁶, R. Nicolaidou ¹³⁵, J. Nielsen ¹³⁶,
M. Niemeyer ⁵⁵, N. Nikiforou ³⁶, V. Nikolaenko ^{37,a}, I. Nikolic-Audit ¹²⁷, K. Nikolopoulos ²⁰,
P. Nilsson ²⁹, I. Ninca ⁴⁸, H.R. Nindhito ⁵⁶, A. Nisati ^{75a}, N. Nishu ², R. Nisius ¹¹⁰,
J-E. Nitschke ⁵⁰, E.K. Nkadimeng ^{33g}, S.J. Noacco Rosende ⁹⁰, T. Nobe ¹⁵³, D.L. Noel ³²,
Y. Noguchi ⁸⁷, T. Nommensen ¹⁴⁷, M.A. Nomura ²⁹, M.B. Norfolk ¹³⁹, R.R.B. Norisam ⁹⁶,
B.J. Norman ³⁴, J. Novak ⁹³, T. Novak ⁴⁸, O. Novgorodova ⁵⁰, L. Novotny ¹³², R. Novotny ¹¹²,
L. Nozka ¹²², K. Ntekas ¹⁶⁰, N.M.J. Nunes De Moura Junior ^{82b}, E. Nurse ⁹⁶, F.G. Oakham ^{34,al},
J. Ocariz ¹²⁷, A. Ochi ⁸⁴, I. Ochoa ^{130a}, S. Oerdek ¹⁶¹, J.T. Offermann ³⁹, A. Ogrodnik ^{85a},
A. Oh ¹⁰¹, C.C. Ohm ¹⁴⁴, H. Oide ⁸³, R. Oishi ¹⁵³, M.L. Ojeda ⁴⁸, Y. Okazaki ⁸⁷,
M.W. O'Keefe ⁹², Y. Okumura ¹⁵³, A. Olariu ^{27b}, L.F. Oleiro Seabra ^{130a}, S.A. Olivares Pino ^{137e},
D. Oliveira Damazio ²⁹, D. Oliveira Goncalves ^{82a}, J.L. Oliver ¹⁶⁰, M.J.R. Olsson ¹⁶⁰,
A. Olszewski ⁸⁶, J. Olszowska ^{86,*}, Ö.O. Öncel ⁵⁴, D.C. O'Neil ¹⁴², A.P. O'Neill ¹⁹,
A. Onofre ^{130a,130e}, P.U.E. Onyisi ¹¹, M.J. Oreglia ³⁹, G.E. Orellana ⁹⁰, D. Orestano ^{77a,77b},
N. Orlando ¹³, R.S. Orr ¹⁵⁵, V. O'Shea ⁵⁹, R. Ospanov ^{62a}, G. Otero y Garzon ³⁰, H. Otono ⁸⁹,
P.S. Ott ^{63a}, G.J. Ottino ^{17a}, M. Ouchrif ^{35d}, J. Ouellette ^{29,ao}, F. Ould-Saada ¹²⁵, M. Owen ⁵⁹,
R.E. Owen ¹³⁴, K.Y. Oyulmaz ^{21a}, V.E. Ozcan ^{21a}, N. Ozturk ⁸, S. Ozturk ^{21d}, J. Pacalt ¹²²,
H.A. Pacey ³², K. Pachal ⁵¹, A. Pacheco Pages ¹³, C. Padilla Aranda ¹³, G. Padovano ^{75a,75b},
S. Pagan Griso ^{17a}, G. Palacino ⁶⁸, A. Palazzo ^{70a,70b}, S. Palestini ³⁶, M. Palka ^{85b}, J. Pan ¹⁷²,
T. Pan ^{64a}, D.K. Panchal ¹¹, C.E. Pandini ¹¹⁴, J.G. Panduro Vazquez ⁹⁵, H. Pang ^{14b}, P. Pani ⁴⁸,
G. Panizzo ^{69a,69c}, L. Paolozzi ⁵⁶, C. Papadatos ¹⁰⁸, S. Parajuli ⁴⁴, A. Paramonov ⁶,
C. Paraskevopoulos ¹⁰, D. Paredes Hernandez ^{64b}, T.H. Park ¹⁵⁵, M.A. Parker ³², F. Parodi ^{57b,57a},
E.W. Parrish ¹¹⁵, V.A. Parrish ⁵², J.A. Parsons ⁴¹, U. Parzefall ⁵⁴, B. Pascual Dias ¹⁰⁸,
L. Pascual Dominguez ¹⁵¹, V.R. Pascuzzi ^{17a}, F. Pasquali ¹¹⁴, E. Pasqualucci ^{75a}, S. Passaggio ^{57b},
F. Pastore ⁹⁵, P. Pasuwan ^{47a,47b}, P. Patel ⁸⁶, J.R. Pater ¹⁰¹, T. Pauly ³⁶, J. Pearkes ¹⁴³,
M. Pedersen ¹²⁵, R. Pedro ^{130a}, S.V. Peleganchuk ³⁷, O. Penc ³⁶, E.A. Pender ⁵², C. Peng ^{64b},
H. Peng ^{62a}, K.E. Pensi ¹⁰⁹, M. Penzin ³⁷, B.S. Peralva ^{82d}, A.P. Pereira Peixoto ⁶⁰,
L. Pereira Sanchez ^{47a,47b}, D.V. Perepelitsa ^{29,ao}, E. Perez Codina ^{156a}, M. Perganti ¹⁰,
L. Perini ^{71a,71b,*}, H. Pernegger ³⁶, S. Perrella ³⁶, A. Perrevoort ¹¹³, O. Perrin ⁴⁰, K. Peters ⁴⁸,
R.F.Y. Peters ¹⁰¹, B.A. Petersen ³⁶, T.C. Petersen ⁴², E. Petit ¹⁰², V. Petousis ¹³²,
C. Petridou ^{152,f}, A. Petrukhin ¹⁴¹, M. Pettee ^{17a}, N.E. Pettersson ³⁶, A. Petukhov ³⁷,
K. Petukhova ¹³³, A. Peyaud ¹³⁵, R. Pezoa ^{137f}, L. Pezzotti ³⁶, G. Pezzullo ¹⁷², T.M. Pham ¹⁷⁰,
T. Pham ¹⁰⁵, P.W. Phillips ¹³⁴, M.W. Phipps ¹⁶², G. Piacquadio ¹⁴⁵, E. Pianori ^{17a},
F. Piazza ^{71a,71b}, R. Piegai ³⁰, D. Pietreanu ^{27b}, A.D. Pilkington ¹⁰¹, M. Pinamonti ^{69a,69c},
J.L. Pinfeld ², B.C. Pinheiro Pereira ^{130a}, C. Pitman Donaldson ⁹⁶, D.A. Pizzi ³⁴,
L. Pizzimento ^{76a,76b}, A. Pizzini ¹¹⁴, M.-A. Pleier ²⁹, V. Plesanovs ⁵⁴, V. Pleskot ¹³³, E. Plotnikova ³⁸,
G. Poddar ⁴, R. Poettgen ⁹⁸, L. Poggioli ¹²⁷, I. Pogrebnyak ¹⁰⁷, D. Pohl ²⁴, I. Pokharel ⁵⁵,
S. Polacek ¹³³, G. Polesello ^{73a}, A. Poley ^{142,156a}, R. Polifka ¹³², A. Polini ^{23b}, C.S. Pollard ¹⁶⁷,
Z.B. Pollock ¹¹⁹, V. Polychronakos ²⁹, E. Pompa Pacchi ^{75a,75b}, D. Ponomarenko ³⁷,
L. Pontecorvo ³⁶, S. Popa ^{27a}, G.A. Popeneciu ^{27d}, D.M. Portillo Quintero ^{156a}, S. Pospisil ¹³²,

P. Postolache [ID27c](#), K. Potamianos [ID126](#), I.N. Potrap [ID38](#), C.J. Potter [ID32](#), H. Potti [ID1](#), T. Poulsen [ID48](#),
 J. Poveda [ID163](#), M.E. Pozo Astigarraga [ID36](#), A. Prades Ibanez [ID163](#), M.M. Prapa [ID46](#), J. Pretel [ID54](#),
 D. Price [ID101](#), M. Primavera [ID70a](#), M.A. Principe Martin [ID99](#), R. Privara [ID122](#), M.L. Proffitt [ID138](#),
 N. Proklova [ID128](#), K. Prokofiev [ID64c](#), G. Proto [ID76a,76b](#), S. Protopopescu [ID29](#), J. Proudfoot [ID6](#),
 M. Przybycien [ID85a](#), J.E. Puddefoot [ID139](#), D. Pudzha [ID37](#), P. Puzo [ID66](#), D. Pyatiizbyantseva [ID37](#),
 J. Qian [ID106](#), D. Qichen [ID101](#), Y. Qin [ID101](#), T. Qiu [ID94](#), A. Quadt [ID55](#), M. Queitsch-Maitland [ID101](#),
 G. Quetant [ID56](#), G. Rabanal Bolanos [ID61](#), D. Rafanoharana [ID54](#), F. Ragusa [ID71a,71b](#), J.L. Rainbolt [ID39](#),
 J.A. Raine [ID56](#), S. Rajagopalan [ID29](#), E. Ramakoti [ID37](#), K. Ran [ID48,14d](#), N.P. Rapheeha [ID33g](#),
 V. Raskina [ID127](#), D.F. Rassloff [ID63a](#), S. Rave [ID100](#), B. Ravina [ID55](#), I. Ravinovich [ID169](#), M. Raymond [ID36](#),
 A.L. Read [ID125](#), N.P. Readioff [ID139](#), D.M. Rebutzi [ID73a,73b](#), G. Redlinger [ID29](#), K. Reeves [ID45](#),
 J.A. Reidelsturz [ID171](#), D. Reikher [ID151](#), A. Rej [ID141](#), C. Rembser [ID36](#), A. Renardi [ID48](#), M. Renda [ID27b](#),
 M.B. Rendel [ID110](#), F. Renner [ID48](#), A.G. Rennie [ID59](#), S. Resconi [ID71a](#), M. Ressegotti [ID57b,57a](#),
 E.D. Resseguie [ID17a](#), S. Rettie [ID36](#), J.G. Reyes Rivera [ID107](#), B. Reynolds [ID119](#), E. Reynolds [ID17a](#),
 M. Rezaei Estabragh [ID171](#), O.L. Rezanova [ID37](#), P. Reznicek [ID133](#), N. Ribaric [ID91](#), E. Ricci [ID78a,78b](#),
 R. Richter [ID110](#), S. Richter [ID47a,47b](#), E. Richter-Was [ID85b](#), M. Ridel [ID127](#), S. Ridouani [ID35d](#), P. Rieck [ID117](#),
 P. Riedler [ID36](#), M. Rijssenbeek [ID145](#), A. Rimoldi [ID73a,73b](#), M. Rimoldi [ID48](#), L. Rinaldi [ID23b,23a](#),
 T.T. Rinn [ID29](#), M.P. Rinnagel [ID109](#), G. Ripellino [ID144](#), I. Riu [ID13](#), P. Rivadeneira [ID48](#),
 J.C. Rivera Vergara [ID165](#), F. Rizatdinova [ID121](#), E. Rizvi [ID94](#), C. Rizzi [ID56](#), B.A. Roberts [ID167](#),
 B.R. Roberts [ID17a](#), S.H. Robertson [ID104,ab](#), M. Robin [ID48](#), D. Robinson [ID32](#), C.M. Robles Gajardo [ID137f](#),
 M. Robles Manzano [ID100](#), A. Robson [ID59](#), A. Rocchi [ID76a,76b](#), C. Roda [ID74a,74b](#), S. Rodriguez Bosca [ID63a](#),
 Y. Rodriguez Garcia [ID22a](#), A. Rodriguez Rodriguez [ID54](#), A.M. Rodríguez Vera [ID156b](#), S. Roe [ID36](#),
 J.T. Roemer [ID160](#), A.R. Roepe-Gier [ID120](#), J. Roggel [ID171](#), O. Røhne [ID125](#), R.A. Rojas [ID103](#),
 B. Roland [ID54](#), C.P.A. Roland [ID68](#), J. Roloff [ID29](#), A. Romaniouk [ID37](#), E. Romano [ID73a,73b](#),
 M. Romano [ID23b](#), A.C. Romero Hernandez [ID162](#), N. Rompotis [ID92](#), L. Roos [ID127](#), S. Rosati [ID75a](#),
 B.J. Rosser [ID39](#), E. Rossi [ID4](#), E. Rossi [ID72a,72b](#), L.P. Rossi [ID57b](#), L. Rossini [ID48](#), R. Rosten [ID119](#),
 M. Rotaru [ID27b](#), B. Rottler [ID54](#), C. Rougier [ID102,af](#), D. Rousseau [ID66](#), D. Rousso [ID32](#), G. Rovelli [ID73a,73b](#),
 A. Roy [ID162](#), A. Rozanov [ID102](#), Y. Rozen [ID150](#), X. Ruan [ID33g](#), A. Rubio Jimenez [ID163](#), A.J. Ruby [ID92](#),
 V.H. Ruelas Rivera [ID18](#), T.A. Ruggeri [ID1](#), F. Rühr [ID54](#), A. Ruiz-Martinez [ID163](#), A. Rummler [ID36](#),
 Z. Rurikova [ID54](#), N.A. Rusakovich [ID38](#), H.L. Russell [ID165](#), J.P. Rutherford [ID7](#), K. Rybacki [ID91](#),
 M. Rybar [ID133](#), E.B. Rye [ID125](#), A. Ryzhov [ID37](#), J.A. Sabater Iglesias [ID56](#), P. Sabatini [ID163](#),
 L. Sabetta [ID75a,75b](#), H.F-W. Sadrozinski [ID136](#), F. Safai Tehrani [ID75a](#), B. Safarzadeh Samani [ID146](#),
 M. Safdari [ID143](#), S. Saha [ID104](#), M. Sahinsoy [ID110](#), M. Saimpert [ID135](#), M. Saito [ID153](#), T. Saito [ID153](#),
 D. Salamani [ID36](#), G. Salamanna [ID77a,77b](#), A. Salnikov [ID143](#), J. Salt [ID163](#), A. Salvador Salas [ID13](#),
 D. Salvatore [ID43b,43a](#), F. Salvatore [ID146](#), A. Salzburger [ID36](#), D. Sammel [ID54](#), D. Sampsonidis [ID152,f](#),
 D. Sampsonidou [ID62d,62c](#), J. Sánchez [ID163](#), A. Sanchez Pineda [ID4](#), V. Sanchez Sebastian [ID163](#),
 H. Sandaker [ID125](#), C.O. Sander [ID48](#), J.A. Sandesara [ID103](#), M. Sandhoff [ID171](#), C. Sandoval [ID22b](#),
 D.P.C. Sankey [ID134](#), T. Sano [ID87](#), A. Sansoni [ID53](#), L. Santi [ID75a,75b](#), C. Santoni [ID40](#), H. Santos [ID130a,130b](#),
 S.N. Santpur [ID17a](#), A. Santra [ID169](#), K.A. Saoucha [ID139](#), J.G. Saraiva [ID130a,130d](#), J. Sardain [ID7](#),
 O. Sasaki [ID83](#), K. Sato [ID157](#), C. Sauer [ID63b](#), F. Sauerburger [ID54](#), E. Sauvan [ID4](#), P. Savard [ID155,al](#),
 R. Sawada [ID153](#), C. Sawyer [ID134](#), L. Sawyer [ID97](#), I. Sayago Galvan [ID163](#), C. Sbarra [ID23b](#), A. Sbrizzi [ID23b,23a](#),
 T. Scanlon [ID96](#), J. Schaarschmidt [ID138](#), P. Schacht [ID110](#), D. Schaefer [ID39](#), U. Schäfer [ID100](#),
 A.C. Schaffer [ID66,44](#), D. Schaile [ID109](#), R.D. Schamberger [ID145](#), E. Schanet [ID109](#), C. Scharf [ID18](#),
 M.M. Schefer [ID19](#), V.A. Schegelsky [ID37](#), D. Scheirich [ID133](#), F. Schenck [ID18](#), M. Schernau [ID160](#),
 C. Scheulen [ID55](#), C. Schiavi [ID57b,57a](#), Z.M. Schillaci [ID26](#), E.J. Schioppa [ID70a,70b](#), M. Schioppa [ID43b,43a](#),
 B. Schlag [ID100](#), K.E. Schleicher [ID54](#), S. Schlenker [ID36](#), J. Schmeing [ID171](#), M.A. Schmidt [ID171](#),
 K. Schmieden [ID100](#), C. Schmitt [ID100](#), S. Schmitt [ID48](#), L. Schoeffel [ID135](#), A. Schoening [ID63b](#),
 P.G. Scholer [ID54](#), E. Schopf [ID126](#), M. Schott [ID100](#), J. Schovancova [ID36](#), S. Schramm [ID56](#),

F. Schroeder ¹⁷¹, H-C. Schultz-Coulon ^{63a}, M. Schumacher ⁵⁴, B.A. Schumm ¹³⁶, Ph. Schune ¹³⁵,
 H.R. Schwartz ¹³⁶, A. Schwartzman ¹⁴³, T.A. Schwarz ¹⁰⁶, Ph. Schwemling ¹³⁵,
 R. Schwienhorst ¹⁰⁷, A. Sciandra ¹³⁶, G. Sciolla ²⁶, F. Scuri ^{74a}, F. Scutti ¹⁰⁵, C.D. Sebastiani ⁹²,
 K. Sedlaczek ⁴⁹, P. Seema ¹⁸, S.C. Seidel ¹¹², A. Seiden ¹³⁶, B.D. Seidlitz ⁴¹, C. Seitz ⁴⁸,
 J.M. Seixas ^{82b}, G. Sekhniaidze ^{72a}, S.J. Sekula ⁴⁴, L. Selem ⁴, N. Semprini-Cesari ^{23b,23a},
 S. Sen ⁵¹, D. Sengupta ⁵⁶, V. Senthilkumar ¹⁶³, L. Serin ⁶⁶, L. Serkin ^{69a,69b}, M. Sessa ^{77a,77b},
 H. Severini ¹²⁰, F. Sforza ^{57b,57a}, A. Sfyrta ⁵⁶, E. Shabalina ⁵⁵, R. Shaheen ¹⁴⁴,
 J.D. Shahinian ¹²⁸, D. Shaked Renous ¹⁶⁹, L.Y. Shan ^{14a}, M. Shapiro ^{17a}, A. Sharma ³⁶,
 A.S. Sharma ¹⁶⁴, P. Sharma ⁸⁰, S. Sharma ⁴⁸, P.B. Shatalov ³⁷, K. Shaw ¹⁴⁶, S.M. Shaw ¹⁰¹,
 Q. Shen ^{62c,5}, P. Sherwood ⁹⁶, L. Shi ⁹⁶, C.O. Shimmin ¹⁷², Y. Shimogama ¹⁶⁸, J.D. Shinner ⁹⁵,
 I.P.J. Shipsey ¹²⁶, S. Shirabe ⁶⁰, M. Shiyakova ^{38,z}, J. Shlomi ¹⁶⁹, M.J. Shochet ³⁹, J. Shojaii ¹⁰⁵,
 D.R. Shope ¹²⁵, S. Shrestha ^{119,ap}, E.M. Shrif ^{33g}, M.J. Shroff ¹⁶⁵, P. Sicho ¹³¹,
 A.M. Sickles ¹⁶², E. Sideras Haddad ^{33g}, A. Sidoti ^{23b}, F. Siegert ⁵⁰, Dj. Sijacki ¹⁵,
 R. Sikora ^{85a}, F. Sili ⁹⁰, J.M. Silva ²⁰, M.V. Silva Oliveira ³⁶, S.B. Silverstein ^{47a}, S. Simion ⁶⁶,
 R. Simoniello ³⁶, E.L. Simpson ⁵⁹, L.R. Simpson ¹⁰⁶, N.D. Simpson ⁹⁸, S. Simsek ^{21d},
 S. Sindhu ⁵⁵, P. Sinervo ¹⁵⁵, S. Singh ¹⁴², S. Singh ¹⁵⁵, S. Sinha ⁴⁸, S. Sinha ^{33g},
 M. Sioli ^{23b,23a}, I. Siral ³⁶, S.Yu. Sivoklov ^{37,*}, J. Sjölin ^{47a,47b}, A. Skaf ⁵⁵, E. Skorda ⁹⁸,
 P. Skubic ¹²⁰, M. Slawinska ⁸⁶, V. Smakhtin ¹⁶⁹, B.H. Smart ¹³⁴, J. Smiesko ³⁶, S.Yu. Smirnov ³⁷,
 Y. Smirnov ³⁷, L.N. Smirnova ^{37,a}, O. Smirnova ⁹⁸, A.C. Smith ⁴¹, E.A. Smith ³⁹,
 H.A. Smith ¹²⁶, J.L. Smith ⁹², R. Smith ¹⁴³, M. Smizanska ⁹¹, K. Smolek ¹³², A. Smykiewicz ⁸⁶,
 A.A. Snesarev ³⁷, H.L. Snoek ¹¹⁴, S. Snyder ²⁹, R. Sobie ^{165,ab}, A. Soffer ¹⁵¹,
 C.A. Solans Sanchez ³⁶, E.Yu. Soldatov ³⁷, U. Soldevila ¹⁶³, A.A. Solodkov ³⁷, S. Solomon ⁵⁴,
 A. Soloshenko ³⁸, K. Solovieva ⁵⁴, O.V. Solovyanov ⁴⁰, V. Solovyev ³⁷, P. Sommer ³⁶,
 A. Sonay ¹³, W.Y. Song ^{156b}, J.M. Sonneveld ¹¹⁴, A. Sopczak ¹³², A.L. Sopio ⁹⁶,
 F. Sopkova ^{28b}, V. Sothilingam ^{63a}, S. Sottocornola ⁶⁸, R. Soualah ^{116b}, Z. Soumami ^{35e},
 D. South ⁴⁸, S. Spagnolo ^{70a,70b}, M. Spalla ¹¹⁰, F. Spanò ⁹⁵, D. Sperlich ⁵⁴, G. Spigo ³⁶,
 M. Spina ¹⁴⁶, S. Spinali ⁹¹, D.P. Spiteri ⁵⁹, M. Spousta ¹³³, E.J. Staats ³⁴, A. Stabile ^{71a,71b},
 R. Stamen ^{63a}, M. Stamenkovic ¹¹⁴, A. Stampekis ²⁰, M. Standke ²⁴, E. Stanecka ⁸⁶,
 M.V. Stange ⁵⁰, B. Stanislaus ^{17a}, M.M. Stanitzki ⁴⁸, M. Stankaityte ¹²⁶, B. Stapf ⁴⁸,
 E.A. Starchenko ³⁷, G.H. Stark ¹³⁶, J. Stark ^{102,af}, D.M. Starko ^{156b}, P. Staroba ¹³¹,
 P. Starovoitov ^{63a}, S. Stärz ¹⁰⁴, R. Staszewski ⁸⁶, G. Stavropoulos ⁴⁶, J. Steentoft ¹⁶¹,
 P. Steinberg ²⁹, A.L. Steinhebel ¹²³, B. Stelzer ^{142,156a}, H.J. Stelzer ¹²⁹, O. Stelzer-Chilton ^{156a},
 H. Stenzel ⁵⁸, T.J. Stevenson ¹⁴⁶, G.A. Stewart ³⁶, M.C. Stockton ³⁶, G. Stoicea ^{27b},
 M. Stolarski ^{130a}, S. Stonjek ¹¹⁰, A. Straessner ⁵⁰, J. Strandberg ¹⁴⁴, S. Strandberg ^{47a,47b},
 M. Strauss ¹²⁰, T. Strebler ¹⁰², P. Strizenec ^{28b}, R. Ströhmer ¹⁶⁶, D.M. Strom ¹²³, L.R. Strom ⁴⁸,
 R. Stroynowski ⁴⁴, A. Strubig ^{47a,47b}, S.A. Stucci ²⁹, B. Stugu ¹⁶, J. Stupak ¹²⁰, N.A. Styles ⁴⁸,
 D. Su ¹⁴³, S. Su ^{62a}, W. Su ^{62d,138,62c}, X. Su ^{62a,66}, K. Sugizaki ¹⁵³, V.V. Sulin ³⁷,
 M.J. Sullivan ⁹², D.M.S. Sultan ^{78a,78b}, L. Sultanaliyeva ³⁷, S. Sultansoy ^{3b}, T. Sumida ⁸⁷,
 S. Sun ¹⁰⁶, S. Sun ¹⁷⁰, O. Sunneborn Gudnadottir ¹⁶¹, M.R. Sutton ¹⁴⁶, M. Svatos ¹³¹,
 M. Swiatlowski ^{156a}, T. Swirski ¹⁶⁶, I. Sykora ^{28a}, M. Sykora ¹³³, T. Sykora ¹³³, D. Ta ¹⁰⁰,
 K. Tackmann ^{48,y}, A. Taffard ¹⁶⁰, R. Tafirout ^{156a}, J.S. Tafoya Vargas ⁶⁶, R.H.M. Taibah ¹²⁷,
 R. Takashima ⁸⁸, K. Takeda ⁸⁴, E.P. Takeva ⁵², Y. Takubo ⁸³, M. Talby ¹⁰², A.A. Talyshv ³⁷,
 K.C. Tam ^{64b}, N.M. Tamir ¹⁵¹, A. Tanaka ¹⁵³, J. Tanaka ¹⁵³, R. Tanaka ⁶⁶, M. Tanasini ^{57b,57a},
 J. Tang ^{62c}, Z. Tao ¹⁶⁴, S. Tapia Araya ^{137f}, S. Tapprogge ¹⁰⁰, A. Tarek Abouelfadl Mohamed ¹⁰⁷,
 S. Tarem ¹⁵⁰, K. Tariq ^{62b}, G. Tarna ^{102,27b}, G.F. Tartarelli ^{71a}, P. Tas ¹³³, M. Tasevsky ¹³¹,
 E. Tassi ^{43b,43a}, A.C. Tate ¹⁶², G. Tateno ¹⁵³, Y. Tayalati ^{35e,aa}, G.N. Taylor ¹⁰⁵, W. Taylor ^{156b},
 H. Teagle ⁹², A.S. Tee ¹⁷⁰, R. Teixeira De Lima ¹⁴³, P. Teixeira-Dias ⁹⁵, J.J. Teoh ¹⁵⁵,

K. Terashi ¹⁵³, J. Terron ⁹⁹, S. Terzo ¹³, M. Testa ⁵³, R.J. Teuscher ^{155,ab}, A. Thaler ⁷⁹,
 O. Theiner ⁵⁶, N. Themistokleous ⁵², T. Thevenaux-Pelzer ¹⁸, O. Thielmann ¹⁷¹, D.W. Thomas ⁹⁵,
 J.P. Thomas ²⁰, E.A. Thompson ⁴⁸, P.D. Thompson ²⁰, E. Thomson ¹²⁸, E.J. Thorpe ⁹⁴,
 Y. Tian ⁵⁵, V. Tikhomirov ^{37,a}, Yu.A. Tikhonov ³⁷, S. Timoshenko ³⁷, E.X.L. Ting ¹, P. Tipton ¹⁷²,
 S. Tisserant ¹⁰², S.H. Tlou ^{33g}, A. Tnourji ⁴⁰, K. Todome ^{23b,23a}, S. Todorova-Nova ¹³³, S. Todt ⁵⁰,
 M. Togawa ⁸³, J. Tojo ⁸⁹, S. Tokár ^{28a}, K. Tokushuku ⁸³, O. Toldaiev ⁶⁸, R. Tombs ³²,
 M. Tomoto ^{83,111}, L. Tompkins ^{143,s}, K.W. Topolnicki ^{85b}, P. Tornambe ¹⁰³, E. Torrence ¹²³,
 H. Torres ⁵⁰, E. Torró Pastor ¹⁶³, M. Toscani ³⁰, C. Tosciri ³⁹, M. Tost ¹¹, D.R. Tovey ¹³⁹,
 A. Traeet ¹⁶, I.S. Trandafir ^{27b}, T. Trefzger ¹⁶⁶, A. Tricoli ²⁹, I.M. Trigger ^{156a},
 S. Trincaz-Duvoid ¹²⁷, D.A. Trischuk ²⁶, B. Trocmé ⁶⁰, A. Trofymov ⁶⁶, C. Troncon ^{71a},
 L. Truong ^{33c}, M. Trzebinski ⁸⁶, A. Trzupiek ⁸⁶, F. Tsai ¹⁴⁵, M. Tsai ¹⁰⁶, A. Tsiamis ^{152,f},
 P.V. Tsiareshka ³⁷, S. Tsigaridas ^{156a}, A. Tsirigotis ^{152,w}, V. Tsiskaridze ¹⁴⁵, E.G. Tskhadadze ^{149a},
 M. Tsopoulou ^{152,f}, Y. Tsujikawa ⁸⁷, I.I. Tsukerman ³⁷, V. Tsulaia ^{17a}, S. Tsuno ⁸³, O. Tsur ¹⁵⁰,
 D. Tsybychev ¹⁴⁵, Y. Tu ^{64b}, A. Tudorache ^{27b}, V. Tudorache ^{27b}, A.N. Tuna ³⁶, S. Turchikhin ³⁸,
 I. Turk Cakir ^{3a}, R. Turra ^{71a}, T. Turtuvshin ^{38,ac}, P.M. Tuts ⁴¹, S. Tzamarias ^{152,f}, P. Tzanis ¹⁰,
 E. Tzovara ¹⁰⁰, K. Uchida ¹⁵³, F. Ukegawa ¹⁵⁷, P.A. Ulloa Poblete ^{137c}, E.N. Umaka ²⁹,
 G. Unal ³⁶, M. Unal ¹¹, A. Undrus ²⁹, G. Unel ¹⁶⁰, J. Urban ^{28b}, P. Urquijo ¹⁰⁵, G. Usai ⁸,
 R. Ushioda ¹⁵⁴, M. Usman ¹⁰⁸, Z. Uysal ^{21b}, L. Vacavant ¹⁰², V. Vacek ¹³², B. Vachon ¹⁰⁴,
 K.O.H. Vadla ¹²⁵, T. Vafeiadis ³⁶, A. Vaitkus ⁹⁶, C. Valderanis ¹⁰⁹, E. Valdes Santurio ^{47a,47b},
 M. Valente ^{156a}, S. Valentinetti ^{23b,23a}, A. Valero ¹⁶³, A. Vallier ^{102,af}, J.A. Valls Ferrer ¹⁶³,
 D.R. Van Arneeman ¹¹⁴, T.R. Van Daalen ¹³⁸, P. Van Gemmeren ⁶, M. Van Rijnbach ^{125,36},
 S. Van Stroud ⁹⁶, I. Van Vulpen ¹¹⁴, M. Vanadia ^{76a,76b}, W. Vandelli ³⁶, M. Vandenbroucke ¹³⁵,
 E.R. Vandewall ¹²¹, D. Vannicola ¹⁵¹, L. Vannoli ^{57b,57a}, R. Vari ^{75a}, E.W. Varnes ⁷,
 C. Varni ^{17a}, T. Varol ¹⁴⁸, D. Varouchas ⁶⁶, L. Varriale ¹⁶³, K.E. Varvell ¹⁴⁷, M.E. Vasile ^{27b},
 L. Vaslin ⁴⁰, G.A. Vasquez ¹⁶⁵, F. Vazeille ⁴⁰, T. Vazquez Schroeder ³⁶, J. Veatch ³¹,
 V. Vecchio ¹⁰¹, M.J. Veen ¹⁰³, I. Veliscek ¹²⁶, L.M. Veloce ¹⁵⁵, F. Veloso ^{130a,130c},
 S. Veneziano ^{75a}, A. Ventura ^{70a,70b}, A. Verbytskyi ¹¹⁰, M. Verducci ^{74a,74b}, C. Vergis ²⁴,
 M. Verissimo De Araujo ^{82b}, W. Verkerke ¹¹⁴, J.C. Vermeulen ¹¹⁴, C. Vernieri ¹⁴³,
 P.J. Verschuuren ⁹⁵, M. Vessella ¹⁰³, M.C. Vetterli ^{142,al}, A. Vgenopoulos ^{152,f},
 N. Viaux Maira ^{137f}, T. Vickey ¹³⁹, O.E. Vickey Boeriu ¹³⁹, G.H.A. Viehhauser ¹²⁶, L. Vignani ^{63b},
 M. Villa ^{23b,23a}, M. Villaplana Perez ¹⁶³, E.M. Villhauer ⁵², E. Vilucchi ⁵³, M.G. Vincter ³⁴,
 G.S. Virdee ²⁰, A. Vishwakarma ⁵², C. Vittori ^{23b,23a}, I. Vivarelli ¹⁴⁶, V. Vladimirov ¹⁶⁷,
 E. Voevodina ¹¹⁰, F. Vogel ¹⁰⁹, P. Vokac ¹³², J. Von Ahnen ⁴⁸, E. Von Toerne ²⁴,
 B. Vormwald ³⁶, V. Vorobel ¹³³, K. Vorobev ³⁷, M. Vos ¹⁶³, K. Voss ¹⁴¹, J.H. Vossebeld ⁹²,
 M. Vozak ¹¹⁴, L. Vozdecky ⁹⁴, N. Vranjes ¹⁵, M. Vranjes Milosavljevic ¹⁵, M. Vreeswijk ¹¹⁴,
 R. Vuillermet ³⁶, O. Vujanovic ¹⁰⁰, I. Vukotic ³⁹, S. Wada ¹⁵⁷, C. Wagner ¹⁰³, W. Wagner ¹⁷¹,
 S. Wahdan ¹⁷¹, H. Wahlberg ⁹⁰, R. Wakasa ¹⁵⁷, M. Wakida ¹¹¹, V.M. Walbrecht ¹¹⁰,
 J. Walder ¹³⁴, R. Walker ¹⁰⁹, W. Walkowiak ¹⁴¹, A.M. Wang ⁶¹, A.Z. Wang ¹⁷⁰, C. Wang ^{62a},
 C. Wang ^{62c}, H. Wang ^{17a}, J. Wang ^{64a}, R.-J. Wang ¹⁰⁰, R. Wang ⁶¹, R. Wang ⁶,
 S.M. Wang ¹⁴⁸, S. Wang ^{62b}, T. Wang ^{62a}, W.T. Wang ⁸⁰, X. Wang ^{14c}, X. Wang ¹⁶²,
 X. Wang ^{62c}, Y. Wang ^{62d}, Y. Wang ^{14c}, Z. Wang ¹⁰⁶, Z. Wang ^{62d,51,62c}, Z. Wang ¹⁰⁶,
 A. Warburton ¹⁰⁴, R.J. Ward ²⁰, N. Warrack ⁵⁹, A.T. Watson ²⁰, H. Watson ⁵⁹, M.F. Watson ²⁰,
 G. Watts ¹³⁸, B.M. Waugh ⁹⁶, A.F. Webb ¹¹, C. Weber ²⁹, H.A. Weber ¹⁸, M.S. Weber ¹⁹,
 S.M. Weber ^{63a}, C. Wei ^{62a}, Y. Wei ¹²⁶, A.R. Weidberg ¹²⁶, J. Weingarten ⁴⁹, M. Weirich ¹⁰⁰,
 C. Weiser ⁵⁴, C.J. Wells ⁴⁸, T. Wenaus ²⁹, B. Wendland ⁴⁹, T. Wengler ³⁶, N.S. Wenke ¹¹⁰,
 N. Wermes ²⁴, M. Wessels ^{63a}, K. Whalen ¹²³, A.M. Wharton ⁹¹, A.S. White ⁶¹, A. White ⁸,
 M.J. White ¹, D. Whiteson ¹⁶⁰, L. Wickremasinghe ¹²⁴, W. Wiedenmann ¹⁷⁰, C. Wiel ⁵⁰,

M. Wielers ¹³⁴, C. Wigglesworth ⁴², L.A.M. Wiik-Fuchs ⁵⁴, D.J. Wilbern ¹²⁰, H.G. Wilkens ³⁶, D.M. Williams ⁴¹, H.H. Williams ¹²⁸, S. Williams ³², S. Willocq ¹⁰³, P.J. Windischhofer ¹²⁶, F. Winklmeier ¹²³, B.T. Winter ⁵⁴, J.K. Winter ¹⁰¹, M. Wittgen ¹⁴³, M. Wobisch ⁹⁷, R. Wölker ¹²⁶, J. Wollrath ¹⁶⁰, M.W. Wolter ⁸⁶, H. Wolters ^{130a,130c}, V.W.S. Wong ¹⁶⁴, A.F. Wongel ⁴⁸, S.D. Worm ⁴⁸, B.K. Wosiek ⁸⁶, K.W. Woźniak ⁸⁶, K. Wraight ⁵⁹, J. Wu ^{14a,14d}, M. Wu ^{64a}, M. Wu ¹¹³, S.L. Wu ¹⁷⁰, X. Wu ⁵⁶, Y. Wu ^{62a}, Z. Wu ^{135,62a}, J. Wuerzinger ¹²⁶, T.R. Wyatt ¹⁰¹, B.M. Wynne ⁵², S. Xella ⁴², L. Xia ^{14c}, M. Xia ^{14b}, J. Xiang ^{64c}, X. Xiao ¹⁰⁶, M. Xie ^{62a}, X. Xie ^{62a}, S. Xin ^{14a,14d}, J. Xiong ^{17a}, I. Xiotidis ¹⁴⁶, D. Xu ^{14a}, H. Xu ^{62a}, H. Xu ^{62a}, L. Xu ^{62a}, R. Xu ¹²⁸, T. Xu ¹⁰⁶, W. Xu ¹⁰⁶, Y. Xu ^{14b}, Z. Xu ^{62b}, Z. Xu ^{14a}, B. Yabsley ¹⁴⁷, S. Yacoob ^{33a}, N. Yamaguchi ⁸⁹, Y. Yamaguchi ¹⁵⁴, H. Yamauchi ¹⁵⁷, T. Yamazaki ^{17a}, Y. Yamazaki ⁸⁴, J. Yan ^{62c}, S. Yan ¹²⁶, Z. Yan ²⁵, H.J. Yang ^{62c,62d}, H.T. Yang ^{62a}, S. Yang ^{62a}, T. Yang ^{64c}, X. Yang ^{62a}, X. Yang ^{14a}, Y. Yang ⁴⁴, Z. Yang ^{62a,106}, W.-M. Yao ^{17a}, Y.C. Yap ⁴⁸, H. Ye ^{14c}, H. Ye ⁵⁵, J. Ye ⁴⁴, S. Ye ²⁹, X. Ye ^{62a}, Y. Yeh ⁹⁶, I. Yeletsikh ³⁸, B.K. Yeo ^{17a}, M.R. Yexley ⁹¹, P. Yin ⁴¹, K. Yorita ¹⁶⁸, S. Younas ^{27b}, C.J.S. Young ⁵⁴, C. Young ¹⁴³, Y. Yu ^{62a}, M. Yuan ¹⁰⁶, R. Yuan ^{62b,m}, L. Yue ⁹⁶, X. Yue ^{63a}, M. Zaazoua ^{35e}, B. Zabinski ⁸⁶, E. Zaid ⁵², T. Zakareishvili ^{149b}, N. Zakharchuk ³⁴, S. Zambito ⁵⁶, J.A. Zamora Saa ^{137d,137b}, J. Zang ¹⁵³, D. Zanzi ⁵⁴, O. Zaplatilek ¹³², S.V. Zeißner ⁴⁹, C. Zeitnitz ¹⁷¹, J.C. Zeng ¹⁶², D.T. Zenger Jr ²⁶, O. Zenin ³⁷, T. Ženiš ^{28a}, S. Zenz ⁹⁴, S. Zerradi ^{35a}, D. Zerwas ⁶⁶, M. Zhai ^{14a,14d}, B. Zhang ^{14c}, D.F. Zhang ¹³⁹, J. Zhang ^{62b}, J. Zhang ⁶, K. Zhang ^{14a,14d}, L. Zhang ^{14c}, P. Zhang ^{14a,14d}, R. Zhang ¹⁷⁰, S. Zhang ¹⁰⁶, T. Zhang ¹⁵³, X. Zhang ^{62c}, X. Zhang ^{62b}, Y. Zhang ^{62c,5}, Z. Zhang ^{17a}, Z. Zhang ⁶⁶, H. Zhao ¹³⁸, P. Zhao ⁵¹, T. Zhao ^{62b}, Y. Zhao ¹³⁶, Z. Zhao ^{62a}, A. Zhemchugov ³⁸, X. Zheng ^{62a}, Z. Zheng ¹⁴³, D. Zhong ¹⁶², B. Zhou ¹⁰⁶, C. Zhou ¹⁷⁰, H. Zhou ⁷, N. Zhou ^{62c}, Y. Zhou ⁷, C.G. Zhu ^{62b}, C. Zhu ^{14a,14d}, H.L. Zhu ^{62a}, H. Zhu ^{14a}, J. Zhu ¹⁰⁶, Y. Zhu ^{62c}, Y. Zhu ^{62a}, X. Zhuang ^{14a}, K. Zhukov ³⁷, V. Zhulanov ³⁷, N.I. Zimine ³⁸, J. Zinsser ^{63b}, M. Ziolkowski ¹⁴¹, L. Živković ¹⁵, A. Zoccoli ^{23b,23a}, K. Zoch ⁵⁶, T.G. Zorbas ¹³⁹, O. Zormpa ⁴⁶, W. Zou ⁴¹, L. Zwalinski ³⁶.

¹Department of Physics, University of Adelaide, Adelaide; Australia.

²Department of Physics, University of Alberta, Edmonton AB; Canada.

³(^a)Department of Physics, Ankara University, Ankara; (^b)Division of Physics, TOBB University of Economics and Technology, Ankara; Türkiye.

⁴LAPP, Université Savoie Mont Blanc, CNRS/IN2P3, Annecy; France.

⁵APC, Université Paris Cité, CNRS/IN2P3, Paris; France.

⁶High Energy Physics Division, Argonne National Laboratory, Argonne IL; United States of America.

⁷Department of Physics, University of Arizona, Tucson AZ; United States of America.

⁸Department of Physics, University of Texas at Arlington, Arlington TX; United States of America.

⁹Physics Department, National and Kapodistrian University of Athens, Athens; Greece.

¹⁰Physics Department, National Technical University of Athens, Zografou; Greece.

¹¹Department of Physics, University of Texas at Austin, Austin TX; United States of America.

¹²Institute of Physics, Azerbaijan Academy of Sciences, Baku; Azerbaijan.

¹³Institut de Física d'Altes Energies (IFAE), Barcelona Institute of Science and Technology, Barcelona; Spain.

¹⁴(^a)Institute of High Energy Physics, Chinese Academy of Sciences, Beijing; (^b)Physics Department, Tsinghua University, Beijing; (^c)Department of Physics, Nanjing University, Nanjing; (^d)University of Chinese Academy of Science (UCAS), Beijing; China.

¹⁵Institute of Physics, University of Belgrade, Belgrade; Serbia.

¹⁶Department for Physics and Technology, University of Bergen, Bergen; Norway.

- ^{17(a)}Physics Division, Lawrence Berkeley National Laboratory, Berkeley CA;^(b)University of California, Berkeley CA; United States of America.
- ¹⁸Institut für Physik, Humboldt Universität zu Berlin, Berlin; Germany.
- ¹⁹Albert Einstein Center for Fundamental Physics and Laboratory for High Energy Physics, University of Bern, Bern; Switzerland.
- ²⁰School of Physics and Astronomy, University of Birmingham, Birmingham; United Kingdom.
- ^{21(a)}Department of Physics, Bogazici University, Istanbul;^(b)Department of Physics Engineering, Gaziantep University, Gaziantep;^(c)Department of Physics, Istanbul University, Istanbul;^(d)Istinye University, Sariyer, Istanbul; Türkiye.
- ^{22(a)}Facultad de Ciencias y Centro de Investigaciones, Universidad Antonio Nariño, Bogotá;^(b)Departamento de Física, Universidad Nacional de Colombia, Bogotá; Colombia.
- ^{23(a)}Dipartimento di Fisica e Astronomia A. Righi, Università di Bologna, Bologna;^(b)INFN Sezione di Bologna; Italy.
- ²⁴Physikalisches Institut, Universität Bonn, Bonn; Germany.
- ²⁵Department of Physics, Boston University, Boston MA; United States of America.
- ²⁶Department of Physics, Brandeis University, Waltham MA; United States of America.
- ^{27(a)}Transilvania University of Brasov, Brasov;^(b)Horia Hulubei National Institute of Physics and Nuclear Engineering, Bucharest;^(c)Department of Physics, Alexandru Ioan Cuza University of Iasi, Iasi;^(d)National Institute for Research and Development of Isotopic and Molecular Technologies, Physics Department, Cluj-Napoca;^(e)University Politehnica Bucharest, Bucharest;^(f)West University in Timisoara, Timisoara;^(g)Faculty of Physics, University of Bucharest, Bucharest; Romania.
- ^{28(a)}Faculty of Mathematics, Physics and Informatics, Comenius University, Bratislava;^(b)Department of Subnuclear Physics, Institute of Experimental Physics of the Slovak Academy of Sciences, Kosice; Slovak Republic.
- ²⁹Physics Department, Brookhaven National Laboratory, Upton NY; United States of America.
- ³⁰Universidad de Buenos Aires, Facultad de Ciencias Exactas y Naturales, Departamento de Física, y CONICET, Instituto de Física de Buenos Aires (IFIBA), Buenos Aires; Argentina.
- ³¹California State University, CA; United States of America.
- ³²Cavendish Laboratory, University of Cambridge, Cambridge; United Kingdom.
- ^{33(a)}Department of Physics, University of Cape Town, Cape Town;^(b)iThemba Labs, Western Cape;^(c)Department of Mechanical Engineering Science, University of Johannesburg, Johannesburg;^(d)National Institute of Physics, University of the Philippines Diliman (Philippines);^(e)University of South Africa, Department of Physics, Pretoria;^(f)University of Zululand, KwaDlangezwa;^(g)School of Physics, University of the Witwatersrand, Johannesburg; South Africa.
- ³⁴Department of Physics, Carleton University, Ottawa ON; Canada.
- ^{35(a)}Faculté des Sciences Ain Chock, Réseau Universitaire de Physique des Hautes Energies - Université Hassan II, Casablanca;^(b)Faculté des Sciences, Université Ibn-Tofail, Kénitra;^(c)Faculté des Sciences Semlalia, Université Cadi Ayyad, LPHEA-Marrakech;^(d)LPMR, Faculté des Sciences, Université Mohamed Premier, Oujda;^(e)Faculté des sciences, Université Mohammed V, Rabat;^(f)Institute of Applied Physics, Mohammed VI Polytechnic University, Ben Guerir; Morocco.
- ³⁶CERN, Geneva; Switzerland.
- ³⁷Affiliated with an institute covered by a cooperation agreement with CERN.
- ³⁸Affiliated with an international laboratory covered by a cooperation agreement with CERN.
- ³⁹Enrico Fermi Institute, University of Chicago, Chicago IL; United States of America.
- ⁴⁰LPC, Université Clermont Auvergne, CNRS/IN2P3, Clermont-Ferrand; France.
- ⁴¹Nevis Laboratory, Columbia University, Irvington NY; United States of America.
- ⁴²Niels Bohr Institute, University of Copenhagen, Copenhagen; Denmark.

- ^{43(a)}Dipartimento di Fisica, Università della Calabria, Rende; ^(b)INFN Gruppo Collegato di Cosenza, Laboratori Nazionali di Frascati; Italy.
- ⁴⁴Physics Department, Southern Methodist University, Dallas TX; United States of America.
- ⁴⁵Physics Department, University of Texas at Dallas, Richardson TX; United States of America.
- ⁴⁶National Centre for Scientific Research "Demokritos", Agia Paraskevi; Greece.
- ^{47(a)}Department of Physics, Stockholm University; ^(b)Oskar Klein Centre, Stockholm; Sweden.
- ⁴⁸Deutsches Elektronen-Synchrotron DESY, Hamburg and Zeuthen; Germany.
- ⁴⁹Fakultät Physik, Technische Universität Dortmund, Dortmund; Germany.
- ⁵⁰Institut für Kern- und Teilchenphysik, Technische Universität Dresden, Dresden; Germany.
- ⁵¹Department of Physics, Duke University, Durham NC; United States of America.
- ⁵²SUPA - School of Physics and Astronomy, University of Edinburgh, Edinburgh; United Kingdom.
- ⁵³INFN e Laboratori Nazionali di Frascati, Frascati; Italy.
- ⁵⁴Physikalisches Institut, Albert-Ludwigs-Universität Freiburg, Freiburg; Germany.
- ⁵⁵II. Physikalisches Institut, Georg-August-Universität Göttingen, Göttingen; Germany.
- ⁵⁶Département de Physique Nucléaire et Corpusculaire, Université de Genève, Genève; Switzerland.
- ^{57(a)}Dipartimento di Fisica, Università di Genova, Genova; ^(b)INFN Sezione di Genova; Italy.
- ⁵⁸II. Physikalisches Institut, Justus-Liebig-Universität Giessen, Giessen; Germany.
- ⁵⁹SUPA - School of Physics and Astronomy, University of Glasgow, Glasgow; United Kingdom.
- ⁶⁰LPSC, Université Grenoble Alpes, CNRS/IN2P3, Grenoble INP, Grenoble; France.
- ⁶¹Laboratory for Particle Physics and Cosmology, Harvard University, Cambridge MA; United States of America.
- ^{62(a)}Department of Modern Physics and State Key Laboratory of Particle Detection and Electronics, University of Science and Technology of China, Hefei; ^(b)Institute of Frontier and Interdisciplinary Science and Key Laboratory of Particle Physics and Particle Irradiation (MOE), Shandong University, Qingdao; ^(c)School of Physics and Astronomy, Shanghai Jiao Tong University, Key Laboratory for Particle Astrophysics and Cosmology (MOE), SKLPPC, Shanghai; ^(d)Tsung-Dao Lee Institute, Shanghai; China.
- ^{63(a)}Kirchhoff-Institut für Physik, Ruprecht-Karls-Universität Heidelberg, Heidelberg; ^(b)Physikalisches Institut, Ruprecht-Karls-Universität Heidelberg, Heidelberg; Germany.
- ^{64(a)}Department of Physics, Chinese University of Hong Kong, Shatin, N.T., Hong Kong; ^(b)Department of Physics, University of Hong Kong, Hong Kong; ^(c)Department of Physics and Institute for Advanced Study, Hong Kong University of Science and Technology, Clear Water Bay, Kowloon, Hong Kong; China.
- ⁶⁵Department of Physics, National Tsing Hua University, Hsinchu; Taiwan.
- ⁶⁶IJCLab, Université Paris-Saclay, CNRS/IN2P3, 91405, Orsay; France.
- ⁶⁷Centro Nacional de Microelectrónica (IMB-CNM-CSIC), Barcelona; Spain.
- ⁶⁸Department of Physics, Indiana University, Bloomington IN; United States of America.
- ^{69(a)}INFN Gruppo Collegato di Udine, Sezione di Trieste, Udine; ^(b)ICTP, Trieste; ^(c)Dipartimento Politecnico di Ingegneria e Architettura, Università di Udine, Udine; Italy.
- ^{70(a)}INFN Sezione di Lecce; ^(b)Dipartimento di Matematica e Fisica, Università del Salento, Lecce; Italy.
- ^{71(a)}INFN Sezione di Milano; ^(b)Dipartimento di Fisica, Università di Milano, Milano; Italy.
- ^{72(a)}INFN Sezione di Napoli; ^(b)Dipartimento di Fisica, Università di Napoli, Napoli; Italy.
- ^{73(a)}INFN Sezione di Pavia; ^(b)Dipartimento di Fisica, Università di Pavia, Pavia; Italy.
- ^{74(a)}INFN Sezione di Pisa; ^(b)Dipartimento di Fisica E. Fermi, Università di Pisa, Pisa; Italy.
- ^{75(a)}INFN Sezione di Roma; ^(b)Dipartimento di Fisica, Sapienza Università di Roma, Roma; Italy.
- ^{76(a)}INFN Sezione di Roma Tor Vergata; ^(b)Dipartimento di Fisica, Università di Roma Tor Vergata, Roma; Italy.
- ^{77(a)}INFN Sezione di Roma Tre; ^(b)Dipartimento di Matematica e Fisica, Università Roma Tre, Roma; Italy.

- ⁷⁸(*a*) INFN-TIFPA; (*b*) Università degli Studi di Trento, Trento; Italy.
- ⁷⁹Universität Innsbruck, Department of Astro and Particle Physics, Innsbruck; Austria.
- ⁸⁰University of Iowa, Iowa City IA; United States of America.
- ⁸¹Department of Physics and Astronomy, Iowa State University, Ames IA; United States of America.
- ⁸²(*a*) Departamento de Engenharia Elétrica, Universidade Federal de Juiz de Fora (UFJF), Juiz de Fora; (*b*) Universidade Federal do Rio De Janeiro COPPE/EE/IF, Rio de Janeiro; (*c*) Instituto de Física, Universidade de São Paulo, São Paulo; (*d*) Rio de Janeiro State University, Rio de Janeiro; Brazil.
- ⁸³KEK, High Energy Accelerator Research Organization, Tsukuba; Japan.
- ⁸⁴Graduate School of Science, Kobe University, Kobe; Japan.
- ⁸⁵(*a*) AGH University of Krakow, Faculty of Physics and Applied Computer Science, Krakow; (*b*) Marian Smoluchowski Institute of Physics, Jagiellonian University, Krakow; Poland.
- ⁸⁶Institute of Nuclear Physics Polish Academy of Sciences, Krakow; Poland.
- ⁸⁷Faculty of Science, Kyoto University, Kyoto; Japan.
- ⁸⁸Kyoto University of Education, Kyoto; Japan.
- ⁸⁹Research Center for Advanced Particle Physics and Department of Physics, Kyushu University, Fukuoka ; Japan.
- ⁹⁰Instituto de Física La Plata, Universidad Nacional de La Plata and CONICET, La Plata; Argentina.
- ⁹¹Physics Department, Lancaster University, Lancaster; United Kingdom.
- ⁹²Oliver Lodge Laboratory, University of Liverpool, Liverpool; United Kingdom.
- ⁹³Department of Experimental Particle Physics, Jožef Stefan Institute and Department of Physics, University of Ljubljana, Ljubljana; Slovenia.
- ⁹⁴School of Physics and Astronomy, Queen Mary University of London, London; United Kingdom.
- ⁹⁵Department of Physics, Royal Holloway University of London, Egham; United Kingdom.
- ⁹⁶Department of Physics and Astronomy, University College London, London; United Kingdom.
- ⁹⁷Louisiana Tech University, Ruston LA; United States of America.
- ⁹⁸Fysiska institutionen, Lunds universitet, Lund; Sweden.
- ⁹⁹Departamento de Física Teórica C-15 and CIAFF, Universidad Autónoma de Madrid, Madrid; Spain.
- ¹⁰⁰Institut für Physik, Universität Mainz, Mainz; Germany.
- ¹⁰¹School of Physics and Astronomy, University of Manchester, Manchester; United Kingdom.
- ¹⁰²CPPM, Aix-Marseille Université, CNRS/IN2P3, Marseille; France.
- ¹⁰³Department of Physics, University of Massachusetts, Amherst MA; United States of America.
- ¹⁰⁴Department of Physics, McGill University, Montreal QC; Canada.
- ¹⁰⁵School of Physics, University of Melbourne, Victoria; Australia.
- ¹⁰⁶Department of Physics, University of Michigan, Ann Arbor MI; United States of America.
- ¹⁰⁷Department of Physics and Astronomy, Michigan State University, East Lansing MI; United States of America.
- ¹⁰⁸Group of Particle Physics, University of Montreal, Montreal QC; Canada.
- ¹⁰⁹Fakultät für Physik, Ludwig-Maximilians-Universität München, München; Germany.
- ¹¹⁰Max-Planck-Institut für Physik (Werner-Heisenberg-Institut), München; Germany.
- ¹¹¹Graduate School of Science and Kobayashi-Maskawa Institute, Nagoya University, Nagoya; Japan.
- ¹¹²Department of Physics and Astronomy, University of New Mexico, Albuquerque NM; United States of America.
- ¹¹³Institute for Mathematics, Astrophysics and Particle Physics, Radboud University/Nikhef, Nijmegen; Netherlands.
- ¹¹⁴Nikhef National Institute for Subatomic Physics and University of Amsterdam, Amsterdam; Netherlands.
- ¹¹⁵Department of Physics, Northern Illinois University, DeKalb IL; United States of America.

- ¹¹⁶(*a*) New York University Abu Dhabi, Abu Dhabi; (*b*) University of Sharjah, Sharjah; United Arab Emirates.
- ¹¹⁷Department of Physics, New York University, New York NY; United States of America.
- ¹¹⁸Ochanomizu University, Otsuka, Bunkyo-ku, Tokyo; Japan.
- ¹¹⁹Ohio State University, Columbus OH; United States of America.
- ¹²⁰Homer L. Dodge Department of Physics and Astronomy, University of Oklahoma, Norman OK; United States of America.
- ¹²¹Department of Physics, Oklahoma State University, Stillwater OK; United States of America.
- ¹²²Palacký University, Joint Laboratory of Optics, Olomouc; Czech Republic.
- ¹²³Institute for Fundamental Science, University of Oregon, Eugene, OR; United States of America.
- ¹²⁴Graduate School of Science, Osaka University, Osaka; Japan.
- ¹²⁵Department of Physics, University of Oslo, Oslo; Norway.
- ¹²⁶Department of Physics, Oxford University, Oxford; United Kingdom.
- ¹²⁷LPNHE, Sorbonne Université, Université Paris Cité, CNRS/IN2P3, Paris; France.
- ¹²⁸Department of Physics, University of Pennsylvania, Philadelphia PA; United States of America.
- ¹²⁹Department of Physics and Astronomy, University of Pittsburgh, Pittsburgh PA; United States of America.
- ¹³⁰(*a*) Laboratório de Instrumentação e Física Experimental de Partículas - LIP, Lisboa; (*b*) Departamento de Física, Faculdade de Ciências, Universidade de Lisboa, Lisboa; (*c*) Departamento de Física, Universidade de Coimbra, Coimbra; (*d*) Centro de Física Nuclear da Universidade de Lisboa, Lisboa; (*e*) Departamento de Física, Universidade do Minho, Braga; (*f*) Departamento de Física Teórica y del Cosmos, Universidad de Granada, Granada (Spain); (*g*) Departamento de Física, Instituto Superior Técnico, Universidade de Lisboa, Lisboa; Portugal.
- ¹³¹Institute of Physics of the Czech Academy of Sciences, Prague; Czech Republic.
- ¹³²Czech Technical University in Prague, Prague; Czech Republic.
- ¹³³Charles University, Faculty of Mathematics and Physics, Prague; Czech Republic.
- ¹³⁴Particle Physics Department, Rutherford Appleton Laboratory, Didcot; United Kingdom.
- ¹³⁵IRFU, CEA, Université Paris-Saclay, Gif-sur-Yvette; France.
- ¹³⁶Santa Cruz Institute for Particle Physics, University of California Santa Cruz, Santa Cruz CA; United States of America.
- ¹³⁷(*a*) Departamento de Física, Pontificia Universidad Católica de Chile, Santiago; (*b*) Millennium Institute for Subatomic physics at high energy frontier (SAPHIR), Santiago; (*c*) Instituto de Investigación Multidisciplinario en Ciencia y Tecnología, y Departamento de Física, Universidad de La Serena; (*d*) Universidad Andres Bello, Department of Physics, Santiago; (*e*) Instituto de Alta Investigación, Universidad de Tarapacá, Arica; (*f*) Departamento de Física, Universidad Técnica Federico Santa María, Valparaíso; Chile.
- ¹³⁸Department of Physics, University of Washington, Seattle WA; United States of America.
- ¹³⁹Department of Physics and Astronomy, University of Sheffield, Sheffield; United Kingdom.
- ¹⁴⁰Department of Physics, Shinshu University, Nagano; Japan.
- ¹⁴¹Department Physik, Universität Siegen, Siegen; Germany.
- ¹⁴²Department of Physics, Simon Fraser University, Burnaby BC; Canada.
- ¹⁴³SLAC National Accelerator Laboratory, Stanford CA; United States of America.
- ¹⁴⁴Department of Physics, Royal Institute of Technology, Stockholm; Sweden.
- ¹⁴⁵Departments of Physics and Astronomy, Stony Brook University, Stony Brook NY; United States of America.
- ¹⁴⁶Department of Physics and Astronomy, University of Sussex, Brighton; United Kingdom.
- ¹⁴⁷School of Physics, University of Sydney, Sydney; Australia.

- ¹⁴⁸Institute of Physics, Academia Sinica, Taipei; Taiwan.
- ¹⁴⁹^(a)E. Andronikashvili Institute of Physics, Iv. Javakhishvili Tbilisi State University, Tbilisi;^(b)High Energy Physics Institute, Tbilisi State University, Tbilisi;^(c)University of Georgia, Tbilisi; Georgia.
- ¹⁵⁰Department of Physics, Technion, Israel Institute of Technology, Haifa; Israel.
- ¹⁵¹Raymond and Beverly Sackler School of Physics and Astronomy, Tel Aviv University, Tel Aviv; Israel.
- ¹⁵²Department of Physics, Aristotle University of Thessaloniki, Thessaloniki; Greece.
- ¹⁵³International Center for Elementary Particle Physics and Department of Physics, University of Tokyo, Tokyo; Japan.
- ¹⁵⁴Department of Physics, Tokyo Institute of Technology, Tokyo; Japan.
- ¹⁵⁵Department of Physics, University of Toronto, Toronto ON; Canada.
- ¹⁵⁶^(a)TRIUMF, Vancouver BC;^(b)Department of Physics and Astronomy, York University, Toronto ON; Canada.
- ¹⁵⁷Division of Physics and Tomonaga Center for the History of the Universe, Faculty of Pure and Applied Sciences, University of Tsukuba, Tsukuba; Japan.
- ¹⁵⁸Department of Physics and Astronomy, Tufts University, Medford MA; United States of America.
- ¹⁵⁹United Arab Emirates University, Al Ain; United Arab Emirates.
- ¹⁶⁰Department of Physics and Astronomy, University of California Irvine, Irvine CA; United States of America.
- ¹⁶¹Department of Physics and Astronomy, University of Uppsala, Uppsala; Sweden.
- ¹⁶²Department of Physics, University of Illinois, Urbana IL; United States of America.
- ¹⁶³Instituto de Física Corpuscular (IFIC), Centro Mixto Universidad de Valencia - CSIC, Valencia; Spain.
- ¹⁶⁴Department of Physics, University of British Columbia, Vancouver BC; Canada.
- ¹⁶⁵Department of Physics and Astronomy, University of Victoria, Victoria BC; Canada.
- ¹⁶⁶Fakultät für Physik und Astronomie, Julius-Maximilians-Universität Würzburg, Würzburg; Germany.
- ¹⁶⁷Department of Physics, University of Warwick, Coventry; United Kingdom.
- ¹⁶⁸Waseda University, Tokyo; Japan.
- ¹⁶⁹Department of Particle Physics and Astrophysics, Weizmann Institute of Science, Rehovot; Israel.
- ¹⁷⁰Department of Physics, University of Wisconsin, Madison WI; United States of America.
- ¹⁷¹Fakultät für Mathematik und Naturwissenschaften, Fachgruppe Physik, Bergische Universität Wuppertal, Wuppertal; Germany.
- ¹⁷²Department of Physics, Yale University, New Haven CT; United States of America.
- ^a Also Affiliated with an institute covered by a cooperation agreement with CERN.
- ^b Also at An-Najah National University, Nablus; Palestine.
- ^c Also at Borough of Manhattan Community College, City University of New York, New York NY; United States of America.
- ^d Also at Bruno Kessler Foundation, Trento; Italy.
- ^e Also at Center for High Energy Physics, Peking University; China.
- ^f Also at Center for Interdisciplinary Research and Innovation (CIRI-AUTH), Thessaloniki ; Greece.
- ^g Associated at Center for Theoretical Physics, MIT, Cambridge MA; United States of America.
- ^h Also at Centro Studi e Ricerche Enrico Fermi; Italy.
- ⁱ Also at CERN, Geneva; Switzerland.
- ^j Also at Département de Physique Nucléaire et Corpusculaire, Université de Genève, Genève; Switzerland.
- ^k Also at Departament de Física de la Universitat Autònoma de Barcelona, Barcelona; Spain.
- ^l Also at Department of Financial and Management Engineering, University of the Aegean, Chios; Greece.
- ^m Also at Department of Physics and Astronomy, Michigan State University, East Lansing MI; United States of America.

ⁿ Also at Department of Physics and Astronomy, University of Louisville, Louisville, KY; United States of America.

^o Also at Department of Physics, Ben Gurion University of the Negev, Beer Sheva; Israel.

^p Also at Department of Physics, California State University, East Bay; United States of America.

^q Also at Department of Physics, California State University, Sacramento; United States of America.

^r Also at Department of Physics, King's College London, London; United Kingdom.

^s Also at Department of Physics, Stanford University, Stanford CA; United States of America.

^t Also at Department of Physics, University of Fribourg, Fribourg; Switzerland.

^u Also at Department of Physics, University of Thessaly; Greece.

^v Also at Department of Physics, Westmont College, Santa Barbara; United States of America.

^w Also at Hellenic Open University, Patras; Greece.

^x Also at Institutio Catalana de Recerca i Estudis Avancats, ICREA, Barcelona; Spain.

^y Also at Institut für Experimentalphysik, Universität Hamburg, Hamburg; Germany.

^z Also at Institute for Nuclear Research and Nuclear Energy (INRNE) of the Bulgarian Academy of Sciences, Sofia; Bulgaria.

^{aa} Also at Institute of Applied Physics, Mohammed VI Polytechnic University, Ben Guerir; Morocco.

^{ab} Also at Institute of Particle Physics (IPP); Canada.

^{ac} Also at Institute of Physics and Technology, Ulaanbaatar; Mongolia.

^{ad} Also at Institute of Physics, Azerbaijan Academy of Sciences, Baku; Azerbaijan.

^{ae} Also at Institute of Theoretical Physics, Ilia State University, Tbilisi; Georgia.

^{af} Also at L2IT, Université de Toulouse, CNRS/IN2P3, UPS, Toulouse; France.

^{ag} Also at Lawrence Livermore National Laboratory, Livermore; United States of America.

^{ah} Also at National Institute of Physics, University of the Philippines Diliman (Philippines); Philippines.

^{ai} Also at RWTH Aachen University, III. Physikalisches Institut A, Aachen; Germany.

^{aj} Also at Technical University of Munich, Munich; Germany.

^{ak} Also at The Collaborative Innovation Center of Quantum Matter (CICQM), Beijing; China.

^{al} Also at TRIUMF, Vancouver BC; Canada.

^{am} Also at Università di Napoli Parthenope, Napoli; Italy.

^{an} Also at University of Chinese Academy of Sciences (UCAS), Beijing; China.

^{ao} Also at University of Colorado Boulder, Department of Physics, Colorado; United States of America.

^{ap} Also at Washington College, Maryland; United States of America.

^{aq} Also at Yeditepe University, Physics Department, Istanbul; Türkiye.

* Deceased